A STUDY OF THE ROLE OF THE SIX FAMILY OF TRANSCRIPTION FACTORS IN ADULT SKELETAL MUSCLE HOMEOSTASIS

By

John Girgis

July 2018

A Thesis submitted to the
University of Ottawa
in partial fulfillment of the requirements
for the degree of
Master of Science in Biochemistry

Department of Biochemistry, Microbiology and Immunology
Faculty of Medicine
University of Ottawa

Abstract

Duchenne Muscular Dystrophy (DMD) is characterized by persistent deterioration and regeneration of skeletal muscles. This occurs when ablation of the Dystrophin protein – through deleterious, nonsense, or frameshift mutations in the coding gene – destabilizes the Dystrophin-Associated Glycoprotein Complex (DAPC), resulting in a multitude of signaling defects. Upregulation of a closely related protein, Utrophin A, has been shown to alleviate the DMD phenotype, and slow-twitch oxidative muscle fibers express innately increased sarcolemmal Utrophin levels conferring resistance to the disease. Studies have shown that the Six family of Transcription Factors (TFs) promote the formation and maintenance of fast-twitch muscle, suggesting that antagonizing the Six TFs and causing a fiber type switch may be a therapeutic approach to treating DMD. In this study, partial loss-of function through RNA interference methodologies in adult skeletal muscles were combined with bioinformatic analyses, to elucidate the therapeutic potential of the antagonism of the Six TFs. Knockdown of Six1 is shown to increase Utrophin levels, with a suggested increase in Nuclear factor of activated T-cells (NFAT) activity. This may be partially mediated by Six1 regulation of a known inhibitor of the NFAT pathway, Myoz1, described herein. Six1 knockdown is also shown to modulate thyroid hormone regulated gene expression, mediated through a novel target, MCT10. This thesis elucidates putative mechanisms by which Six TFs may regulate pro-fast-twitch skeletal muscle fiber type by both antagonizing NFAT activity and promoting thyroid hormone signaling.

Acknowledgements

I would like to gratefully acknowledge all the people without whom the work presented herein could not have been accomplished.
First, and most importantly, I would like to thank Dr. Alexandre Blais for his guidance, patience, kindness and sense of direction these past few years. I would be a different person entirely without having your supervision.

I would like to express my gratitude to Dr. Bernard Jasmin and Dr. Mary-Ellen Harper for being supportive and understanding as members of my Thesis Advisory Committee, and more importantly, for always showing me my blind spots to help me improve as a researcher.

I would like to thank our lab manager, Dabo Yang, for being both the first person to teach me molecular biology techniques in the lab, the last person standing ensuring every experiment I performed was as immaculately performed as can be, and, most significantly, for meeting me with a warm smile every time I asked him for help working after hours or during weekends. I would like to thank Dr. Iman Chakroun and Dr. Yubing Liu for their constant encouragement and support with every tiny question, difficulty and experimental mistake I came up with. I'd like to thank my students over the years, Kimmy Yang, Sara Hemens and Jack Guthrie, for being my extra sets of hands and spare brain whenever my project seemed too daunting in size. The help of previous lab members did not go unnoticed and I appreciate every tiny thing I have learnt from each person, including Ellias Horner, Alphonse Chu, and Atchayaa Gunasekharan.

I would like to thank my mother, Mary Ishak, for being my personal giant whose shoulders I stand on. To my brothers Michael and Andrew, I appreciate every time you were willing to sacrifice your personal comfort for me, and all the nights you suffocated me with hugs when I felt defeated.

To the members of the Nemer Lab, especially Jamie Whitcomb, Lara Gharibeh and Waël Maharsy, the members of the Jasmin lab, especially John Lunde, Christine Péladeau and Tara Crawford, and the members of the Wiper-Bergeron lab, especially Hamood Al-Sudais, thank you for every time you allowed me to borrow a reagent on a moment's notice, or allowed me to skip ahead of you to use a shared piece of equipment.

Finally, and in no particular order, I would like to give a shout-out to Sumanthan Selvarajah, Amali Kannangara, Vaibhav Gupta, Gaëlle Groux, Shagana Visuvanathan, Melissa Govindaraju, Vipal Jain, Annie Ng, Daniel O'Neil, Paula Adler, Jun Yu Gao, Julie Fiala, Graeme McDowell, Stephanie Schoen, Naveeda Hussain, Shalah Mohammed, Liam St. Louis, Danny Salem, Ian Roney, Amy Prouty, Matthieu Leduc, Nick Zhang, Warren Chang and Lionel Chow for being the greatest friends and social support (read: time-wasting) systems one could dream of.

Funding for this work was kindly provided by The Canadian Institutes of Health Research (CIHR).

Contents

Abstract ii

Acknowledgements iii

Glossary x

1 Introduction 1

1.1 Muscle . . . 1

1.1.1 Skeletal muscle . . . 1

1.1.2 Muscle diseases . . . 2

1.2 Duchenne & Becker muscular dystrophy . . . 4

1.2.1 Dystrophin and the DAPC . . . 5

1.2.2 The molecular basis of DMD . . . 5

1.2.3 The scale of DMD . . . 6

1.2.4 Current treatment options . . . 8

1.2.5 Therapies under research . . . 9

1.2.6 Utrophin . . . 11

1.2.7 Utrophin upregulation to treat DMD . . . 13

1.3 The Six TFs . . . 14

1.3.1 Embryonic myogenesis and the Six TFs . . . 16

1.3.2 Adult myogenesis and the Six TFs . . . 18

1.3.3 Fiber-type specification and the Six TFs . . . 19

1.4 The NFAT TFs . . . 20

1.4.1 The NFAT TFs and skeletal muscles 21
1.4.2 The NFAT TFs and the Six TFs 22
1.5 Thyroid hormone 22
1.5.1 Thyroid Hormone and skeletal muscles 23
1.5.2 Thyroid hormone and the Six TFs 24
1.6 Hypothesis & Aims 25

2 Materials and Methods 27
2.1 Tissue Culture Techniques 27
2.1.1 Cell Growth and Maintenance 27
2.1.2 Lipofectamine siRNA Transfections 27
2.1.3 Lipofectamine 3000 Plasmid Transfections 28
2.2 Animal Model Techniques 28
2.2.1 Animal Care 28
2.2.2 Nucleic Acid Electroporation 29
2.2.3 Muscle Section Processing 30
2.2.4 Immunofluorescent Staining 30
2.2.5 Luciferase 31
2.3 General Techniques 32
2.3.1 RNA Extraction 32
2.3.2 Reverse-Transcription PCR 33
2.3.3 ChIP 33
2.3.4 qPCR and qChIP 34
2.3.5 Protein Extraction 35
2.3.6 Protein Quantification Assay 36
2.3.7 Western Blotting 36
2.3.8 Densitometry 37
2.3.9 Bioinformatics Analyses 37
2.3.10 Statistical Analyses 38

3 Results 39
3.1 Optimizing *in vivo* knockdown of Six TFs 39
3.2 Effect of *in vivo* Six TFs knockdown on Utrophin expression . . . 44
3.3 Effect of *in vivo* Six TFs knockdown on Myosin Isoform expression 50
3.4 Elucidating regulatory mechanisms of Utrophin overexpression 53
3.5 Elucidating regulatory mechanisms of NFAT pathway upregulation 57
3.6 Exploring the Six1 regulome for fiber-type specific targets 64
3.7 MCT10, a thyroid transporter, is under Six1 regulatory control . . 69
3.8 Thyroid pathway is impacted negatively in Six1 knockdown conditions 72

4 Discussion 80
4.1 Achieving Six TFs knockdown in skeletal muscle 83
4.2 Six1 knockdown promotes Utrophin upregulation 84
4.3 Six1 knockdown effect on Myosin expression 89
4.4 Six1 knockdown promotes NFAT pathway activity 90
4.5 Six1 effect on Thyroid hormone signaling pathway 93
4.6 Conclusion 97

Bibliography 98

Contributions of Collaborators 124

Appendices 125

Glossary

AAV Adeno-Associated Virus 9

AICAR 5-Aminoimidazole-4-Carboxamide Ribonucleotide 12, 86

AMPK AMP-activated protein kinase 12, 13, 18

ANOVA Analysis of Variance 37, 40

APS Ammonium Persulfate 36

ATCC American Type Culture Collection 27

ATP Adenosine triphosphate 50, 71

BMD Becker Muscular Dystrophy 4, 6, 9

BOR Branchio-Oto-Renal Syndrome 15

BSA Bovine Serum Albumin 35

cDNA Complementary-DNA 11, 34

ChIP Chromatin Immunoprecipitation 33, 37, 50, 57, 59, 60, 64, 66, 67, 70, 71, 73, 76, 93, 94, 124, 138

CIHR The Canadian Institutes of Health Research iv

CK Creatine Kinase 5

CMD Congenital muscular dystrophy 4

CRISPR Clustered Regularly Interspaced Short Palindromic Repeats 94

DAPC Dystrophin-Associated Glycoprotein Complex ii, 4, 6, 11, 87

DEPC Diethyl Pyrocarbonate 31, 32

DM Differentiation Medium 27

DMD Duchenne Muscular Dystrophy ii, 2, 4, 5, 6, 7, 8, 9, 10, 12, 86, 97

DMSO Dimethyl Sulfoxide 36

DNA Deoxyribonucleic Acid 15, 28, 31, 33, 50, 60, 64, 71, 136

dNTP Deoxynucleotide Triphosphate 32

DPI Dots Per Inch 37

DTT Dithiothreitol 32

EDL Extensor digitorum longus 85

eMHC Embryonic Myosin Heavy Chain 39, 40, 83, 84

FIJI FIJI Is Just ImageJ 37

GABP GA-Binding Protein 11

GFP Green Fluorescent Protein 39, 40, 83, 136

GM Growth Medium 27, 28

HRP Horseradish Peroxidase 36

LGMD Limb-girdle muscular dystrophy 4

MDs Muscular Dystrophies 2, 4

MRF Myogenic Regulatory Factor 16, 17, 18, 23, 88

mRNA messenger RNA xi, xii, 7, 20, 23, 37, 39, 40, 44, 47, 50, 54, 57, 60, 64, 67, 71, 72, 73, 76, 80, 83, 84, 85, 86, 89, 90, 91, 92, 94, 136

NFAT Nuclear factor of activated T-cells ii, vii, xi, 8, 11, 12, 18, 20, 21, 50, 54, 57, 60, 76, 80, 90, 91, 92, 93

nNOS Neuronal Nitric Oxide Synthase 4, 6, 10

OCT Optimal Cutting Temperature Compound 30

PBS Phosphate-Buffered Saline 27, 30, 31, 33

PCR Polymerase Chain Reaction 32

PFA Paraformaldehyde 30

PGC-1α Peroxisome proliferator-activated receptor Gamma Coactivator 1-α 11, 12

PVDF Polyvinylidene Fluoride 36

qChIP Quantitative ChIP 34

qPCR Quantitative PCR 33, 34, 37, 60, 67, 71, 94, 138

qRT-PCR Quantitative Reverse-Transcription PCR 25, 40, 44, 47, 50, 54, 60, 67, 71, 73, 76, 84, 85, 89, 94, 95, 138, 139

RCAN Regulator of Calcineurin 21, 76

RIPA Radioimmunoprecipitation assay buffer 33

RLS Restless Legs Syndrome 11

RNA Ribonucleic Acid ii, 9, 20, 25, 31, 32, 96

ROS Reactive Oxygen Species 6

RPM Rotations Per Minute 31

SDS Sodium Dodecyl Sulfate 33, 35, 36

SEM Standard Error over the Mean 37, 40, 44, 47, 50, 54, 57, 60, 71, 73, 76, 136

shRNA short hairpin RNA 28, 39

siNS Short-Interfering Non-Specific RNA 37, 40, 44, 47, 50, 54, 57, 60, 71, 73, 76, 83, 87, 89, 136

siRNA short interfering RNA xi, xii, 27, 28, 31, 37, 40, 44, 47, 50, 54, 57, 60, 71, 73, 76, 80, 83, 92, 95, 136, 138

so sine oculis 14

T_3 Triiodothyronine hormone 22, 23, 24, 72, 80, 94, 96

TA Tibialis Anterior 25, 28, 30, 31, 39, 40, 44, 47, 50, 54, 60, 64, 66, 67, 71, 72, 73, 76, 85, 86, 87

TEMED Tetramethylethylenediamine 36

TFs Transcription Factors ii, vii, xii, 2, 13, 14, 15, 16, 17, 18, 19, 20, 21, 22, 24, 25, 39, 40, 47, 67, 70, 80, 83, 84, 91, 92, 93, 95, 124

TRE Thyroid Response Element 22, 76

TRP Transient Receptor Potential 5

List of Figures

1 Diagrams of skeletal muscle Transcriptional Regulation 3
2 Schematic of hypothesis 26
3 Optimization of *in vivo* transfection efficiency 41
4 Optimization of *in vivo* transfection efficacy 42
5 Six TF protein levels under knockdown conditions 43
6 Effect of Six1 knockdown on Utrophin mRNA 45
7 Effect of Six4 and Double knockdown 46
8 Six1 knockdown regulates Utrophin protein levels 48
9 Utrophin protein localization under Six1 knockdown conditions 49
10 Effect of Six1 knockdown on Myosin mRNA 51
11 Myosin isoform expression under Six1 knockdown conditions . . 52
12 Effect of Six1 knockdown on NFAT pathway mRNA 55
13 Effect of Six4 and Double knockdown on NFAT pathway mRNA 56
14 Myoz1 is a potential Six1 target 58
15 ChIP-Seq of Six1 binding at Myoz1 locus 59
16 Myoz1 is a Six1 target *in vivo* 61
17 Six1 knockdown regulates Myoz1 protein levels 62
18 Recapitulation of NFAT pathway effects with siRNA targeting Myoz1 63
19 Fiber-type independent bioinformatics analysis performed to identify Six1 target genes 65

20 Fiber-type specific bioinformatics analysis performed to identify Six1 target genes 66
21 ChIP-Seq of Six TFs binding at Slc16a10/MCT10 locus 70
22 Slc16a10/MCT10 is a Six1 target *in vivo* 71
23 Effect of Six1 knockdown on Thyroid pathway mRNA 74
24 Effect of Six4 and Double knockdown on Thyroid pathway mRNA 75
25 Recapitulation of Thyroid pathway effects with siRNA targeting MCT10 77
26 Thyroid signaling pathway overlaps with Six1 regulome 78
27 Thyroid-regulated Rcan proteins are not affected by Six1 knockdown 79
28 Model of Six1 action in adult skeletal muscle homeostasis 82
29 Optimization of *in vitro* transfection efficiency 136
30 C2C12 Myotubes are a poor model for studying adult muscle . . . 137

List of Tables

1 Genes affected by Six1 knockout independently of fiber-type . . . 67

2 Genes affected by Six1 knockout dependent on fiber-type 68

3 List of used oligonucleotides for qPCR and siRNA 138

4 List of used Antibodies and Dilutions 140

Chapter 1

Introduction

1.1 Muscle

Muscle tissue is a soft tissue that confers animals with their locomotion and internal organ movement, through the activity of muscle cells. Muscle cells, or myocytes, are typified by being composed of Myosin, Actin and Titin protein filaments, or myofibrils, that contract and relax in response to signals received at the cell membrane. The human body contains three major types of muscle. The first, smooth muscle, found for example in the gastrointestinal tract or blood vessel lining, is under involuntary control, is non-striated and centrally mono-nucleated. The second, cardiac muscle, found in the heart, is under involuntary control, is striated and is usually mono-nucleated. Third, and finally, skeletal muscle, the only type under voluntary control, is made up of striated and peripherally multi-nucleated myofibers, due to its formation from the fusion of multiple mono-nucleated precursor cells.

1.1.1 Skeletal muscle

Skeletal muscles account for about 40% of total body mass for an adult human and are unique in both being anchored to bone and being composed of multiple bundles of myofibers, held together by connective tissue, known as fascicles.

Each myofiber contains complete contractile apparatus of the protein filaments required for contraction and movement (Frontera and Ochala, 2015). Skeletal muscles maintain one more unique ability: their ability to regenerate rapidly in response to stress or damage. This ability is due to a constantly maintained pool of reserve stem cells, known as satellite cells, that can proliferate, differentiate and even fuse with pre-existing myofibers to re-establish healthy muscle. A representative diagram exhibiting these modes of action can be found in Figure 1A. These properties allow skeletal muscles to effect voluntary movement, to be highly resistance to stress, and to be capable of modulating cellular regulation in order to more optimally fulfill their functions.

There are four major types of skeletal muscle. At one end of the spectrum slow-twitch skeletal muscle fibers exist, typified by containing Myosin type I myofibrils. Slow-twitch myofibers are resistant to fatigue, rely on oxidative phosphorylation for their energy source, are rich in mitochondria, and so consequentially require more access to capillaries. Fast-twitch skeletal muscle fibers are at the other end of the spectrum, typified by being composed of Myosin type IIb myofibrils. Fast-twitch myofibers produce a higher maximal force output than slow-twitch myofibers, but are more susceptible to fatigue due to their reliance on glycolytic, anaerobic pathways for energy production, leading to lactate buildup. Intermediary fiber types also exist with variable potential for fatigue resistance and power output, expressing Myosin type IIa or IIx myofibrils, and in some cases concurrently expressing more than one type of Myosin myofibril (Banas et al., 2011).

1.1.2 Muscle diseases

The main diseases that affect skeletal muscles include sarcopenia, or progressive muscle wasting due to age-onset depletion of satellite cells (Fulle et al., 2004), muscle atrophy, a disease of myocyte wasting and shrinkage due to the loss of cytoplasmic organelles and proteins (Sartorelli and Fulco, 2004), and

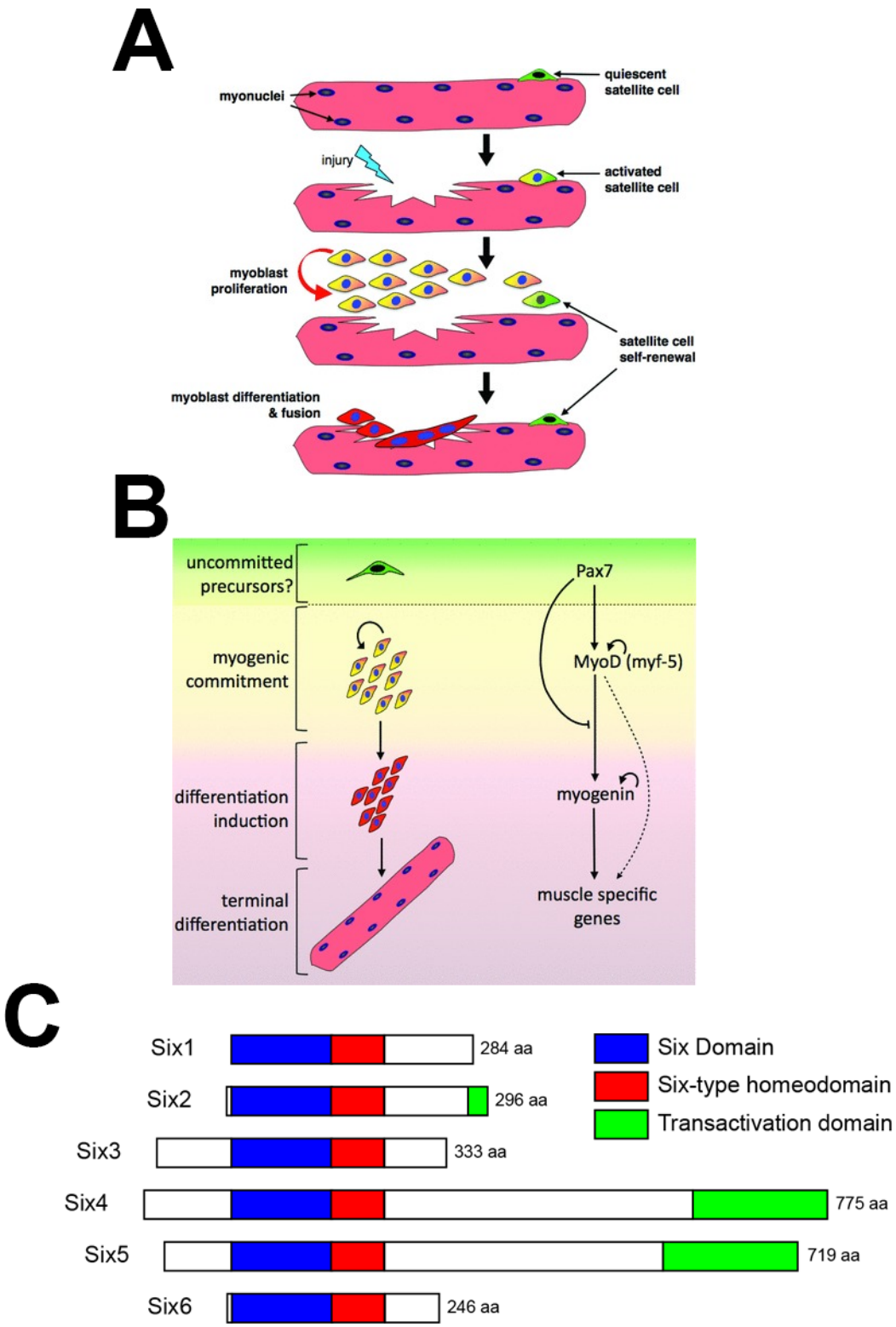

Figure 1: **Diagrams of skeletal muscle Transcriptional Regulation**
(**A**) Basic steps involved in muscle regeneration. Figure borrowed from (Olguín and Pisconti, 2012).
(**B**) Temporal expression of various skeletal muscle TFs based on myogenic development phases. Figure borrowed from (Olguín and Pisconti, 2012).
(**C**) Six TFs homology and protein domain distribution. Figure borrowed from (Kawakami et al., 2000).

the Muscular Dystrophies (MDs), a group of hereditary neuromuscular diseases typified by early-onset progressive muscle wasting and weakness. While MDs may be caused by disruptions in the contractile apparatus, for example through mutations of the Titin gene (Hackman et al., 2008), or disruptions of the nuclear envelope, through mutations of Emerin (Bione et al., 1994), a main objective of this research, is to investigate the treatment potential of targeting the Six TFs in the context of Duchenne Muscular Dystrophy (DMD).

1.2 Duchenne & Becker muscular dystrophy

DMD, the most lethal and prevalent of the MDs, is X-linked and affects about 1 in 5,000 males (Romitti et al., 2015). Patients with DMD usually exhibit their first symptoms by age two in their motor reflexes, and exhibit difficulties walking and standing. Patients are typically wheelchair bound by their second decade of life and succumb to the condition within their third, due to a variety of reasons, including cardiac arrest, respiratory distress, and multi-organ failure. At the cellular level, DMD presents itself as repetitive cycles of myocyte weakness and susceptibility to stress-induced damage, leading to cycles of degeneration and regeneration, decreased potential for successful regeneration, and fat cell infiltration of muscle tissue.

DMD is caused by deleterious or nonsense mutations in the Dystrophin gene, while patients of the closely related Becker Muscular Dystrophy (BMD) suffer from truncated or functionally compromised copies of the Dystrophin gene. BMD patients present with delayed onset of symptoms and longer life expectancy, but nonetheless exhibit milder phenotypes of progressive muscle weakness and wasting. To describe the complexity of the disease, a short explanation of the biochemical role of Dystrophin will be presented, followed by descriptions of the mechanistic complexity of Dystrophin function, and the therapeutic challenges in addressing the disease.

1.2.1 Dystrophin and the DAPC

Dystrophin is a rod-shaped cytoplasmic protein, and is encoded by the DMD gene at locus Xp21. The DMD gene spans 2.3 megabases in length, encompassing 79 exons and 8 promoters. Dystrophin protein binds the intracellular actin cytoskeleton of muscle cells, at its N-Terminus, and connects the apparatus to the extracellular Laminin matrix by anchoring and associating with the Dystrophin-Associated Glycoprotein Complex (DAPC) at its C-Terminus. The DAPC is a protein complex anchored within the cellular membrane (sarcolemma) of skeletal and cardiac muscle cells and its members include Dystrophin, α1-, and ß1-Syntrophin, α-, and ß-Dystroglycan, α-, ß-, γ-, and δ-Sarcoglycan, Neuronal Nitric Oxide Synthase (nNOS), and Laminin-2 (Yoshida and Ozawa, 1990; Ervasti et al., 1990; Murphy et al., 2017). Normal DAPC structure and protein composition regulates many functions, including intracellular signaling (Rando, 2001) and development of the blood-brain barrier in higher mammals (Nico et al., 2004). When Dystrophin, or other members of the DAPC are missing, membrane and cellular structural fragility cause muscle cells to rupture during cycles of contractions. For example, abnormalities in the expression of the Sarcoglycan proteins results in Limb-girdle muscular dystrophy (LGMD) and mutations of Laminin can cause Congenital muscular dystrophy (CMD).

1.2.2 The molecular basis of DMD

Current consensus on the mechanism for fiber type degeneration in DMD suggests that absence of Dystrophin causes a force drop with lengthening contractions (Blaauw et al., 2008) caused by cell rupturing due to sarcolemmal fragility (Petrof et al., 1993; Moens et al., 1993). Afflicted cells display reduced excitability to neuromuscular transmission (Roy et al., 2016), coupled with an excess influx of calcium ions through calcium leak and Transient Receptor

Potential (TRP) channels (McCarter and Steinhardt, 2000; Vandebrouck et al., 2002), and an increased sarcolemmal permeability that allows Creatine Kinase (CK) to leak out (Whitehead et al., 2006). Combined, these effects lead to a cascade of increased protease activity, due to spurious activation of the calcium-dependent Calpains (Hollinger and Selsby, 2013), activation of the proinflammatory response (Gumerson and Michele, 2011), and mitochondrial dysfunction (Vila et al., 2017).

Mutations to ablate Dystrophin binding to microtubules do not induce muscular dystrophy, suggesting that anchoring of the cytoskeleton to the sarcolemma is not a causative factor in the disease (Belanto et al., 2016). Additionally, mutants that cause BMD have been shown to have increased sarcolemmal lipid association (Ameziane-Le Hir et al., 2016) and dissociation of Dystrophin from the sarcolemma in adult mice is insufficient to induce the dystrophic phenotype (Ghahramani Seno et al., 2008), suggesting that unfulfilled structural roles of the DAPC may not be the exclusive cause of DMD.

The DAPC regulates multiple intra-cellular cascades, including calcium and calmodulin metabolism, nNOS production, PI3K/Akt pathway, and RhoGTP'ases signaling, among many others (Bhat et al., 2017). Truncated forms of Dystrophin retaining nNOS anchoring domains (Reza et al., 2016) and counteracting resultant Reactive Oxygen Species (ROS) productions are both sufficient to normalize dystrophic muscular morphology (Whitehead et al., 2008), and increased calcium ion influx recapitulates the dystrophic phenotype in healthy muscle (Millay et al., 2009), suggesting that signalling cascades are implicated in the dystrophic phenotype.

1.2.3 The scale of DMD

While the above results hint that the role of Dystrophin in adult myofibers is more nuanced than being a simple structural component, it is also expressed and functionally relevant in satellite cells. In mice, the ability of dystrophic

satellite cells exhibit proliferation defects, inability to respond to injury, and decreased potential to regenerate muscle compared to wildtype satellite cells transplanted in dystrophic muscle (Sacco et al., 2010). Additionally, satellite cells in dystrophic muscle exhibit spurious activation that is not dependent on myofiber degeneration (Nielsen et al., 2017), decreased asymmetric division potential along with impaired mitotic spindle orientation and prolonged cell cycles (Dumont et al., 2015), and epigenetic modifications that inhibit the transcription of genes required for differentiation such as Myf5 (Chang et al., 2018). Combined, the data suggest that therapeutic considerations should account for the reduced readiness of DMD patients to form or repair new muscle readily. Chimeric mice produced by introduction of dystrophic embryonic stem cells in wild type blastocysts present with a severe dystrophic phenotype, lacking endogenous compensatory mechanisms (Gonzalez et al., 2017), suggesting that Dystrophin expression may be critical even at the embryonic stem cell level.

One major source of complexity to treat DMD is the sheer scale of the disease within a patient. Dystrophin protein is expressed in the human brain and muscle tissues, but transcription from at least one the 8 promoters within the locus and expression of one of the 7 protein isoforms is present in many tissues, including reproductive organs, the liver, and endocrine tissues. This can cause a molecular abnormality to become a systemic point of failure. A third of all patients suffer from intellectual disability (Dubowitz, 1965) and develop cardiomyopathies, even in females carrying a diseased allele (Hoogerwaard et al., 1999). Misregulation of cytoskeleton structuring and energy metabolism in lymphocytes has been reported in DMD (Carr et al., 2017). This necessitates potential therapeutic approaches to have the ability to achieve global treatment in the body.

An added source of complexity in treating DMD comes from the population-wide heterogeneity of the disease. Due to the complexity and size

of the Dystrophin gene, a combinatorial approach between patient genome sequencing, and mRNA expression and splicing change analysis is required to diagnose the effect of certain mutations (Santos et al., 2014). *De novo* mutations are found at a rate of one in every three patients (Bladen et al., 2015), suggesting research into corrective methodologies that could provide treatment for all patients will always be crucial in an eventual cure. Germline mosaicism means that even non-carrier parents may still pass on DMD mutations to their offspring, even though this possibility is a rare one (Wang et al., 2017), making genetic counseling an effective but not preventative measure against DMD.

Combined, these characteristics of DMD paint a picture where development and maintenance is affected in a huge proportion of cells per patient, in a patient population that can be extremely heterogeneous in presentation and disease severity. While current treatments exist that improve patient muscle strength and life expectancy, the search for a cure persists.

1.2.4 Current treatment options

Currently, two treatments exist for patients suffering from DMD. The first, is the administration of corticosteroids, such as Prednisone (Drachman et al., 1974) and Deflazacort (Biggar et al., 2001). Corticosteroids can delay loss of ambulation by over a year, and increase patient lifespan by more than five (Gloss et al., 2016). Corticosteroids may function by increasing α7-integrin and Laminin-α2 expression (Wuebbles et al., 2013), by increasing Calcineurin/NFAT activity (Pierre et al., 2004) - a pathway known to ameliorate the dystrophic phenotype - through inhibition of the mTOR pathway (Mu et al., 2017) - a pathway promoted due to inflammation that accompanies disease progression - or even through downregulation of the expression of Versican (McRae et al., 2017) - a myoblast fusion inhibitor. Common side-effects of corticosteroid treatment, however, is their potential to cause a cushingoid appearance or weight gain in patients (Mendell et al., 1989). Additionally, they

do not drastically improve patient quality of life or life expectancy, demonstrating the need for improved therapy research.

Due to the severity of the disease, Eteplirsen, the first approved exon-skipping drug, was accelerated in its acceptance (Syed, 2016) and is the second treatment option available to patients. Eteplirsen targets exon 51 of the Dystrophin gene and will only be effective for the 13% of all DMD patients who exhibit mutations in that specific exon (Young and Pyle, 2016), causing about 20% increase in Dystrophin expressing myofibers (Mendell et al., 2013). However, due to the size of the Dystrophin gene the development of many exon-skipping drugs to cover the entire range of possible mutations is required (Bladen et al., 2015). Unfortunately, some exons cannot be skipped, such as exon 5 which is necessary for actin-binding (Muntoni et al., 1994), and heterogeneous presentation of symptoms within the BMD patient population suggests limitations preventing exon-skipping from being the methodology of an eventual cure.

1.2.5 Therapies under research

One option to treat DMD is the use of genetic therapies. Two approaches using genetic therapies are in research right now. The first is the use of truncated forms of the Dystrophin gene, mini- or micro-Dystrophins, delivered using viral vectors (Harper et al., 2002). This approach has shown promise in alleviating the DMD phenotype, but host immune-system rejection of the novel introduced proteins has been noted (Mendell et al., 2010), and difficulties exist in scaling up from the *mdx* mouse model into efficacious human patient clinical results (Arechavala-Gomeza et al., 2010). Additionally, complications exist in maintaining stable high transfection efficiency of viral vectors in the context of DMD due to the increased oxidative stress, constantly regenerating muscle and immune pathology of the disease (Dupont, 2016).

The second genetic therapy approach is to directly treat the mutation

causing the disease, either through nonsense suppression, exon skipping, or CRISPR-mediated corrections. Methods include the use of antisense oligonucleotides to correct the splicing of the Dystrophin gene product mRNA (Goyenvalle et al., 2004), the use of premature nonsense mutation suppressing drugs such as Ataluren (Finkel et al., 2013), and multiple potential routes of delivery for Adeno-Associated Virus (AAV) encoding CRISPR-Cas9 and a corrective guide-RNA to induce exon-skipping (Ousterout et al., 2015; Long et al., 2016). However, difficulties in sustained long-term benefits of these treatments are documented and the phenotypic improvements over placebo can be marginal (Voit et al., 2014; Bushby et al., 2014). Additonally, the investment in order to determine the toxicity and efficacy of multiple drug candidates for the ever increasing candidate exons requiring treatment across the population could prove logistically difficult with this approach (Lu et al., 2011). Finally, genetic therapies all share an inherent structural limitation, in the obligate global delivery of the vector into all afflicted tissues of a patient.

Another option is to use therapeutic satellite cell transplantation in affected patients with the hope that the expanding population would repopulate the muscle with Dystrophin-positive myofibers. The ideal methodology would be to expand patient cells *in vitro*, correct their mutations and transplant them back into patients (Filareto et al., 2015). Complications with this method of treatment arise due to questionnable viability of the transplanted cells (Asakura, 2012) and poor potential for expansion *in vivo* (Cossu et al., 2015). An added limitation of this method of treatment is that the adaptive immune response can reject donor cells expressing Dystrophin in patients (Sitzia et al., 2016). Finally, the long-term efficacy of this approach has yet to be determined (Briggs and Morgan, 2013), as the half-life of Dystrophin in healthy muscle has been demonstrated to be around five months (Ghahramani Seno et al., 2008), and it remains to be seen if repeated transplantation will be necessary as part of the therapeutic intervention.

Treatment of secondary cascades caused by misregulation of satellite components represent another avenue for treatment of DMD. Vitamin E treatment has shown positive results in ameliorating the dystrophic phenotype by counteracting the oxidative stress symptoms that are part of the progression of the disease (Mâncio et al., 2017), and promoting mitochondrial function through stimulation of NAD+ synthesis is similarly beneficial (Ryu et al., 2016). However, improving the function of secondary cascades is not always therapeutically viable. While proteasome dysfunction seems to recapitulate the dystrophic phenotype (Kitajima et al., 2014), suggesting a therapeutic target, proteasome inhibition improved the dystrophic phenotype in models of muscular dystrophy (Bonuccelli et al., 2003; Winder et al., 2011; Carmignac et al., 2011) and attempting to rescue the nNOS deficit by nitrate supplementation exacerbates the dystrophic phenotype (Timpani et al., 2017). These results suggest that while one or multiple of these treatments could ameliorate the phenotype, a combinatorial approach will likely be the end-result of this research, and all-encompassing treatments may not be capable of covering the ever-increasing gamut of patient symptoms. Literature based attempts have generally focused on combinatorial approaches where one therapy targets the genetic defect, and the other targets recipient muscle health (Abmayr et al., 2005; Kendall et al., 2012; Heller et al., 2017). Finally, promotion of inherent compensatory mechanisms against the disease can be attempted. While these can include the upregulation of α-sarcoglycan, Laminin and β1-integrin (Hughes et al., 2016), the major example of a compensatory mechanism is the upregulation of Utrophin, a Dystrophin homologue.

1.2.6 Utrophin

Utrophin is the closest protein relative to Dystrophin, and was discovered during a Complementary-DNA (cDNA) screen for genes that exhibit homology to the DAPC binding C-Terminal domain of Dystrophin (Love et al., 1989). With

80% amino acid identity match with Dystrophin in their C-Terminus, Utrophin is uniquely capable of structurally replacing Dystrophin in its niche (Tinsley et al., 1998; Tadayoni et al., 2012). Utrophin localization to the sarcolemma precedes Dystrophin expression (Lin and Burgunder, 2000), hinting that a targetable degradation mechanism may exist. In adult muscle Utrophin is almost exclusively expressed at the neuromuscular and myotendinous junctions (Ohlendieck et al., 1991; Khurana et al., 1991) and is regulated by GA-Binding Protein (GABP) (Gramolini et al., 1999; Khurana et al., 1999), PGC-1α (Angus et al., 2005) and NFAT (Chakkalakal et al., 2003) activities. Recent research has linked skeletal muscles and Restless Legs Syndrome (RLS), with Utrophin mutations being identified as having a key linked factor in the pathogenesis of the disease (Cho et al., 2017), implying our incomplete understanding of the role of Utrophin in muscle health and pathology.

In the context of DMD, double knockout mice of both Dystrophin and Utrophin exhibit exacerbated pathology in part due to additional rapid stem cell depletion (Lu et al., 2014). This suggests functional overlap between the two proteins. Crucially, both truncated and full-length forms of Utrophin are able to rescue the dystrophic phenotype (Tinsley et al., 1996; Tinsley et al., 1998), and compensatory Interleukin-6 and Neuregulin-1 signaling cascades increase Utrophin expression in adult dystrophic fibers confering some resistance to the disease (Juretic et al., 2017). Debate exists over whether Utrophin upregulation is required for slow-twitch muscle resistance to the dystrophic phenotype or is a byproduct of mitochondrial amelioration (Chan et al., 2014). However, both PGC-1α and Utrophin can promote disease-resistant muscle simultaneously and independently of one another, as promoting mitochondrial pathways is known to mitigate disease symptoms (Ryu et al., 2016). One main advantage of Utrophin upregulation as a potential therapy for DMD is bypassing problems of immune system rejection, issues of delivery and concerns of treatment universality since Utrophin is an endogenous protein.

1.2.7 Utrophin upregulation to treat DMD

Multiple avenues of Utrophin upregulation are being explored. Research into the positive modulation of the PGC-1α and SIRT1 axis has shown clinically relevant benefits, including the upregulation of Utrophin (Gordon et al., 2013; Handschin et al., 2007). Transplantation of cells is another potential avenue with the ability of sertoli cells to secrete heregulin-ß1, a Utrophin modulator, having been shown to have positive phenotypic effects in DMD (Chiappalupi et al., 2016). Modulation of Promoting Calcineurin/NFAT activity is another pathway through which Utrophin upregulation can be achieved (Chakkalakal et al., 2003). SMT C1100 is a candidate drug for the transcriptional upregulation of Utrophin as a treatment for DMD and is currently in Phase 2 Clinical Trials (Ricotti et al., 2016). Alternative drugs that have been shown to upregulate Utrophin expression include Heparin, acting through p38 post-transcriptional stabilization regulatory pathways (Péladeau et al., 2015), 5-Aminoimidazole-4-Carboxamide Ribonucleotide (AICAR) and Metformin, acting through the AMP-activated protein kinase (AMPK) transcriptional regulatory pathways (Ljubicic et al., 2011; Ljubicic and Jasmin, 2015), Resveratrol, acting through the PGC-1α mitochondrial signaling pathway (Gordon et al., 2013), the use of Kawain, Leflunomide and other drugs to increase Utrophin promoter activity (Khurana et al., 2012), and even the use of Biglycan as a post-translational regulatory target (Fallon and McNally, 2018).

Crucially, it has been noted that slow-twitch skeletal muscles are more resistant to the dystrophic phenotype (Webster et al., 1988). It has been suggested that this inherent resistance to the disease is due to an inherent increased expression of Utrophin in slow-twitch fibersn (Gramolini et al., 2001). Indeed, this theory is supported by the fact that muscles with inherently higher expression of Utrophin are more resistant to the dystrophic phenotype, including the extraocular muscles (Sekulic-Jablanovic et al., 2016). This suggests potential use of fiber type switching, from muscle fiber types

preferentially affected by muscular dystrophy to those more resistant - or from fast to slow - as a therapy. Previous studies have attempted to promote this fiber-type switch for its therapeutic potential through stimulation of AMPK (Ljubicic et al., 2011) or Calcineurin activity (Chakkalakal et al., 2003), both canonically slow-twitch pathways. However, both of these treatment approaches retain some therapeutic limitations, with AMPK stimulation only increasing Utrophin expression by 30% and Calcineurin activation failing to return dystrophic muscle function to wildtype phenotype, suggesting the importance of further research into additional networks that regulate fiber-type plasticity and can be used in a combinatorial approach with pre-existing treatment options in the literature. One such regulatory network involves the Six TFs, and one aim of this research is to investigate the potential for the Six TFs as a therapeutic target in the upregulation of Utrophin expression, mediated through fiber-type regulation.

1.3 The Six TFs

The Six TFs were first discovered in *Drosophila melanogaster*, with the first member, sine oculis (so), identified by a loss-of-function mutant that impeded normal embryonic eye development (Serikaku and O'Tousa, 1994). Related family members, optix and DSix4, were discovered to also be critical for eye development and for mesoderm derivative tissues, such as muscle and gonadal tissues (Seo et al., 1999). Homologues of the so family of proteins have been discovered across the animal kingdom (Oliver et al., 1995a; Kawakami et al., 1996a; Kumar, 2009) and strong evidence exists that the Six TFs and related proteins developed evolutionarily prior to the divergence of vertebrates (Abitua et al., 2015). In mammals, six family members exist: Six1/2, most closely related to so, Six4/5, most closely related to DSix4, and Six3/6, most closely related to optix (Kawakami et al., 1996b). A diagram showing the various Six TFs' protein

domains and relatedness based on sequence homology can be found in Figure 1C. These transcription factors regulate conserved pathways that favor eye, skeletal muscle and gonadal development (Grifone et al., 2005; Fujimoto et al., 2013). Of the Six TFs, Six1 and Six4 are expressed in the widest variety of tissues in the developing embryo, including within somites, suggesting a larger overall role for these two particular members (Ohto et al., 2002; Oliver et al., 1995b). In adult skeletal muscle, the only expressed members are Six1, Six2, Six4, and Six5 (Oliver et al., 1995b; Ohto et al., 2002).

The Six TFs all share a conserved Six domain, to allow for protein interactions with co-factors (Kobayashi et al., 2001; Zhu et al., 2002), and a homeodomain, to allow for direct DNA binding (Kawakami et al., 1996a), although this homeodomain diverges from the universal homeodomain in structure and binding (Noyes et al., 2008; Liu et al., 2012; Patrick et al., 2013). Six2, Six4 and Six5 also contain a transactivation domain at their C-Terminus, suggesting a unique ability to act independently of co-factors in order to regulate target genes. However, in most cases, in order to achieve their regulatory role, the Six TFs cooperate with the Eya co-activators to bind to MEF3 motifs across the genome (Ohto et al., 1999; Liu et al., 2012). An additional family of co-factors, the Dach proteins, complete the list of the most common proteins the Six TFs interact with (Ikeda et al., 2002).

Our understanding of the regulatory network governing the activity of the Six TFs comes from gene studies in flies, which showed that homologues of Six TFs and even Pax are required for regular eye development (Relaix and Buckingham, 1999). Interactions between Six and Eya (Ohto et al., 1999) as well as between Eya and Dach (Chen et al., 1997) have been demonstrated, suggesting a regulatory network between Pax, Six, Eya and Dach TFs.

Binding of Six and Eya proteins promotes nuclear import of Eya, and the phosphatase activity of the Eya coactivators is sufficient to convert the Six-Dach repressor complex into an activator complex (Li et al., 2003). The interaction

between the Six TFs and Eya proteins is particularly important as disruptions lead to Branchio-Oto-Renal Syndrome (BOR) (Kochhar et al., 2008), with multiple Six TFs being implicated in causing BOR (Ruf et al., 2004; Hoskins et al., 2007), and, in the context of muscle disease, while Six4 and Six5 double knockout mice are never born (Yajima et al., 2010) *mdx* mice with reduced Six4 and Six5 expression display an ameliorated dystrophic phenotype (Yajima and Kawakami, 2016). This indicates that research into the Six TFs is of therapeutic relevance. The most studied biological context for the Six TFs remains their role in skeletal muscles, with impact on muscle development, adult muscle regeneration, and fiber-type specification, discussed in the upcoming sections.

1.3.1 Embryonic myogenesis and the Six TFs

Skeletal muscles develop from bilateral segments, that flank the neural tube of the mesoderm in a head-to-tail axis, known as somites. The dorsal component of somites, or dermomyotome, gives rise to skeletal muscle and epithelial cells (Buckingham and Relaix, 2007). Delamination and folding of parts of the dermomyotome allows for the formation of primitive embryonic muscle, or the myotome, during embryonic myogenesis, and both the dermomyotome and myotome give rise to muscle progentior cells which migrate around the embryo to give rise to dorsal, ventral, lateral, and limb muscles during fetal myogenesis (Ordahl and Le Douarin, 1992; Hutcheson et al., 2009). After the progenitor cells have populated their niche with muscles through successive rounds of proliferation, differentiation and fusion during fetal myogenesis, they enter quiescence and become satellite cells - the stem cells of adult muscles (Gros et al., 2005; Schienda et al., 2006).

All these behaviours required for the development of muscles rely on the interactions between a few central families of TFs. The Pax family of TFs signify muscle precursor cells and have been demonstrated to be required for the dermomyotome delamination process and progenitor cell proliferation for the

formation of the primary myotome (Tremblay et al., 1998; Relaix et al., 2005). Expression of the Myogenic Regulatory Factor (MRF) TFs MyoD, Myf5, Mrf4 and Myogenin signifies lineage committed cells in the myotome (Sassoon et al., 1989; Olson and Klein, 1994; Kassar-Duchossoy et al., 2004). The Six TFs are active from embryonic to late stages of embryogenesis (Laclef et al., 2003b), and have been demonstrated to cooperate with the Pax and MRFs in order to form muscle during development. Expression patterns of these important TFs with temporal and commitment phases labeled can be found in figure Figure 1B.

Six TFs are involved in most embryonic myogenesis program steps, including progenitor development in the dermomyotome, the migration of muscle progenitors in the developing embryo, and the eventual proliferation and differentiation of myoblasts (Grifone et al., 2005; Laclef et al., 2003a; Wu et al., 2014). These diverse functions are achieved through regulation of thousands of targets, from connective tissue growth factors (Tian et al., 2015), to even the master MRFs (Le Grand et al., 2012; Liu et al., 2013). Of the six family members, roles for both Six1 and Six4 are the most well understood in the context of skeletal muscle.

Six1 knockout mice die at birth due to respiratory failure caused by improperly formed diaphragms, and exhibit delayed MRF expression (Laclef et al., 2003a). Six4 knockout mice do not demonstrate with an overtly obvious phenotype at birth (Ozaki et al., 2001), suggesting a compensatory role by other Six TFs in the absence of Six4. Mice with a double knockout of both Six1 and Six4 display an exacerbated phenotype of the single knockout mice, however, with complete absence of limb muscle formation and lack of MRF expression (Grifone et al., 2005). The Pax/Six/Eya/Dach axis has been demonstrated to be expressed in embryonic somites and to promote the expression of the MRFs such as MyoD and Myogenin (Heanue et al., 1999).

1.3.2 Adult myogenesis and the Six TFs

The regenerative ability of adult skeletal muscle has been noted since experiments demonstrated the ability of reintroduced crushed explanted muscles to regenerate *in situ* (Studitsky, 1965). While this regenerative potential is mediated by many types of cells including bone-marrow progenitors, pericytes, and PW1-positive cells (Ferrari et al., 1998; Dellavalle et al., 2007; Mitchell et al., 2010), satellite cells are the only population of cells without which muscles become incapable of regeneration (Sambasivan et al., 2011; Lepper et al., 2011; Murphy et al., 2011). Satellite cells are descendants from the central and hypaxial dermomyotome during development (Gros et al., 2005; Schienda et al., 2006), and retain their stemness due to the expression of Pax7 (Seale et al., 2000; Ito et al., 2017) and absence of expression of MyoD (Zammit et al., 2006). In adult tissues satellite cells can be found resting on the sarcolemma of adult myofibers, under the basal lamina (Mauro, 1961). Upon injury or exercise, satellite cells are activated, typified by expression of Myf5, MyoD and Ki67, and undergo multiple cycles of symmetric division, in which both resulting daughter cells retain stemness, and asymmetric division, in which one of the daughter cells commits to differentiate, typified by expression of late differentiation MRF Myogenin, or can return to quiescence depending on the severity of the injury (Tomczak et al., 2004; Kuang et al., 2007).

In adult muscle Six/Eya/Dach are involved in the transcription of Myogenin (Li et al., 2003). Genome analysis reveals that MRF binding sites tend to occur near MEF3 sequences, usually bound by Six TFs (Blais et al., 2005; Cao et al., 2006). Indeed, the interaction between the MRFs and the Six TFs have been demonstrated to regulate both the transcriptional expression of the MRFs and the transcriptional expression of MRF targets regulating myoblast fusion and differentiation (Bryson-Richardson and Currie, 2008; Liu et al., 2010; Liu et al., 2013; Buckingham and Rigby, 2014; Chakroun et al., 2015).

1.3.3 Fiber-type specification and the Six TFs

In adult muscle, fiber-type expression can be modulated depending on various physiological stimuli. The earliest suggestion of fiber-type plasticity was the discovery that renervation of skeletal muscles by opposing fiber-type nerves was able to induce a switch in fiber-type behavior (Buller et al., 1960). Continued work suggested that electrical stimulation could affect the contractile potential of skeletal muscles (Salmons and Vrbova, 1969), and that exercise, a normal physiological process, could recapitulate these experimental findings (Gollnick et al., 1972; Jansson et al., 1978). Two major genetic pathways act downstream of these physiological experiments. The Calcineurin/NFAT pathway promotes the formation of Myosin type I slow-twitch muscle and is required for fiber-type switching under electrical stimulation conditions (Chin et al., 1998). Similarly, the second major genetic regulatory pathway is the AMPK axis, which also promotes plasticity towards a slow-twitch Myosin type I expressing fiber phenotype, with mutants ablating the potential for exercise-induced fiber-type plasticity (Röckl et al., 2007). During development, distinct fiber-type mosaicism can develop in the complete absence of innervation (Condon et al., 1990) suggesting inherent differences within muscle precursor cells to form differentiated fiber-types. Differential expression of various TFs may explain some of these inherent differences.

The first implication of the Six TFs role in fiber-type specification was the discovery that forced expression of Six1 and Eya1 was capable of reprogramming slow-twitch muscle into fast-twitch gene program, promoting the expression of fast Myosin isoforms and shifting muscle energy dependence towards glyoclytic pathways (Grifone et al., 2004). It has since been demonstrated that the Six TFs are critical for the expression of the fast-twitch gene program in developing muscle, with newborn mice failing to form fast-twitch muscle entirely (Niro et al., 2010; Laclef et al., 2003a). Moreover, the Six TFs were determined to be critical for the maintenance of the fast-twitch

gene program, as conditional knockout mice caused adult muscles to convert into the slow-twitch gene program, with muscles exhibiting a switch from expression of fast- to slow-twitch Myosin and Troponin isoforms (Hetzler et al., 2014; Sakakibara et al., 2014). Even though Six1 is expressed to similar levels in both fast and slow-twitch fibers, both Six1 and its principal co-factor Eya1 are preferentially recruited to the nucleus in fast-twitch fibers (Sakakibara et al., 2016).

The main proposed mechanism for Six1 regulation of fiber-type is through direct and positive transcriptional regulation of linc-MYH, a long non-coding RNA (Sakakibara et al., 2014). Linc-MYH knockout recapitulates Six1 knockout condition phenotypes, albeit to about 80% of the magnitude of effect, and is incapable of significantly increasing Myosin type I mRNA expression, suggesting that other pathways that regulate fiber-type specification may also be under Six1 regulatory control. Two such pathways include the NFAT TFs that promote slow-twitch muscle, and the Thyroid hormone pathway, that promotes fast-twitch muscle. One goal of the research presented herein is to elucidate additional regulatory effects the Six1 exhibit over fiber-type specification through these pathways, and the next two sections will explain why these pathways were chosen.

1.4 The NFAT TFs

NFAT factors were first discovered in T Cells, where they promote the expression of cell surface markers and the induction of cytokines (Shaw et al., 1988; McCaffrey et al., 1993). There are five members in the NFAT family, with at least one member expressed in any given tissue type (Macian, 2005), with roles ranging from cardiac development to central nervous system development (Ranger et al., 1998; Graef et al., 2003). NFAT family members serve to transduce calcium signaling into an activated gene program, by acting

downstream of the calcium- and calmodulin-dependent Calcineurin. Phosphorylation of NFAT TFs by Calcineurin allows their translocation into the nucleus (Chow and Davis, 2000), supported by cooperative and synergistic action with the AP-1 axis in T Cells (Chen et al., 1998).

1.4.1 The NFAT TFs and skeletal muscles

The importance of NFAT TFs in skeletal muscles was discovered with the demonstration that electrical stimulation of cultured myotubes induces a fast-to-slow fiber-type switch that is Calcineurin-dependent (Meißner et al., 2001). Further research discovered that expression of a constitutively active NFATc1 was shown to be sufficient to reprogram muscle cells towards the slow-twitch gene program (McCullagh et al., 2004), and that NFAT isoforms are differentially active depending on the fiber-type, with NFATc1 being preferntially located in the nucleus in slow-twitch muscle (Calabria et al., 2009). Over time, research elucidated the breadth of biochemical pathways that induce fiber-type reprogramming through NFAT-dependent activity (Yuan et al., 2011; Wang et al., 2014). Crucially, NFAT signaling activity has been implicated in the regulation of Utrophin gene transcription, both at the synaptic junction and along the extra-synaptic length of myofibers (Chakkalakal et al., 2003).

In skeletal muscles, two main regulatory pathways exist to regulate the activity of the NFAT TFs. The first, is the Regulator of Calcineurin (RCAN) family of inhibitors (Davies et al., 2007) which directly bind to and inhibit Calcineurin protein. The second, is the Calsarcin family of protein inhibitors. The Calsarcins tether Calcineurin to the Z-disc of skeletal muscle fibers (Frey et al., 2000). Myoz1, or Calsarcin-2, knockout mice exhibit a switch towards a slow oxidative fiber-type and an increase in NFAT activity (Frey et al., 2008), and overexpression of NFAT family members does not deplete their localization to the Z-disc mediated through Calsarcin repression (Liu et al., 2001), suggesting a high potency and specificity for the interaction.

1.4.2 The NFAT TFs and the Six TFs

The NFAT TFs and Six1 TFs share multiple regulatory nodes. In developing embryos, NFATc3 cooperates with MyoD to regulate Myogenin transcription, with absence of either alone being insufficient to ablate Myogenin expression (Armand et al., 2008). In the embryo, MyoD expression itself is under Six1 regulatory control (Grifone et al., 2005; Heanue et al., 1999) and a MEF3 binding sequence is required for the induction Myogenin expression (Spitz et al., 1998), suggesting differential temporal regulation by the two families of TFs for embryonic Myogenin expression. In adult muscle, NFATc1 inhibits MyoD activity at fast-twitch gene promoters by inhibiting its interaction with the activator p300 (Ehlers et al., 2014). In slow-twitch muscle, MyoD and the Mef2 TFs, a family under NFAT regulation (Wu et al., 2001), cooperate to promote the expression of Glut4, the main glucose transporter in skeletal muscle (Santaluc1 a et al., 2001), suggesting that MyoD can exhibit fiber-type specific activity. Indeed, it has been demonstrated that MyoD activity can be modulated to promote either fiber-type phenotype, depending either on association with Pbx and Six TFs to promote fast-twitch muscle (Maves et al., 2007), or through association with SIRT1 to promote slow-twitch muscle (Amat et al., 2009). This is additionally supported by data that demonstrated activity of MyoD and Mef2 reporters is ablated in fast-twitch muscle, while MyoD and MEF3 reporters remain active (Spitz et al., 1997). Combined, the data suggests a reciprocally antagonistic relationship between regulatory programs of the NFAT TFs and the Six TFs, and raises the question of whether NFAT activity is increased in Six1 knockout conditions.

1.5 Thyroid hormone

Triiodothyronine hormone (T_3), the most active form of thyroid hormone, is critical for development, differentiation, growth, and metabolic homeostasis of

various tissues, including the brain, muscles, liver, and pancreas (Zhang and Lazar, 2000). Thyroid hormone activity is regulated through expression of various receptors, transporters, and deiodinases (Boelen et al., 2017). Thyroid receptors are TFs that utilize T_3 as a ligand to bind Thyroid Response Element (TRE)s and modulate the transcription of nearby genes (Feng et al., 2000). Intracellularly, the dioidinase Dio2 converts T_4, a form of thyroid hormone with low thyroid receptor binding affinity, into the highly active T_3, and the diodinase Dio3 subsequently converts active T_3 into the least active form, T_2 (Bianco et al., 2002). Finally, thyroid transporters are membrane-bound proteins that allow for the import of thyroid hormones intracellularly and can be regulated based on cell type and transcriptional need for thyroid responsiveness (Mebis et al., 2009).

1.5.1 Thyroid Hormone and skeletal muscles

Thyroid hormone regulates the contractile structure, and myogenesis within skeletal muscle (Simonides and van Hardeveld, 2008; Dentice et al., 2010). T_3 has been demonstrated to regulate the expression of multiple MRFs, with functional thyroid-responsive elements driving mRNA transcription of MyoD (Carnac et al., 1992) and Myogenin (Downes et al., 1993).

In the context of myogenesis T_3 is temporally required in limited amounts, as thyroid pathway activity represses proliferation and induces pro-apoptic axes (Dentice et al., 2014). Hyperthyroidism has been shown to push satellite cells towards expressing higher amounts of MyoD (Anderson et al., 1998). Conversely, hypothyroidism impedes myogenic differentiation (Jacobs et al., 1996). In adult tissues, thyroid hormone activity is capable of suppressing the expression of slow-twitch genes and increasing the expression of fast-twitch genes through a TEAD-1 mediated regulatory pathway (Zhang et al., 2014). In dystrophic muscle, reducing thyroid hormone activity resulted in lower amounts of muscle necrosis in a steady state diseased

muscle (McArdle et al., 1998), however, in response to injury, dystrophic muscle was less capable of repair with impaired thyroid signaling (McIntosh et al., 1994). This could be explained by the finding that under both hypothyroid and hyperthyroid conditions, Dystrophin protein expression is reduced (Zybek-Kocik et al., 2017). In the context of fiber-type specification, hyperthyroidism has been shown to cause a shift towards fast-twitch phenotype, with hypothyroidism promoting the opposite (Muscat et al., 1995; Pette and Staron, 1997).

1.5.2 Thyroid hormone and the Six TFs

In skeletal muscles, T_3 interacts with MyoD to upregulate Glut4, the primary gluocse transporter in skeletal muscles (Santaluc1 a et al., 2001), raising the possibility that coordination between thyroid hormone and the Six TFs could be critical to the proper homeostatic maintenance of skeletal muscle.

Skeletal muscles are not the only tissues that display and interplay between both Six1 and thyroid hormone, with both being required for kidney development (Weil, 1941; Xu et al., 2003). The involvement of impaired thyroid signaling in 70% of hepatocellular carcinomas (Lin et al., 1999), with some cases of the carcinomas demonstrating a significant reduction of Six1 in adult tissues (Ventura-Holman et al., 2011), suggests that an understanding of the interplay between Six1 and the thyroid signaling pathway in additional tissues can help demonstrate parallels during both regular development and diseased states that rely on both. It should be noted that mice knockout models for Eya1 demonstrated a maldeveloped thymus and parathyroid gland, presenting with thyroid hypoplasia and marked reduction in Six1 expression (Xu et al., 2002). This could signify that the Six/Eya regulatory pathway could have importance within the context of thyroid development, signaling and downstream function.

1.6 Hypothesis & Aims

Utrophin overexpression can functionally compensate for the lack of Dystrophin in Dystrophic muscle (Tinsley et al., 1996), methods to promote the overexpression of Utrophin are of clinical importance. Slow-twitch muscles express inherently elevated Utrophin protein levels, and are more resistant to the Dystrophic disease phenotype (Chakkalakal et al., 2003; Webster et al., 1988). Given, that the Six TFs promote the fast-twitch gene program (Grifone et al., 2004), I hypothesized that "antagonism of Six TFs expression in adult fast-twitch Tibialis Anterior (TA) muscle could lead to acquisition of a slow-twitch muscle phenotype, and increased levels of Utrophin expression." Figure 2 presents the graphical hypothesis for this research.

To best address the the experimental hypothesis, following are the actionable aims I set out to accomplish in this study.

Aim 1: To establish a reliable *in vivo* knockdown of Six1, Six4, or both and to confirm and study the fiber-type switch expected. This was performed through electroporating mice with interfering RNA targeting Six1 or Six4 in the TA muscle and measuring the protein and RNA levels of the Six TFs. Once a method for consistent and successful *in vivo* knockdown was confirmed, an analysis of fiber-type switch induced was carried out using Myosin isoform immunofluorescence and Quantitative Reverse-Transcription PCR (qRT-PCR).

Aim 2: To characterize the effect of the fiber-type switch expected with the loss of Six1 and Six4 on Utrophin expression. Using qRT-PCR, western blotting and immunofluorescent staining methodology, I studied changes in Utrophin expression and localization in the TA muscle in the absence of Six1 and/or Six4.

Aim 3: To characterize additional molecular pathways through which Six1, Six4 or both may contribute to fiber type specification. Confirmation of a regulation target in the thyroid response pathway (a thyroid transporter) by Six TFs and the consequential effects on the pathway's target genes was studied through qRT-PCR methodology.

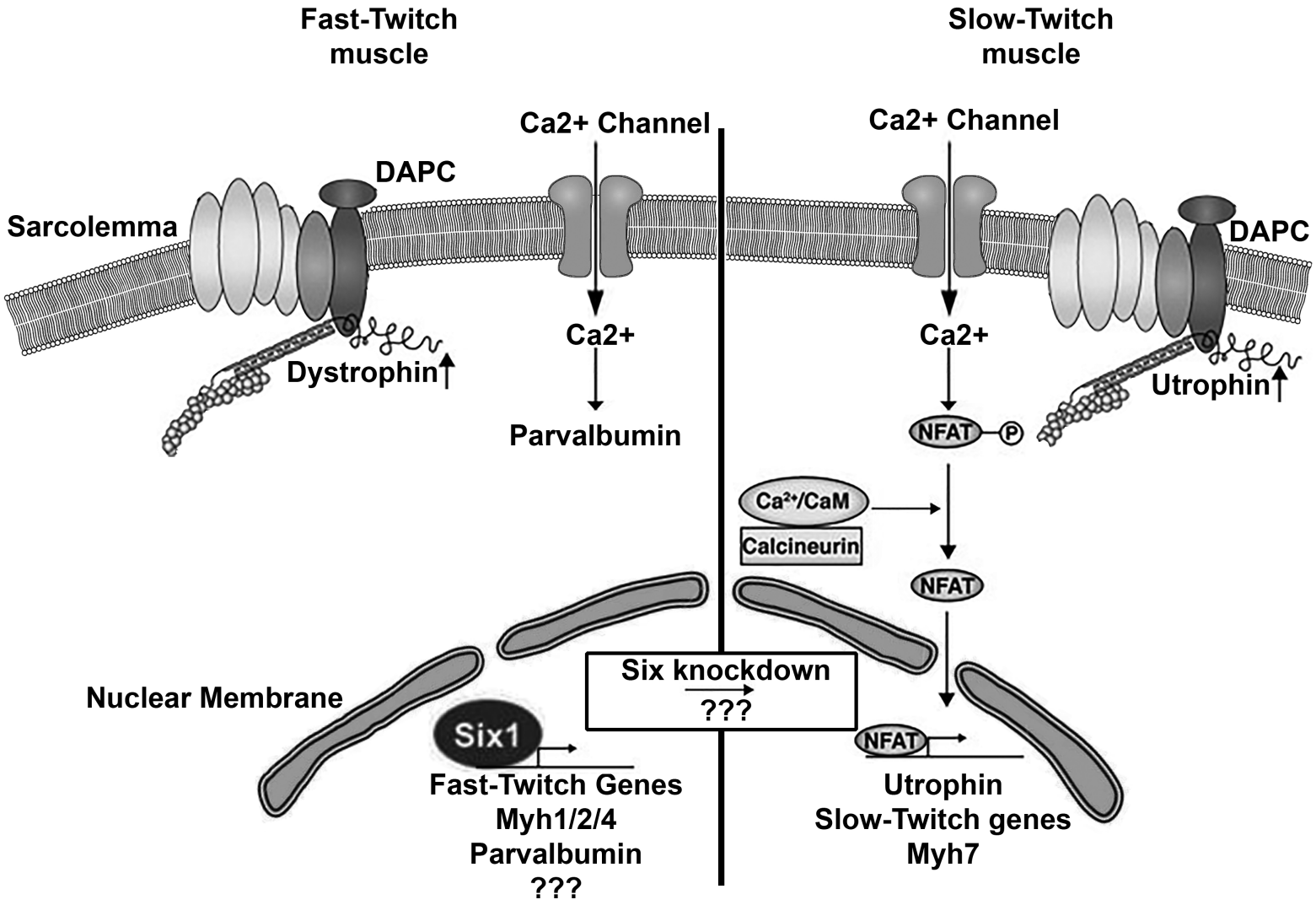

Figure 2: **Schematic of hypothesis**
Relevant regulatory networks active in different skeletal muscle fiber-types. Image adapted from (Frey et al., 2008; Batters et al., 2014).

Chapter 2

Materials and Methods

2.1 Tissue Culture Techniques

2.1.1 Cell Growth and Maintenance

The C2C12 (Yaffe and Saxel, 1977) Murine myoblast cell line, purchased from the American Type Culture Collection (ATCC), was grown in Growth Medium (GM) (88% DMEM, 10% Fetal Bovine Serum, 1% P/S, 1% L-Glutamine) to confluence. When confluent, cells were induced to differentiate by washing off excess GM twice with Phosphate-Buffered Saline (PBS), then were placed in Differentiation Medium (DM) (96% DMEM, 2% Horse Serum, 1% P/S, 1% L-Glutamine). All cells were grown in a humidified water-jacketed incubator at 37°C and 5% CO_2.

2.1.2 Lipofectamine siRNA Transfections

Transfections were carried out using Stealth siRNA technology (Invitrogen) and Lipofectamine RNAiMAX (Invitrogen). siRNA duplexes were suspended and diluted to a final concentration of 20μM in accordance with manufacturer recommendations. siRNA sequences are available in Table 3. In some cases, C2C12 cells were grown to confluence, induced to differentiate, and transfected

with siRNA 48 hours after differentiation was induced. For a 6-well plate, 3μL of siRNA was mixed with 100μL of OptiMEM (Invitrogen). Separately, 5μL of Lipofectamine RNAiMAX was mixed with 100μL of OptiMEM. Both the siRNA and Lipofectamine RNAiMAX mixes, 103μL and 105μL respectively, were combined and incubated at room temperature for five minutes. 208μL of the resultant mixture was added drop-wise to adherent cells in 2mL GM. Concentrations of reagents were determined experimentally (Figure 30).

2.1.3 Lipofectamine 3000 Plasmid Transfections

For a 6-well plate, 10μL of Lipofectamine P3000 Reagent (Invitrogen) was mixed with 100μL of OptiMEM and added to a tube containing 5μg of plasmid DNA. Separately, 10μL of Lipofectamine Lipo3000 reagent was mixed with 125μL of OptiMEM. The Lipo3000 mix was then added to the DNA mix and the resultant transfection mixture was incubated for 5 minutes at room temperature. After the incubation, the transfection mixture added drop-wise to adherent cells in 2mL GM. Concentrations of reagents were determined experimentally (Figure 30).

2.2 Animal Model Techniques

2.2.1 Animal Care

Surgical procedures were performed in compliance with the University of Ottawa Animal Care and Use Committee, the Guidelines of the Canadian Council on Animal Care, and the Animals for Research Act. 6-8 week old female C57BL/6 mice were purchased from Charles River. Mice were sacrificed using cervical dislocation.

2.2.2 Nucleic Acid Electroporation

All work was performed in the TA muscle on 6-8 week old female C57BL/6 mice. For knockdown experiments, on Day 0 of the experiment, the inter-connective tissue of the TA was digested with an intramuscular injection of 25μL Hyaluronidase (Worthington) at 0.4unit/μL concentration through the skin of the hindlimb just above the ankle tendon, in order to ensure genetic material can surround and successfully transfect a majority of muscle fibers once injected (McMahon et al., 2001). One hour later, an intramuscular injection of 22.5μL siRNA at 20μM, for Tweezertrodes experiments, or 30μL shRNA at 833ng/μL, for Needle Array experiments, was administered through the skin of the hindlimb into the belly of the TA. For Needle Array electroporations, 2-Needle 20mm long electrode assemblies were used with 5mm gap between the electrodes (Harvard Apparatus 45-0168). Electrodes were used to pierce through the skin, parallel to the tibia and surrounding the belly of the TA, with one electrode piercing through the skin 2mm inferior to the knee, and the other electrode piercing through 3mm superior to the ankle. Electrical stimulation was carried out using a BTX ECM 630 Electroporation system programmed at a setting of 80 Volts, 5 Pulses, 50ms/pulse, and 500ms interval between pulses. For Tweezertrodes electroporations, 2-paddle electrode assemblies were used with 7mm gap between the electrodes (BTX-Harvard Apparatus 45-0165). After nucleic acid material injection, ultrasound gel was applied to the skin, and two electroporation rounds were applied superficially, with the paddles in the first electroporation oriented transverse and sagittal to the hindlimb, and the second electroporation oriented transverse and contrasagittal to the hindlimb. Electrical stimulation was carried out using a BTX ECM 630 Electroporation system programmed at a setting of 50 Volts, 6 Pulses, 50ms/pulse, and 200ms interval between pulses. Six1-targeted siRNA knockdowns for *in vivo* electroporations used the SIX-A siRNA described in Table 3. In the case of double knockdown experiments, 11.25μL of each siRNA at 20μM concentration

was administered. In the case of multiple-day Tweezertrodes electroporations, the process is repeated on Day 3 of the experiment. All mice were sacrificed on Day 7 of the experiment. For some experiments, an additional 7.5μL of a Luciferase reporter containing plasmid and Renilla Luciferase normalizer plasmid mix, constituted in a half-saline solution, was included during the Day 0 siRNA injection (total injection volume 30μL), at a concentration of 3μg/μL and 1.5 ng/μL, respectively.

2.2.3 Muscle Section Processing

Treated TA muscles were extracted and fixed in cold 2% Paraformaldehyde (PFA) for 30 minutes at 4°C. Muscles were rinsed twice with PBS for 5 minutes at 4°C before being quenched twice with 0.25M Glycine in PBS at 4°C. Muscles were rinsed once in 20% sucrose in PBS for 6 hours at 4°C, then left incubating overnight in 5% sucrose in PBS at 4°C to completely dehydrate muscle. Muscles were frozen in Optimal Cutting Temperature Compound (OCT) dipped in isopentane chilled by liquid Nitrogen. Unfixed tissues were frozen immediately upon extraction. Sectioning was performed on a Microm HM500 Cryostat. Muscles were trimmed at 20μm cuts for 100 cuts starting at the knee tendon to reach the belly of the TA. Sections for the immunofluorescence were cut at 10μm thickness. To avoid sections floating away, positively charged glass slides were used to pick up the sections, and all sections on a single slide were thawed in batch before being stored at -80°C. Before use, slides were thawed for 5 minutes at 37°C.

2.2.4 Immunofluorescent Staining

For all immunostaining, electroporated muscle sections were washed twice with PBS. Dako pens (Agilent) were used to draw hydrophobic barries around individual sections on a slide in the case of using multiple antibodies on

subsequent sections. Slides were blocked for 1 hour at room temperature in IgG Mouse Blocking Reagent diluted 1:18 in PBS (Vector Labs). Protein Concentrate was diluted 1:62.5 in PBS. After blocking, sections were rinsed twice with PBS and were then incubated in protein concentrate dilution for 5 minutes at room temperature. Primary antibodies were then added for 30 minutes at room temperature at concentrations according to manufacturer specifications. The sections were washed 4 times with PBS for 5 minutes at room temperature, and then Biotin diluted 1:250 in protein concentrate dilution was added for 10 minutes at room temperature. Sections were washed again 4 times with PBS for 5 minutes at room temperature, before Streptavidin-conjugated secondary antibodies diluted 1:62.5 in PBS were added for 15 minutes. Slides were mounted with Prolong Gold Antifade with DAPI (Thermo Fisher Scientific). For concurrent stainings including antibodies not derived from mice, multiple antibodies were included during the primary antibody addition and during the final addition of the Streptavidin-conjugated secondaries. For concurrent stainings including more than one mouse-derived antibodies, biotin blocking reagents were used after the Streptavidin-conjugated antibody removal, and the process was repeated starting with the first PBS rinse.

2.2.5 Luciferase

Muscles had 15μg of a luciferase reporter plasmid and 100 ng of a renilla normalizer plasmid delivered in the same injection simultaneously with the siRNA delivery during the electroporation procedure. Muscles were pulverized using liquid nitrogen chilled mortar and pestle (Plattner's) and resuspended in passive lysis buffer (Promega). Luciferase results were obtained by reading 5μL of sample with 50μL Luciferase assay reagents in a Glomax Luminometer according to manufacturer specifications.

2.3 General Techniques

2.3.1 RNA Extraction

All samples were extracted in 1mL of TRIzol Reagent (Invitrogen). Dissected TA samples were placed in TRIzol in Lysing Matrix D Tubes (MP Biomedical) and were homogenized in a MagNa Lyser machine (Roche) programmed to 7,000 Rotations Per Minute (RPM) for a total of three 20-second bursts separated by 10-second cooldowns on ice. The samples were then spun-down for 5 minutes at 12,000g at 4°C to remove fat content. Samples from Tissue Culture were rinsed twice with PBS before TRIzol reagent was added directly into the wells. For all types of samples, the supernatant was then transfered to a new tube. 200μL of Chloroform was added and the resultant mixture was vortexed for 15 seconds until contents were viscous. The samples were then allowed to stand at room temperature for three minutes before being spun down for 15 minutes at 12,000g at 4°C to separate the macromolecular phases. The top aqueous phase, containing the RNA, was transfered to a new tube. The interphase and organic phases containing the DNA and proteins, respectively, were set aside for downstream applications. The RNA was precipitated by adding 500μL of Isopropanol to the isolated aqueous phase. The mixture was vortexed for 10 seconds, allowed to stand at room temperature for 10 minutes and spun-down for 10 minutes at 12,000g at 4°C. RNA pellets were washed twice with 75% Ethanol and centrifuged for 5 minutes at 7,500g at 4°C after each wash. The final pellet was suspended in 25μL Diethyl Pyrocarbonate (DEPC)-treated water. Concentration and quality of the RNA were determined using a Nano-Drop ND-1000 Spectrophotometer (NanoDrop). Quality of RNA was determined on a non-denaturing 1% agarose gel.

2.3.2 Reverse-Transcription PCR

Reverse-transcription Polymerase Chain Reaction (PCR) was performed using 500 ng of DNAse treated RNA with the SuperScript III First-Strand Synthesis System (Thermo Fisher). RNA suspended in a volume of 5μL was mixed with 1μL of 10mM Deoxynucleotide Triphosphate (dNTP), 1μL random hexamers, and 3μL DEPC-treated water. Samples were incubated for five minutes at 65°C then cooled on ice for 3 minutes. Separately, an enzyme mix was prepared as follows: 2μL of 10X Reaction Buffer, 4μL of $MgCl_2$, 2μL of 0.1M Dithiothreitol (DTT), 1μL of RNAse OUT (40 Units/μL), and 1μL of SuperScript III Reverse Transcriptase (200 Units/μL). 10μL of the buffer mix was added to the RNA samples and the mixture was incubated sequentially for 10 minutes at 25°C, 50 minutes at 50°C, and 5 minutes at 85°C. 1μL of RNAse H was added and the samples were incubated for 20 minutes at 37°C. Samples were diluted with 30μL of 10mM Tris pH 8.0 and stored at -20°C.

2.3.3 ChIP

For *in vivo* Chromatin Immunoprecipitation (ChIP) samples, all hindlimb muscles from two mices were extracted per replicate, and homogenized using a benchtop drill in hypotonic buffer (25mM pH 7.8 HEPES, 1.5mM MgCl2, 10mM KCl, 0.1% NP-40 and protease inhibitors) on ice. For *in vitro* samples, cells were grown to confluence in 5 large tissue culture dishes per replicate. To both 1% Formaldehyde was added from an 11X solution (11% Formaldehyde, 0.1M NaCl, 1.0mM EDTA, 0.5M EGTA, 50mM pH 8.0 Hepes) for 10 minutes and 30 minutes, respectively, at room temperature. Quenching was achieved using 0.125M Glycine for 5 minutes at room temperature. *In vivo* samples were spun down at 1,000 g for 5 minutes at 4°C, resuspended in fresh hypotonic buffer, filtered through 70μm cell strainer, spun down again at 1,000 g for 5 minutes at 4°C and resuspended in 650μL sonication buffer (10mM EDTA, 50mM pH8

Tris-HCl 0.1% Sodium Dodecyl Sulfate (SDS) and protease inhibitors). *In vitro* samples were washed with PBS, scraped, had a cell lysis buffer added (50mM 1M pH 7.4 Hepes-KOH, 140mM 5M NaCl, 1mM 0.5M EDTA, 10% Glycerol, 0.75% 10% NP-40 and protease inhibitors) and were Dounce-homogenized for thirty cycles on ice. The nuclear pellet was collected by centrifugation and lysed in nuclear lysis buffer (200mM 5M NaCl, 1mM 0.5M pH 8 EDTA, 0.5mM 0.5M pH 8 EGTA, 10mM 1M pH 8 Tris and protease inhibitors). The DNA pellet was collected by centrifugation and resuspended in 650μL sonication buffer (1mM 0.5M pH 8 EDTA, 0.5mM 0.5M pH 8 EGTA, 10mM 1M pH 8 Tris, 0.5% Sodium sarkosyl and protease inhibitors). All sonication was done using a probe sonicator at an amplitude of 40% power, with 60 cycles of 1 second on to shear DNA and 4 seconds off to cool down. Appropriate chromatin fragmentation was confirmed on a 2% agarose gel. 25μg of chromatin in immunoprecipitation mix (1% NP-40, 0.1% Na-DOC, protease inhibitors and sonication buffer) was pre-cleared with blocked Protein A beads, before having 2μg of antibody added to it for an overnight incubation at 4°C. The next day, pre-blocked beads were added to bind the antibody for 2 hours. The beads were washed 7 times in Radioimmunoprecipitation assay buffer (RIPA) wash buffer, before being subjected to elution buffer (50mM Tris, 10mM EDTA, 1% SDS) and overnight reverse cross-linking at 65°C. Resulting DNA was extracted using a phenol/chloroform/isoamyl alcohol extraction and final pellet was resuspended in water for downstream Quantitative PCR (qPCR).

2.3.4 qPCR and qChIP

qPCR was carried out on the CFX96 platform and CFX Manager software (Bio-Rad). 10μL reaction mixtures were prepared as follows: 1μL of Qiagen HotStarTaq Buffer (Qiagen), 1μL of 1.5% Triton X-100 (Fisher), 0.2μL of 10mM dNTP (Promega), 0.05μL of SYBR Green diluted 1:500 in DMSO (Invitrogen), 0.04μL of HotStarTaq (Qiagen, 5 Units/μL) 4.71μL of water (5.71μL for

Quantitative ChIP (qChIP)), 1μL of 5μM primer pair (Operon), 2μL of cDNA (1μL for qChIP) diluted 1:10 in 10mM Tris pH 8.0. Thermocycler settings included 15 minutes at 94°C to active the HotStarTaq enzyme, followed by 40 cycles of 15 seconds denaturation at 95°C, 30 seconds primer annealing at 60°C and 30 seconds elongation at 72°C, followed by a melting curve. Standard curves for qPCR were prepared as 6 points of 1:5 dilutions and as 4 points of 1:6 dilutions for qChIP. All samples were run as technical duplicates for *in vitro* experiments and as technical triplicates for *in vivo* experiments. GEOMEAN normalization was used with the genes Rps26, 18S ribosomal subunit, and Beta-Actin, which were assumed as invariable under experimental conditions. Oligonucleotide sequences are provided in Table 3.

2.3.5 Protein Extraction

TRIzol extraction interphase and organic phases had 300μL of 100% Ethanol added and were mixed by inversion five times to avoid shearing of genomic DNA contaminating the protein sample. The samples were incubated at room temperature for three minutes, then centrifuged for five minutes at 12,000g at 4°C. Half of the supernatant was added to 1.5mL 100% Isopropanol and mixed by vortexing, and then the second half of the supernatant was added and the combination was mixed by vortexing again. This ensured that high protein concentration samples did not coagulate during the precipitation step. The mixture was incubated at room temperature for 20 minutes, then centrifuged for five minutes at 12,000g at 4°C. Protein pellets were washed thrice with 10mL Guanidine-Ethanol mix (28.5g Guanidine-HCl in 1L 95% Ethanol) and then washed twice in 10mL 100% Ethanol. Protein was pelleted by centrifugation for five minutes at 7,500g at 4°C. Protein pellets had the equivalent of 1μL Urea-SDS Sample Buffer (6M Urea, 1%SDS, 20mM Tris pH 6.8) per 1,000 cells for (in vitro) samples, or 3μL Urea-SDS Sample Buffer per 1mg of tissue for *in vivo* samples added, and were allowed to solubilize overnight at 4°C.

2.3.6 Protein Quantification Assay

Sample protein concentrations were determined using the BCA Protein Assay Kit (Thermo Scientific). The provided Bovine Serum Albumin (BSA) was used to create a standard curve with concentrations of 2,000 ng/μL, 1,000 ng/μL, 500 ng/μL, 250 ng/μL and 0 ng/μL diluted in water. For assay reactions of the standard curve, 2μL of relevant sample buffer was mixed with 8μL of the standard BSA dilution. For assay reactions of unknown samples, 2μL of the sample was mixed with 8μL of water. This ensured that background readings due to sample buffer were consistent across all samples. All samples were run as technical triplicates. BCA Reagent A and BCA Reagent B were mixed in a 50:1 ratio and 200μL of the resultant mixture were added to every assay reaction. The reactions were incubated for 30 minutes at 37°C. Quantification was performed using spectrophotometer readings at a wavelength of 562nm.

2.3.7 Western Blotting

60-100μg of proteins were loaded on a 10% SDS-Page gel (Stacking: 3.15mL water, 2.5mL 0.5M Tris pH 6.8, 1mL 40% 37.5:1 Acrylamide/Bis, 100μL 10% Ammonium Persulfate (APS), 100μL 10% SDS and 16μL Tetramethylethylenediamine (TEMED); Resolving: 4.8mL water, 2.5mL 1.5M Tris pH 8.8, 2.5mL 40% 37.5:1 Acrylamide/Bis, 100μL 10% APS, 100μL 10% SDS and 8μL TEMED). Samples were run through the stacking gel at 50V and then through the resolving gel at 100V. Proteins were transferred to a Polyvinylidene Fluoride (PVDF) membrane in transfer buffer (1.6L water, 400mL methanol, 6g Tris, 28.8g Glycine) for 90 minutes at 100V. Blocking was carried out for 1 hour at room temperature in 5% milk, and primary antibodies (listed in Table 4) were incubated with membranes overnight at 4°C. Secondary antibodies conjugated with Horseradish Peroxidase (HRP) were used for exposure with either the Clarity ECL kit Bio-Rad) as per manufacturer instructions for *in vivo*

samples or a home-made development kit for *in vitro* samples. The home-made kit was prepared as follows: In one tube, 5mL 0.1M Tris pH8.5 was combined with 25μL 90mM Coumaric Acid (dissolved in Dimethyl Sulfoxide (DMSO)) and 50μL 250mM 3-Aminophtalyhydraize Free Azide (Luminol) (dissolved in DMSO). In another tube, 3μL Hydrogen Peroxide was mixed with 5mL 0.1M Tris pH8.5. Both tubes were mixed separately, then combined and the resultant revelation solution was incubated with the membranes for 30 seconds at room temperature.

2.3.8 Densitometry

X-Ray films developed from western blots were scanned at a resolution of 600Dots Per Inch (DPI) and gray-scale 16-bit depth colour setting. Images were imported into FIJI Is Just ImageJ (FIJI). The rectangular selection tool was was used to select the first lane, and cloned vertically-aligned selections were overlayed on all subsequent lanes using the 'Select Next Lane' tool. The 'Plot Lanes' tool was used to produce signal histograms. The straight line tool was used to draw a cutoff point at the bottom of each histogram to gate between signal and background noise. The 'Wand Tool' was used next to measure the area contained within each path created in the previous step and the 'Label Peaks' tool was used to extract relative histogram areas, in pixels.

2.3.9 Bioinformatics Analyses

Analysis was carried out to produce Figures 19 and 20 in the programming language R. Code used to produce the heatmaps can be found in Section 4.6. Data used to produce the heatmaps, and referenced in Subsection 4.6, has already been published by other groups previously, and is publicly available (Sakakibara et al., 2014; Sakakibara et al., 2016).

2.3.10 Statistical Analyses

Required number of replicates was determined empirically for sufficient statistical power. No samples were excluded specifically from analysis. Blinding protocols were used only in the case of Figure 9 in order to achieve unbiased count of Utrophin-positive fibers. Unless otherwise specified, Microsoft Excel was used to carry out statistical analyses. Statistical significance for qPCR, densitometry, and Luciferase assays were determined by paired T-tests, always pairing the experimental muscle electroporated with knockdown siRNA, with its contralateral muscle from the same animal electroporated with Short-Interfering Non-Specific RNA (siNS). mRNA and protein expression was always normalized over siNS expression levels from treated muscle within the same mouse, in order to minimize mouse-to-mouse variability, resulting in siNS expression levels of 1, with Standard Error over the Mean (SEM) of 0. Two-tailed paired T-tests were utilized in Figures 4, 6, 7, and 30 due to the absence of prior data suggesting potential results. One-tailed paired T-Tests were used in subsequent experiments relying on discoveries from the aforementioned figures. Statistical significance for ChIP experiments were determined by unpaired one-tailed T-tests. Statistical significance for Luciferase reporter experiments were determined by Wilcoxon Rank-Sum tests. Statistical significance for all unelectroporated muscle experiments were determined using One-Way Analysis of Variance (ANOVA) tests. P-Values ≤ 0.05 were considered to represent means that were significantly different. Unless otherwise stated, no fewer than 3 biological or technical replicates were studied per experiment. Statistically analyzed control sample groups and experimental sample groups always utilized the same number of technical and biological replicates.

Chapter 3

Results

3.1 Optimizing *in vivo* knockdown of Six TFs

In order to determine the optimal methodology to achieve efficient knockdown of TFs expression in adult tissue, two different electroporation technologies, explained in section 2.2.2, were tested within the TA muscle (Figure 3). Electroporations relying on Needle Array technology (Harvard Apparatus), which involves piercing through the skin of the hindlimb with two electrodes, were the most efficient in delivering a Green Fluorescent Protein (GFP) encoding plasmid, transfecting nearly 100% of fibers in the TA muscle (Figure 3B). However, Needle Array electroporations of shRNA were incapable of inducing Six1 knockdown, instead causing an increase in Six1 mRNA expression (Figure 4A) and protein level (Figure 5A). This could be attributed to induction of damage caused by this electroporation method suggested by increased mRNA expression of Embryonic Myosin Heavy Chain (eMHC), a regeneration marker (Figure 4C), as Six1 expression is known to be upregulated in conditions of muscle regeneration (Liu et al., 2010).

In order to investigate a knockdown avenue capable of causing Six1 knockdown, Tweezertrodes technology (Harvard Apparatus) was investigated. Tweezertrodes technology relies on topical paddle-based electroporations, and

is potentially less likely to induce damage due to the lack of an invasive procedure in their operation, when compared to Needle Array technology. A single application of Tweezertrodes technology was capable of reducing Six1 mRNA expression (Figure 4A) and muscle regeneration marker expression was markedly reduced when compared to Needle Array electroporation (Figure 4C), Six1 protein levels were unaffected by the treatment (Figure 5B).

Due to previous research demonstrating that repeated electroporations increase transfection efficiency of nucleic acids (Manthorpe et al., 1993), and due to the possibility that transfection efficiency being a limiting factor in the success of Tweezertrodes technology electroporations, mice were electroporated twice with siRNA. An experimental timeline of all investigated electroporation methodologies is presented in Figure 3A. multiple-day Tweezertrodes electroporations were capable of doubling the electroporation efficiency of single-shot Tweezertrodes electroporations as demonstrated by GFP plasmid expression (Figure 3B) - transfecting about 70% of muscle fibers. Multiple-day Tweezertrodes electroporation was capable of reducing Six1 mRNA expression significantly and with 13% greater magnitude of reduction over a single Tweezertrodes electroporation (Figure 4A), while maintaining low induction levels of eMHC mRNA expression (Figure 4C). Crucially, multiple-day Tweezertrodes electroporations were the first methodology tested capable of reducing Six1 and Six4 protein levels under knockdown conditions (Figure 5C, D). Due to the obtained results, all subsequent experiments were carried out with multiple-day Tweezertrodes electroporated TA muscle.

In order to validate the lack of an immune response due to nucleic acid electroporation, as has been noted as a possible risk in previous literature (Bridge et al., 2003; Sledz et al., 2003), mRNA expression of interferon pathway genes was verified by qRT-PCR methodology. Expression of the panel of genes did not change significantly between unelectroporated, siNS electroporated, or experimental knockdown samples (Figure 4B).

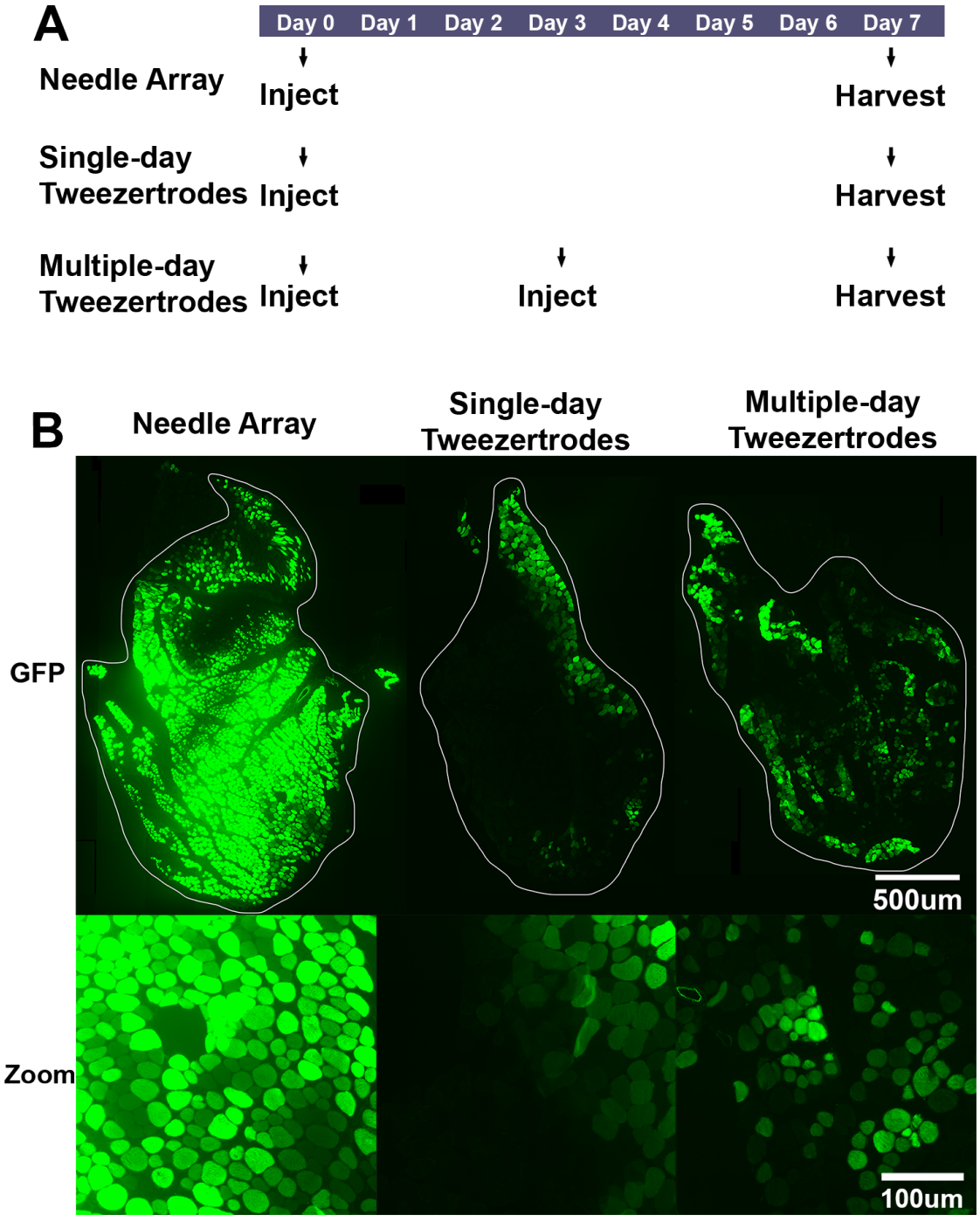

Figure 3: **Optimization of *in vivo* transfection efficiency**
(**A**) Experimental timelines for various electroporation experiments.
(**B**) GFP plasmid electroporation efficiency in mouse TA muscles using different electroporators, seven days post treatment.

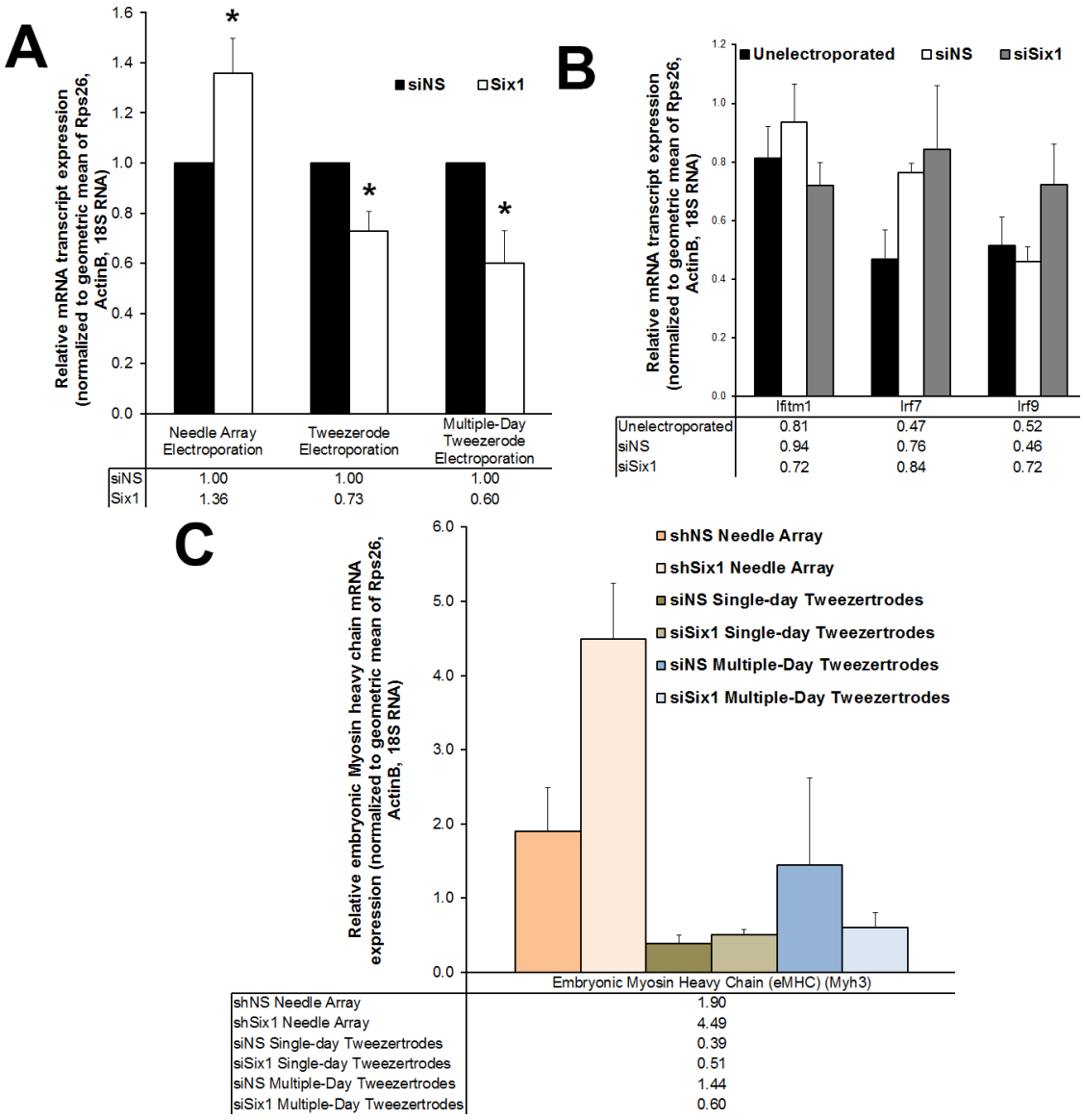

Figure 4: **Optimization of *in vivo* transfection efficacy**
(**A**) Six1, (**B**) interferon pathway regulated genes, and (**C**) eMHC mRNA expression levels in electroporated mouse TA muscle under Six1 knockdown conditions quantified by qRT-PCR. mRNA levels were normalized to the geometric mean of Rps26, 18S and Beta-Actin. Data represents an average of 7 biological replicates. siNS represents a control siRNA targeting a non-specific sequence. Error bars indicate the SEM. * Represents statistically significant changes in levels of expression as determined by an ANOVA statistical test (B), or a two-tailed paired Student's T-Test (A & C) relative to an siNS electroporated TA sample (p-value < 0.05).

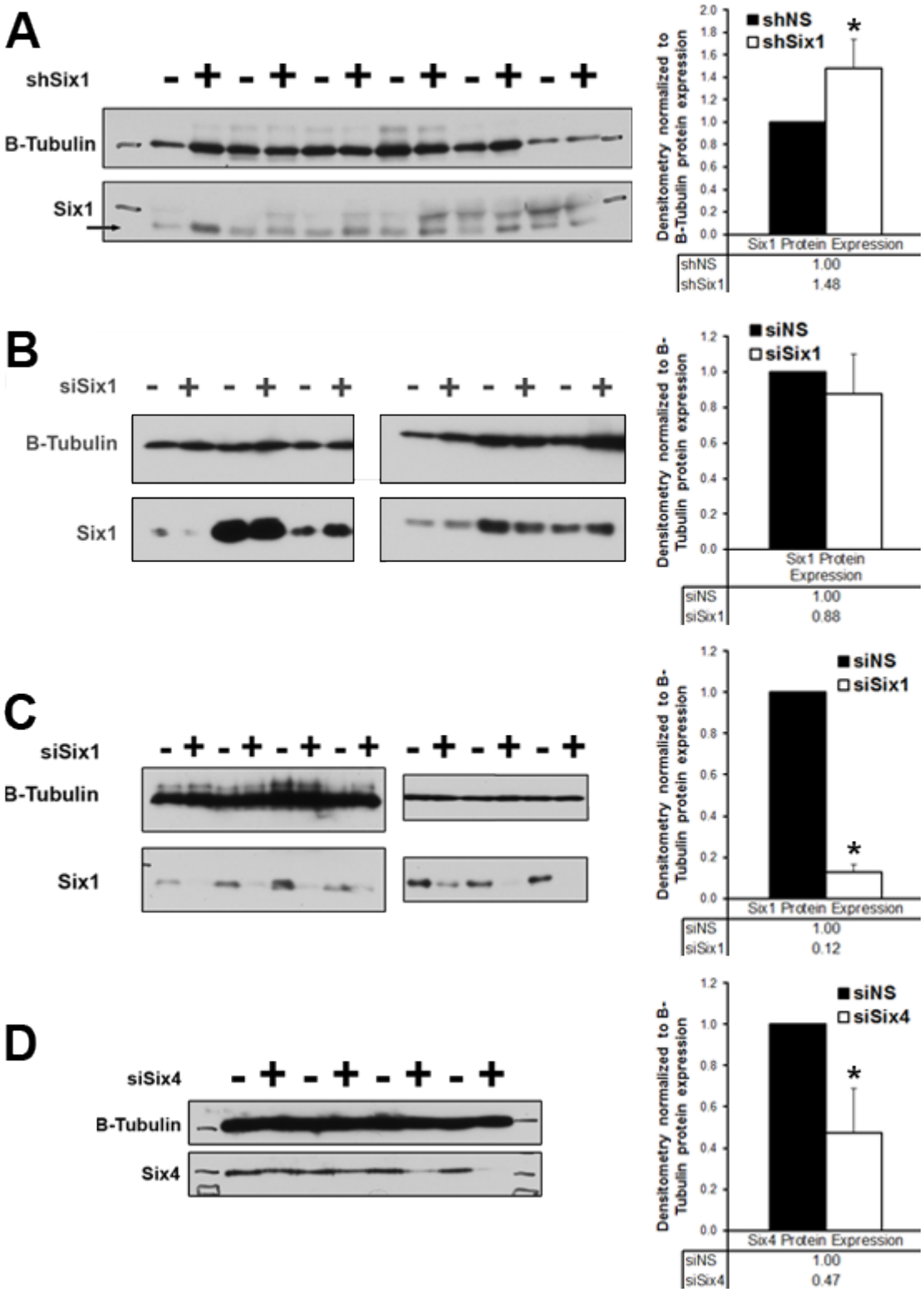

Figure 5: **Six TF protein levels under knockdown conditions**
Western Blots in order to determine Six1 protein expression levels with (**A**) Needle Array electroporation, (**B**) Single-day Tweezertrodes electroporation, (**C**) Multiple-day Tweezertrodes electroporation, and (**D**) Six4 protein expression levels with Multiple-day Tweezertrodes electroporation. siNS represents a control siRNA targeting a non-specific sequence. Error bars indicate the SEM. * Represents statistically significant changes in levels of expression as determined by a one-tailed paired Student's T-Test relative to siNS (p-value < 0.05).

3.2 Effect of *in vivo* Six TFs knockdown on Utrophin expression

To study the effect Six1 knockdown, mRNA expression in samples as detected by qRT-PCR was analyzed. Tweezertrodes multiple-day electroporations that contained siRNA targeting Six1 were uniquely capable of increasing Utrophin expression levels, as detected by Utrophin A-specific primers at the mRNA level (Figure 6A), when compared to either siNS or single-day Tweezertrodes electroporations. This is consistent with the result that only multiple-day Tweezertrodes electroporations were capable of reducing Six1 protein levels (Figure 5), and are therefore capable of effecting changes on the Six1 regulome. Analysis of expression levels in unelectroporated muscles (Figure 6B) revealed that Utrophin mRNA is more highly expressed by a factor of 20% in slow-twitch muscles compared to fast-twitch muscles, indicating that the magnitude of effect observed under post-electroporation conditions could be of biological significance. A similar analysis was carried out with siRNA targeting Six4 mRNA and with a pool of siRNA simultaneously targeting both Six1 and Six4 (Figure 7). While the different siRNA were successful in regulating their targets, and Six4 siRNA was capable of effecting a knockdown on Six4 protein expression (Figure 5D), Utrophin mRNA upregulation was only detected in samples that were electroporated with siRNA targeting Six1, suggesting a unique mechanism under the control of Six1 that can mediate repression of Utophin expression.

Considering the most significant regulatory mechanism determining differential Utrophin mRNA expression is post-transcriptional (Gramolini et al., 2001; Miura et al., 2005), it was important to determine whether the upregulation seen at the mRNA level is accompanied with the same upregulations at the protein level. Western blot analysis confirmed a significant upregulation of Utrophin protein under Six1 knockdown condition,

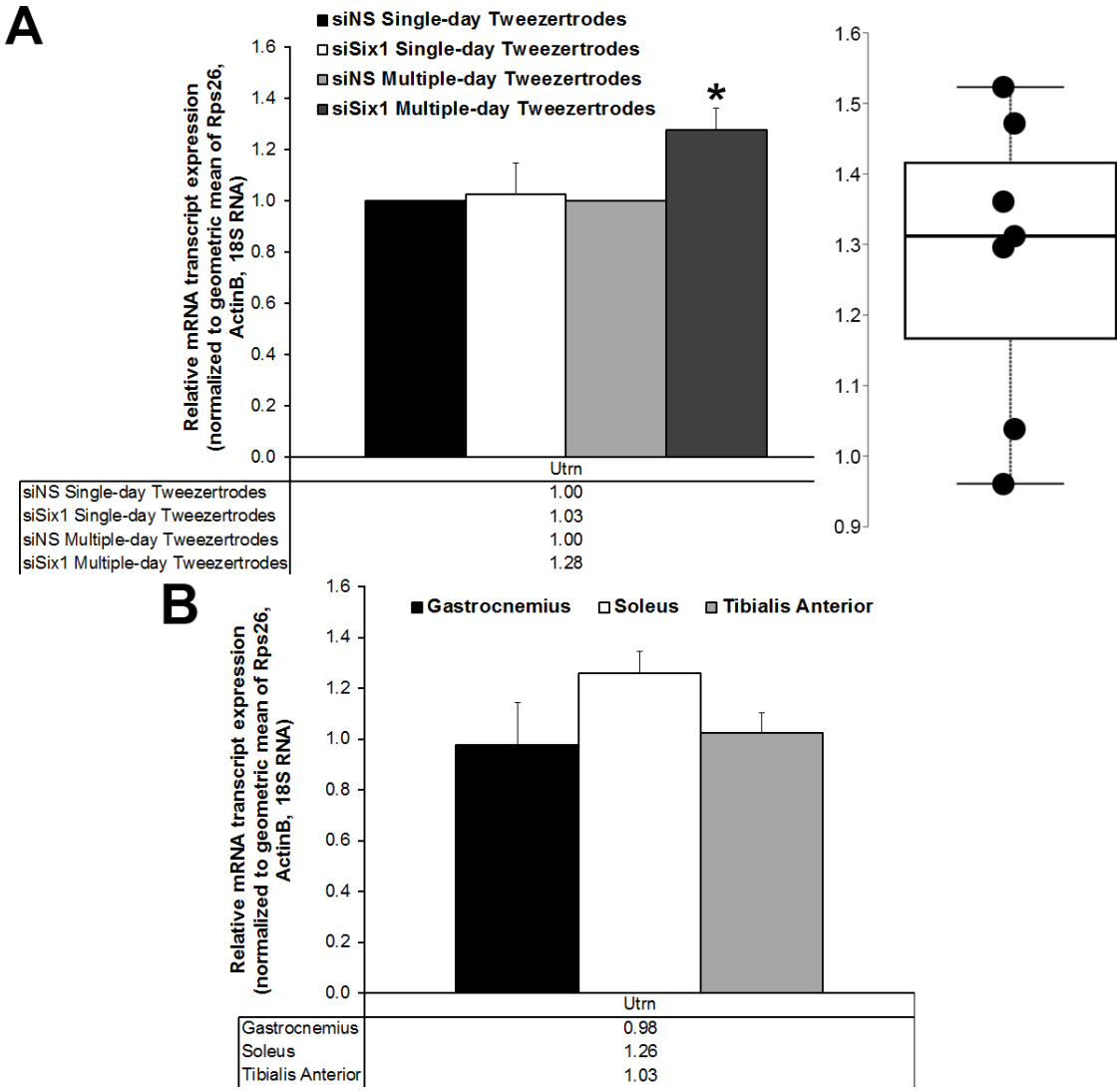

Figure 6: **Effect of Six1 knockdown on Utrophin mRNA**
(A) Utrophin mRNA expression levels in electroporated mouse TA muscle under Six1 knockdown condition. Boxplot represents data distribution and variability under multiple-day Tweezertrodes siSix1 knockdown condition.
(B) Utrophin mRNA expression levels in unelectroporated mouse slow and fast muscles, quantified by qRT-PCR. mRNA levels were normalized to the geometric mean of Rps26, 18S and Beta-Actin. Data represents an average of 7 biological replicates (A) and 4 biological replicates (B). siNS represents a control siRNA targeting a non-specific sequence. Error bars indicate the SEM. * Represents statistically significant changes in levels of expression as determined by a two-tailed paired Student's T-Test relative to siNS (p-value < 0.05).

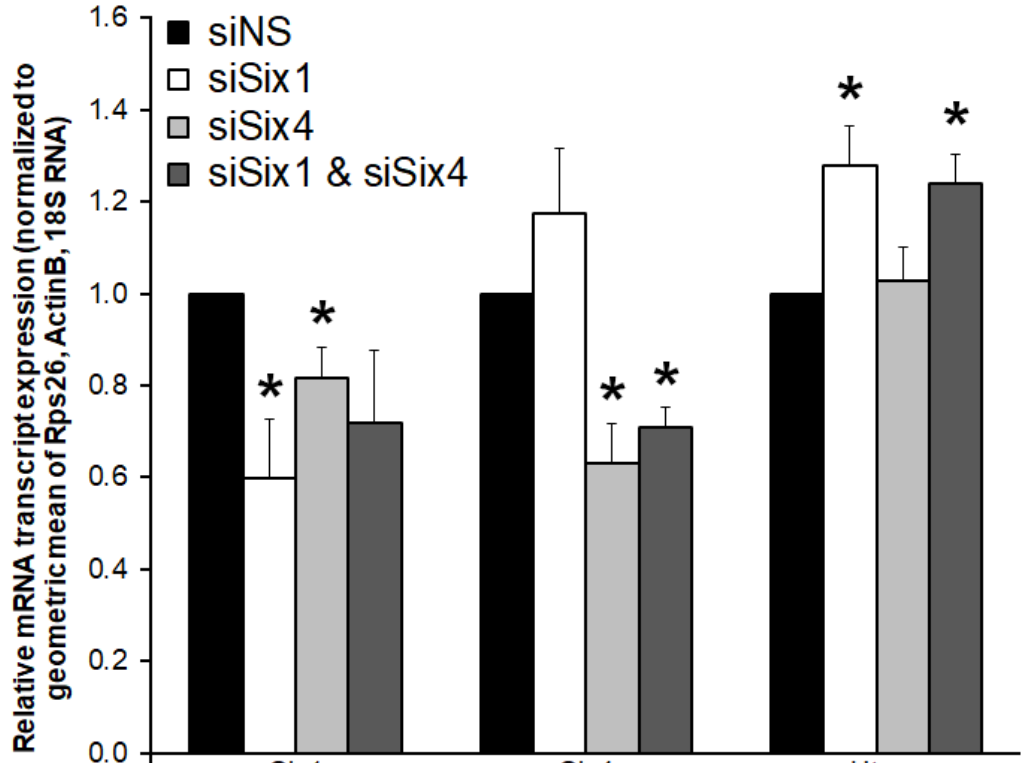

	Six1	Six4	Utrn
siNS	1.00	1.00	1.00
siSix1	0.60	1.17	1.28
siSix4	0.82	0.63	1.03
siSix1 & siSix4	0.72	0.71	1.24

Figure 7: **Effect of Six4 and Double knockdown**
Utrophin mRNA expression levels in electroporated mouse TA muscle under Six4 and double Six1 and Six4 knockdown conditions quantified by qRT-PCR. mRNA levels were normalized to the geometric mean of Rps26, 18S and Beta-Actin. Data represents an average of 7 biological replicates. siNS represents a control siRNA targeting a non-specific sequence. All knockdown conditions were normalized to their respective corresponding contralateral siNS muscles, and a single representative bar for three distinct siNS conditions is presented. Error bars indicate the SEM. * Represents statistically significant changes in levels of expression as determined by a two-tailed paired Student's T-Test relative to siNS (p-value < 0.05).
N.B. siSix1 knockdown effects on both Six1 and Utrophin genes are data already represented in Figure 3B and Figure 6A.

with four of seven biological replicates demonstrating a 1.5-fold upregulation, and an overall average of 2.5-fold protein level upregulation (Figure 8).

Utrophin upregulation can only be functional, and clinically relevant, in conditions where it correctly localizes to the sarcolemma in order to replace the functionally absent Dystrophin (Zubrzycka-Gaarn et al., 1988; Nguyen et al., 1991). To confirm functional Utrophin protein upregulation, immunofluorescent staining was carried out on sections of electroporated TA muscle (Figure 9). Only a small representative field is shown in Figure 9 to avoid confusion with fibers regenerating and expressing Utrophin due to the electroporation process (Lin et al., 1998). Counting of Utrophin positive fibers was only considered in areas with no centrally-located nuclei. Counting only took into consideration Utrophin positive fibers that were directly adjacent to another Utrophin positive fiber to avoid false positive counting of slow-twitch fibers that innately express increased Utrophin levels (Chakkalakal et al., 2003). Slow-twitch fibers comprise fewer than 1% of fibers in the TA muscle (Augusto et al., 2004). Counting based on directly adjacent Utrophin positive fibers decreases the likelihood of mistakenly taking into account a Utrophin-expressing slow-twitch fiber into analysis, especially with the assumption that successful electroporation occurs in regions of the muscle as opposed to disparate fibers (Figure 3). Given the above criteria, an average of 80 fibers were counted for each obtained muscle section. Utrophin localization at the sarcolemma of electroporated muscle was observed (Figure 9A), with a significantly increased count of fibers expressing Utrophin when compared to siNS conditions (Figure 9B). Immunofluorescent co-staining of both Six1 and Utrophin simultaneously is currently not possible due to differing section processing requirements, with Utrophin staining requiring unfixed tissue for optimal staining, and Six1 staining requiring fixed tissue for optimal staining. However, staining of Six1 on similarly treated muscles demonstrated knockdown in similar regions of the muscle (Figure 9A).

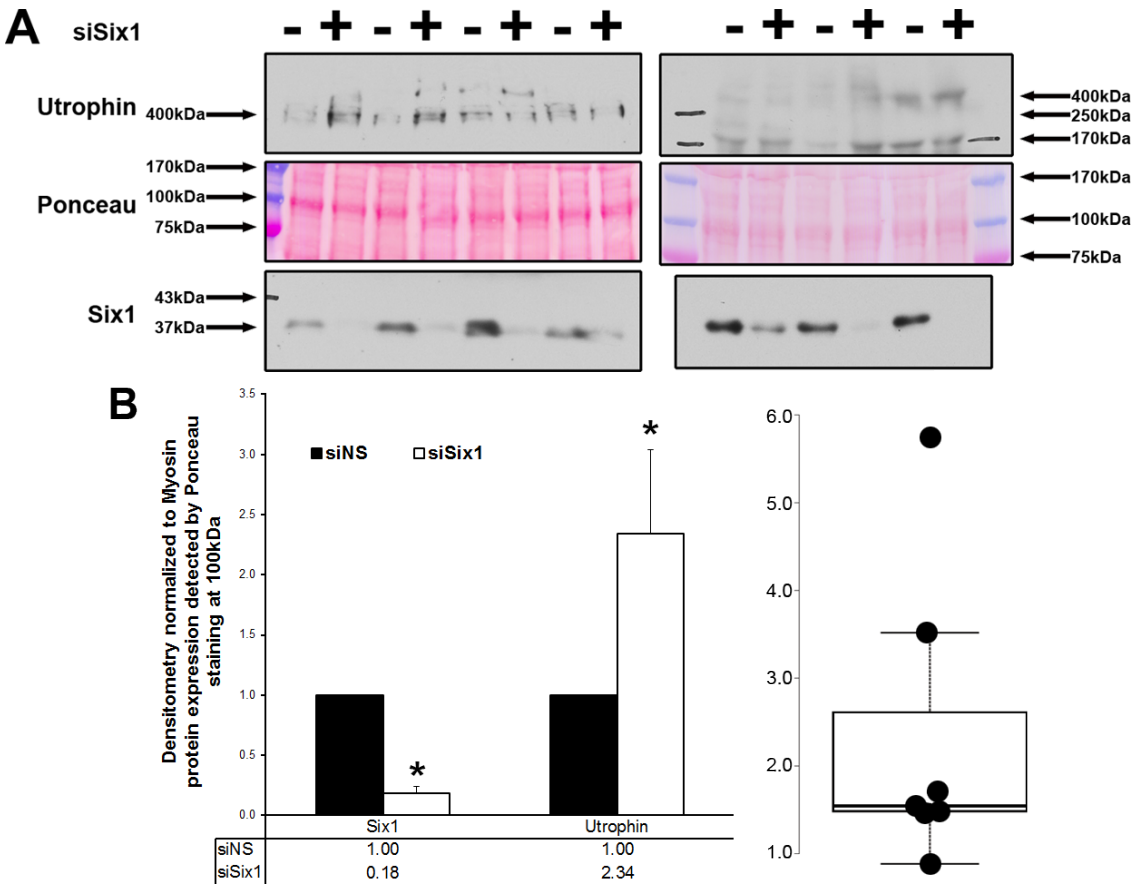

Figure 8: **Six1 knockdown regulates Utrophin protein levels**
(**A**) Western Blots in order to determine Utrophin protein expression levels in electroporated mouse TA muscle under Six1 knockdown condition. Molecular weight markers are annotated on the right-, and left- hand side of the panel.
(**B**) Densitometric quantification of Western Blots seen in (A), normalized to the Ponceau-stained Myosin band seen at 100kDa. Data represents an average of 7 biological replicates. Boxplot represents Utrophin protein level data distribution and variability under multiple-day Tweezertrodes siSix1 knockdown condition. siNS represents a control siRNA targeting a non-specific sequence. Error bars indicate the SEM. * Represents statistically significant changes in levels of expression as determined by a one-tailed paired Student's T-Test relative to siNS (p-value < 0.05).
N.B. siSix1 knockdown effects on Six1 protein levels are data already represented in Figure 5C.

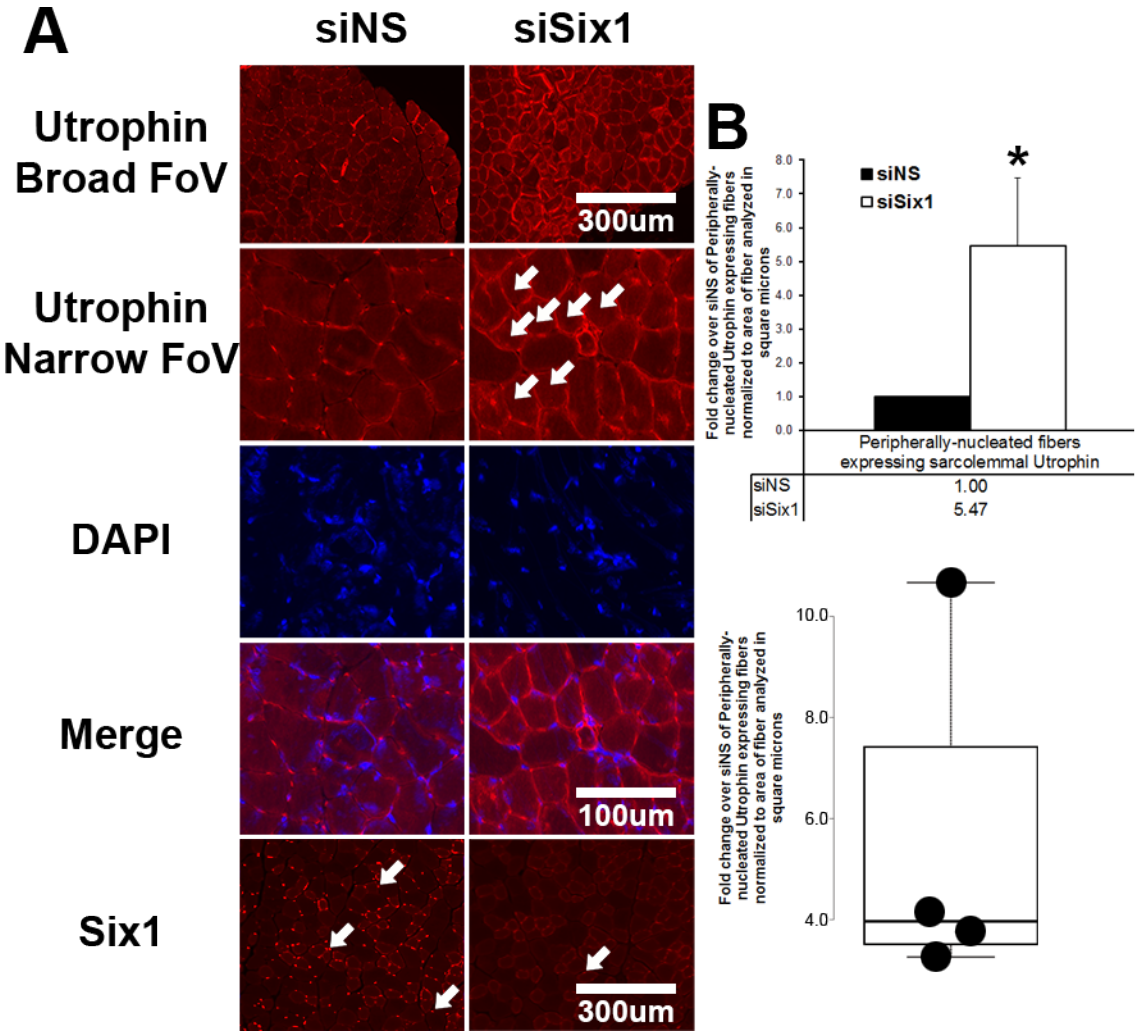

Figure 9: **Utrophin protein localization under Six1 knockdown conditions**
(**A**) Representative Utrophin & Six1 immunofluorescence in electroporated mouse TA muscle under Six1 knockdown condition, showing both an expanded Field of View (FoV) and a zoomed in area. Arrows represent fibers that were considered during the quantification process in Utrophin staining panels, or highlight Six1 expression in Six1 staining panels.
(**B**) Quantification of peripherally-nucleated fibers expressing sarcolemmal Utrophin, normalized to undamaged area of muscle analyzed in square microns and relative to siNS treatment. Data represents an average of 4 biological replicates. Boxplot represents data distribution and variability under multiple-day Tweezertrodes siSix1 knockdown condition. siNS represents a control siRNA targeting a non-specific sequence. Error bars indicate the SEM. * Represents statistically significant changes in levels of expression as determined by a one-tailed paired Student's T-Test relative to siNS (p-value < 0.05).
N.B. Representative Utrophin staining obtained from muscle corresponding to the data-point demonstrating 3.76-fold upregulation.

3.3 Effect of *in vivo* Six TFs knockdown on Myosin Isoform expression

Considering loss of Six1 is known to cause the acquisition of slow-twitch phenotype in skeletal muscle (Hetzler et al., 2014; Sakakibara et al., 2014), and considering Utrophin is more highly expressed in slow-twitch muscle (Chakkalakal et al., 2003), studying Myosin isoform expression was of experimental concern, to determine whether a fiber-type switch is occurring. mRNA expression as detected by qRT-PCR showed that Six1 knockdown is associated with significantly decreased levels of canonical Myosin Isoforms more expressed in fast-twitch muscle (Myosin IIb/*Myh4*, Myosin Type IIa/*Myh2*, and Myosin Type IIx/*Myh1*) (Schiaffino and Reggiani, 1994; Augusto et al., 2004). However, no induction of canonically slow-twitch Myosin Type I (*Myh7*) was observed (Figure 10A). This data is an agreement with other research that has attempted acute Six1 knockdown in adult skeletal muscle (Hetzler et al., 2014). Analysis of unelectroporated slow-twitch and fast-twitch muscles from similar mice demonstrated expected Myosin Isoform expression, with relatively higher expression of *Myh1*, *Myh2* and *Myh4* in the fast-twitch Gastrocnemius and TA, and relatively elevated expression of *Myh7* in the slow Soleus (Figure 10B). To confirm the validity of the obtained mRNA results, and the lack of a fiber-type switch, immunofluorescence analysis was carried out with antibodies detecting Myosin Type IIa and Myosin Type I (Figure 11). No statistically significant differences were observed in fiber-type proportions between siNS and experimental samples. This is counter to the results obtained with the mRNA analysis, where Myosin Type IIa levels were significantly downregulated, but could be explained by Myosin protein turnover rates, which can be measured in months (Poortmans et al., 2012). Attempts to perform immunofluorescent analysis on Myosin IIb and Myosin Type IIx were unsuccessful due to technical difficulties.

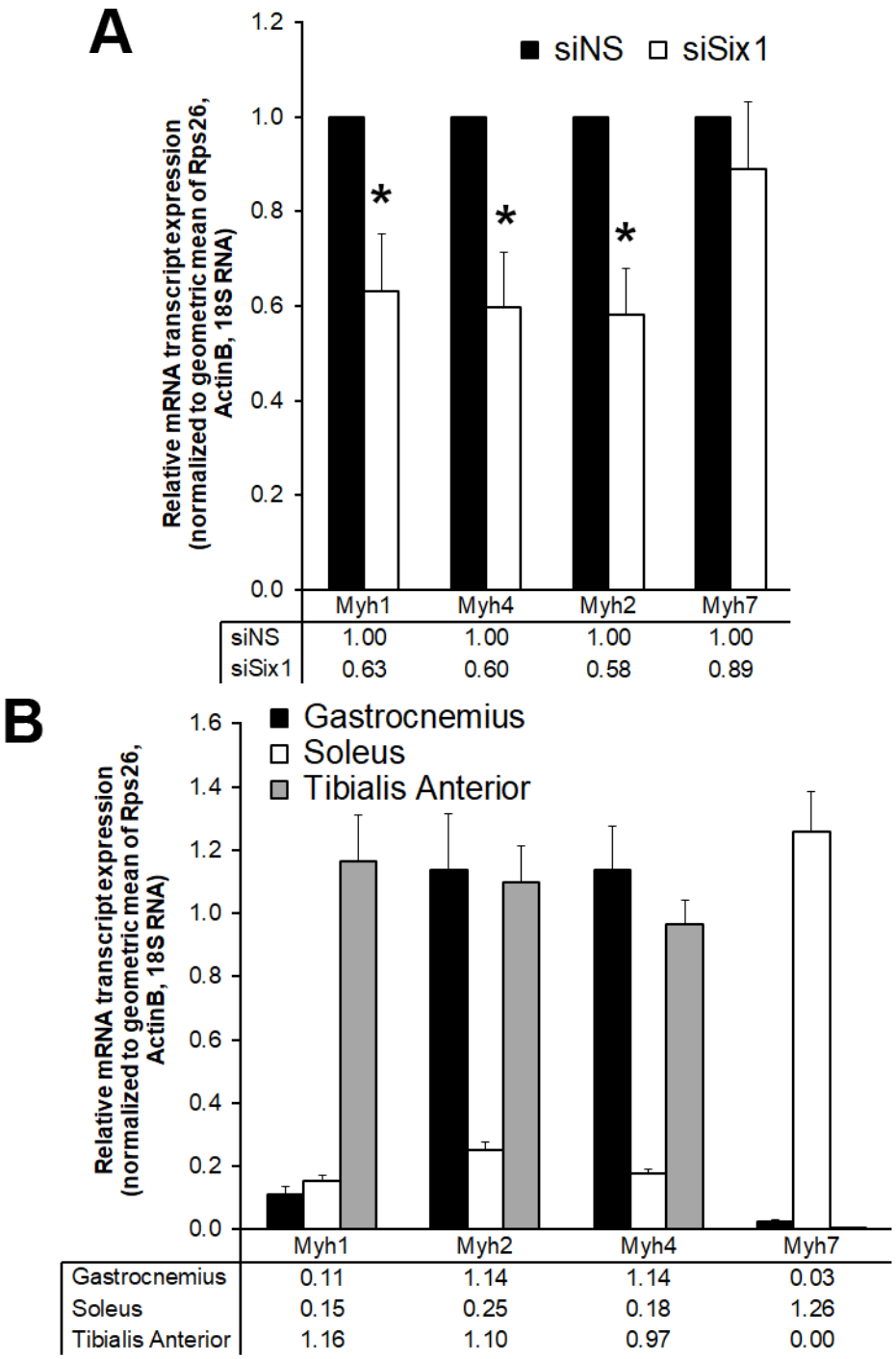

Figure 10: **Effect of Six1 knockdown on Myosin mRNA**
(A) Myosin isoform mRNA expression levels in electroporated mouse TA muscle under Six1 knockdown condition.
(B) Myosin isoform mRNA expression levels in unelectroporated mouse slow and fast muscles, quantified by qRT-PCR. mRNA levels were normalized to the geometric mean of Rps26, 18S and Beta-Actin. Data represents an average of 7 biological replicates (A) and 4 biological replicates (B). *Myh4* represents Myosin IIb/, *Myh2* represents Myosin IIa, *Myh1* represents Myosin IIx/, and *Myh7* represents Myosin I. siNS represents a control siRNA targeting a non-specific sequence. Error bars indicate the SEM. * Represents statistically significant changes in levels of expression as determined by a one-tailed paired Student's T-Test relative to siNS (p-value < 0.05).

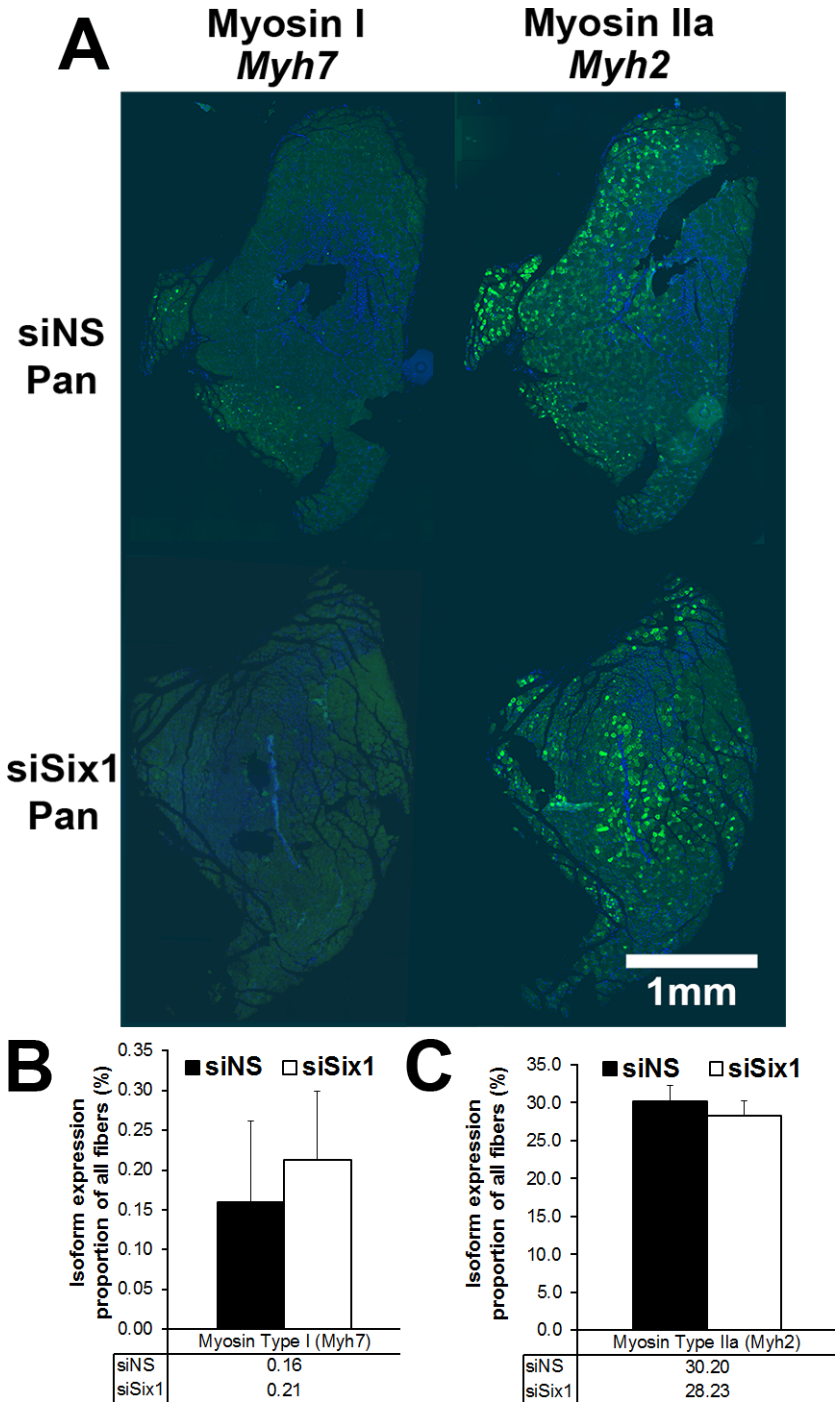

Figure 11: **Myosin isoform expression under Six1 knockdown conditions**
(**A**) Representative Myosin isoform Immunofluorescence in mouse electroporated TA muscle under Six1 knockdown condition.
(**B**) Quantification of fibers expressing Myosin Type I. Whole muscle sections were analyzed, and an average of 5 muscle fibers were counted across all replicates.
(**C**) Quantification of fibers expressing Myosin Type IIa. A 1.7mm² area of muscle analyzed, and an average of 341 muscle fibers were counted across all replicates. Data represents an average of 3 biological replicates. Data represents an average of 3 biological replicates. *Myh2* represents Myosin IIa and *Myh7* represents Myosin I. siNS represents a control siRNA targeting a non-specific sequence. Error bars indicate the SEM.

3.4 Elucidating regulatory mechanisms of Utrophin overexpression

Due to the implication of Utrophin mRNA transcript regulation as a contributing factor in Utrophin upregulation (Figure 6A), mechanisms that regulate Utrophin mRNA expression were explored. Analysis of unpublished ChIP-Seq data revealed a lack of Six1 binding at the Utrophin locus, suggesting indirect effects of Six1 regulation on Utrophin mRNA expression. Canonically, transcriptional and post-transcriptional regulation of Utrophin mRNA expression in extra-synaptic sarcolemmal regions is regulated by NFAT (Chakkalakal et al., 2003). In order to study NFAT pathway transcriptional activity, a bioinformatics approach was employed to determine genes upregulated during fiber-type switching events, with phylogenetically conserved NFAT binding sequences within 1kb of DNA of their promoter region, in order to determine targets for qRT-PCR analysis. The four most highly expressed genes fulfilling this criteria were selected, and they were Atp1b4, an ATPase that may act as a transcriptional regulator during muscle development, Meg3, a tumor inhibitor and p53 interactor, Runx1, a transcription factor required for myofibrillar organization, and Zdbf2, zinc finger protein with chromatin remodelling functions. Additionally, the transcript levels of Mef2d and Mb were analyzed as these were already noted in the literature to be dependent on Calcineurin/NFAT pathway regulation (Chin et al., 1998; Wu et al., 2001). mRNA expression levels of this panel of genes were analyzed under Six1 knockdown conditions by qRT-PCR technology (Figure 12A). Six1 knockdown was capable of upregulating the expression of all four bioinformatics-determined genes in the panel, suggesting Six1 may enact a repressive effect of the NFAT pathway. However, in the case of Mef2d and Mb neither gene was induced under the Six1 knockdown condition. One possible explanation for these conflicting results is that both the Mef2d and Mb may be

tightly regulated genes that are not entirely dependent on NFAT activity, with additional mechanisms in place to ensure their correct induction.

qRT-PCR analysis of this panel of genes in unelectroporated slow-twitch and fast-twitch muscles (Figure 12B) demonstrated that the NFAT pathway bioinformatics-determined genes are not differentially expressed between muscle fiber-types. This suggests that during steady-state conditions these genes are expressed at a basal level, and could highlight the importance of the genes exclusively in fast-to-slow fiber-type transitions. Mef2d demonstrated an increased expression in the slow-twitch Soleus muscle when compared to either the fast-twitch Gastrocnemius or TA, and its levels remained unchanged with Six1 knockdown conditions. Mb demonstrated even expression between the Soleus and the TA, but decreased expression in the Soleus compared to the Gastrocnemius, and Six1 knockdown reduced its expression levels, suggesting that there may be intermediate fiber-type switching effects than just the Utrophin upregulation demonstrated. Considering Utrophin upregulation could only be induced under conditions that included siRNA targeting Six1 (Figure 7), confirmation that effects seen on the upregulation of NFAT pathway activity were also similarly unique to Six1 knockdown conditions was important. Indeed, qRT-PCR analysis demonstrated that Six4 knockdown condition was incapable of upregulating the expression of the panel of NFAT genes. Double knockdown of both Six1 and Six4 was recapitulated some of the trends seen, confirming the unique ability of Six1 to repress the NFAT pathway.

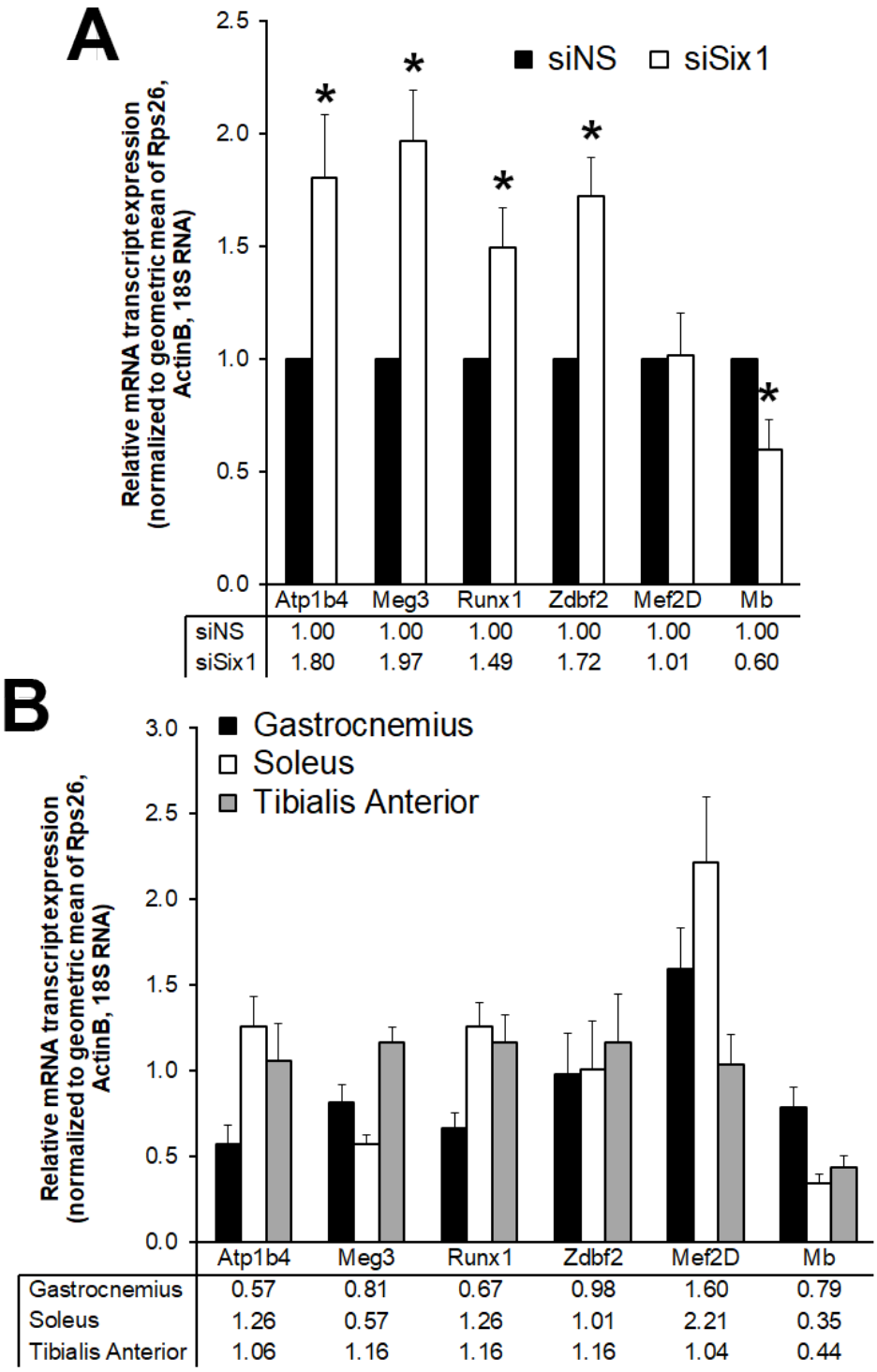

Figure 12: **Effect of Six1 knockdown on NFAT pathway mRNA**
(A) NFAT target genes mRNA expression levels in electroporated mouse TA muscle under Six1 knockdown condition.
(B) NFAT target genes mRNA expression levels in unelectroporated mouse slow and fast muscles, quantified by qRT-PCR. mRNA levels were normalized to the geometric mean of Rps26, 18S and Beta-Actin. Data represents an average of 7 biological replicates (A) and 4 biological replicates (B). siNS represents a control siRNA targeting a non-specific sequence. Error bars indicate the SEM. * Represents statistically significant changes in levels of expression as determined by a one-tailed paired Student's T-Test relative to siNS (p-value < 0.05).

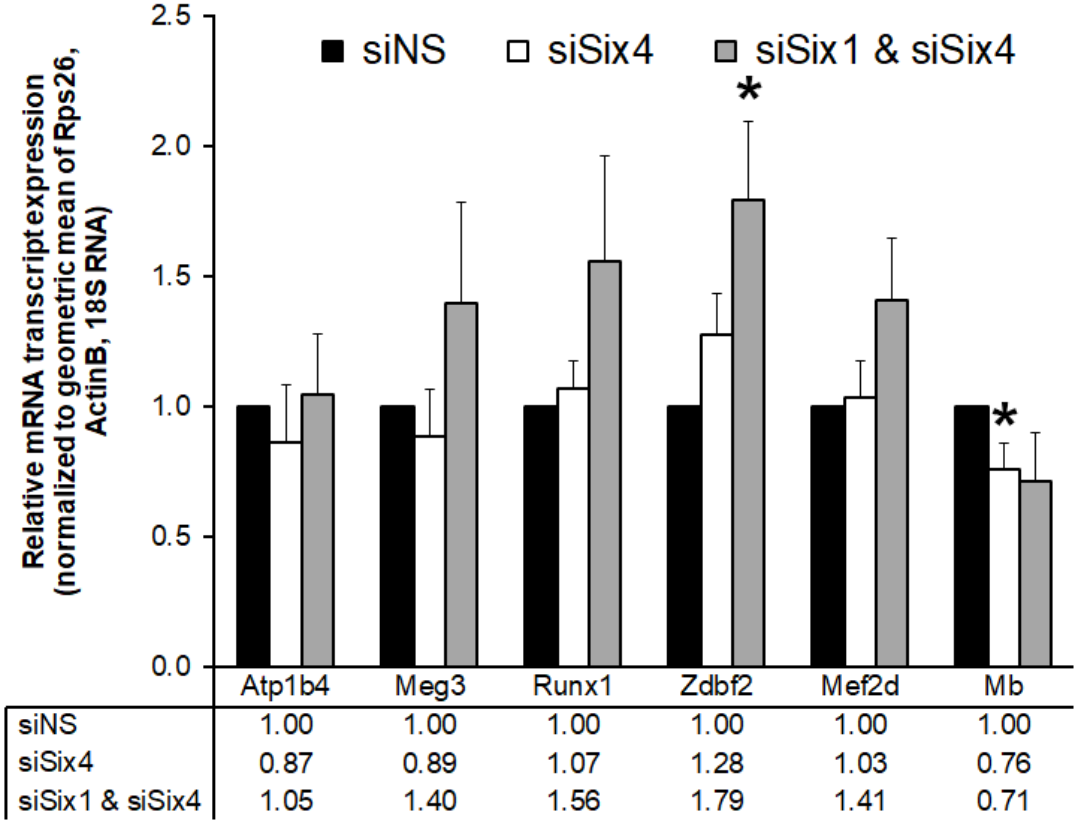

	Atp1b4	Meg3	Runx1	Zdbf2	Mef2d	Mb
siNS	1.00	1.00	1.00	1.00	1.00	1.00
siSix4	0.87	0.89	1.07	1.28	1.03	0.76
siSix1 & siSix4	1.05	1.40	1.56	1.79	1.41	0.71

Figure 13: **Effect of Six4 and Double knockdown on NFAT pathway mRNA** NFAT target genes mRNA expression levels in mouse electroporated TA muscle under Six4 and double Six1 and Six4 knockdown conditions quantified by qRT-PCR. mRNA levels were normalized to the geometric mean of Rps26, 18S and Beta-Actin. Data represents an average of 5 biological replicates. siNS represents a control siRNA targeting a non-specific sequence. All conditions were normalized to their corresponding contralateral siNS muscles. Error bars indicate the SEM. * Represents statistically significant changes in levels of expression as determined by a one-tailed paired Student's T-Test relative to siNS (p-value < 0.05).

3.5 Elucidating regulatory mechanisms of NFAT pathway upregulation

Multiple regulators of the NFAT pathway exist, however, a majority are expressed in slow-twitch muscle. Considering that in our experimental sample no observable fiber-type switch was determined (Figures 10A and 11), regulators of NFAT activity in fast-twitch muscle were explored. One such regulator is the Calsarcin2 protein, also known as the Myoz1 gene (Frey et al., 2000), known to inhibit NFAT activity, and almost exclusively expressed in fast-twitch skeletal muscle (Frey et al., 2000). Analysis of published microarray data (Liu et al., 2010) was carried out (Figure 14). Myoz1 gene expression was significantly induced in C2C12 T96 Myotubes by a factor of more than 10-fold (Figure 14A) and Six1 knockdown in primary myoblasts was capable of reducing Myoz1 levels significantly by a factor of about 40%. Analysis of unpublished ChIP-Seq data revealed a putative MEF3 binding site, with Six1, but not Six4, recruitment in an intronic region within the Myoz1 locus upon induction of differentiation (Figure 15). This criteria was important, as the effects of Six1 observed on Utrophin expression and NFAT activity seem unique to Six1 (Figures 7 and 12A), and the results observed for Utrophin upregulation are active in adult myofibers (Figure 9A).

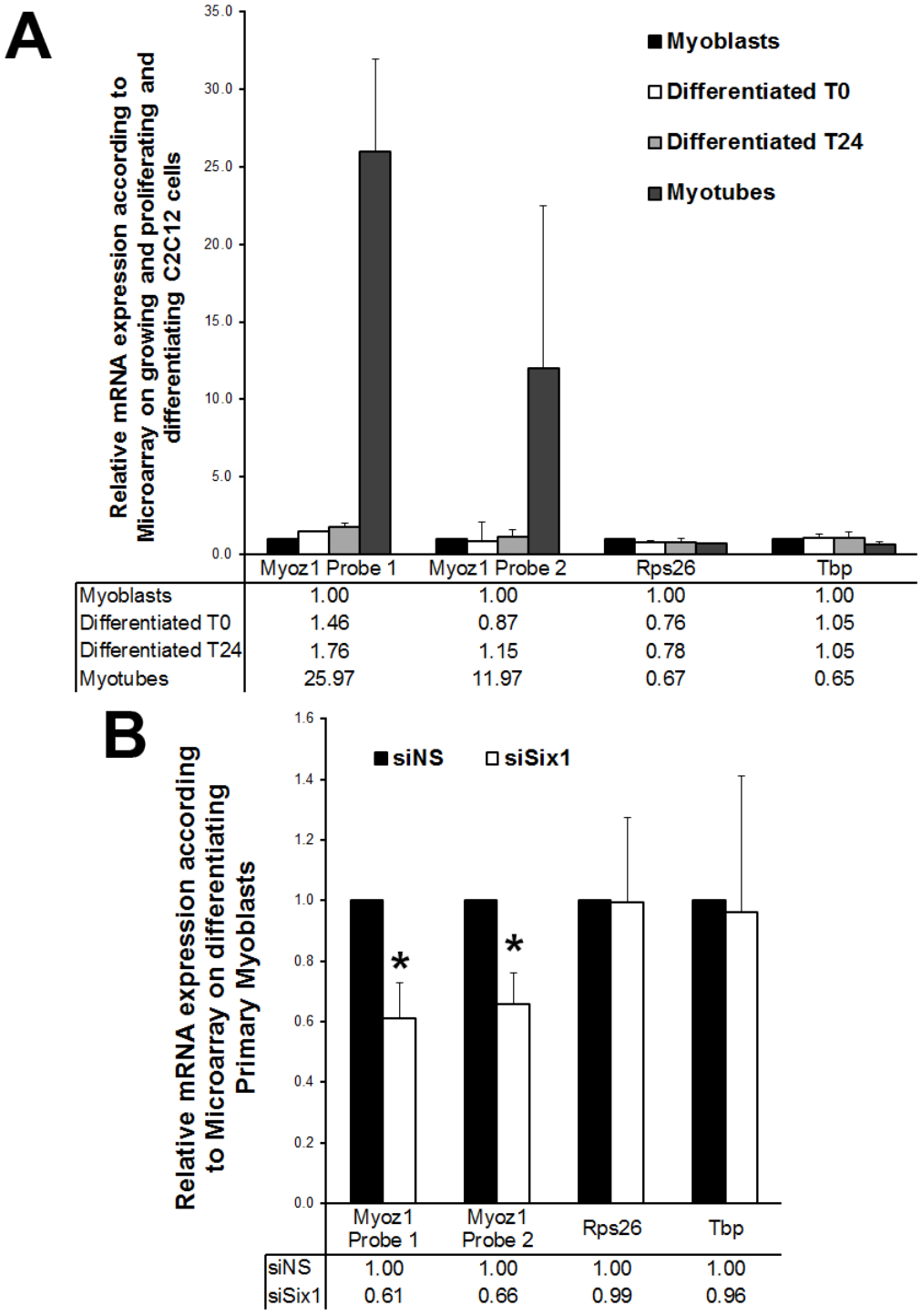

Figure 14: **Myoz1 is a potential Six1 target**
(**A**) Determination of Myoz1 mRNA expression levels based on Microarray time-course analysis of differentiating C2C12 cells.
(**B**) Determination of Myoz1 mRNA expression levels based on Microarray knockdown analysis of T24 differentiating Primary Myoblasts. Data represents an average of 3 biological replicates (A), and 4 biological replicates (B). Myoz1 Probe 1 and Probe 2 represent two separate probes for the Myoz1 transcript within the expression profiling dataset. siNS represents a control siRNA targeting a non-specific sequence. Error bars indicate the SEM. * Represents statistically significant changes in levels of expression as determined by a two-tailed paired Student's T-Test relative to siNS (p-value < 0.05).

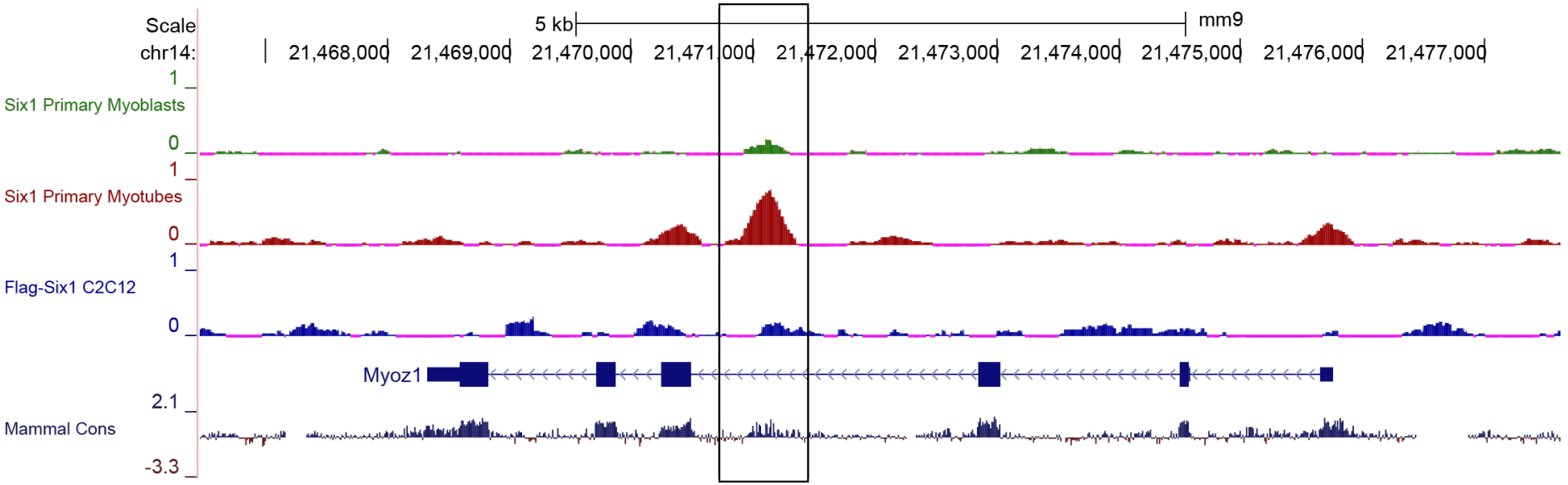

Figure 15: **ChIP-sequencing of Six1 binding at Myoz1 locus**
Peaks represent binding likelihood for Six1 in primary myoblasts (green), Six1 in primary myotubes (T48) (maroon) and Flag-Six1 in growing C2C12 (navy). A black box highlights putative Six1 binding peak. Signals shown have an input ChIP-Seq sample subtracted.

In order to determine if this possible regulation could account for the previously obtained results, *in vivo* experimentation was carried out. Analysis of mRNA expression by qRT-PCR confirmed that Myoz1 is more highly expressed in fast-twitch muscles than slow-twitch muscles (Figure 16A), in agreement with previous literature (Frey et al., 2000), and the relative activity of Six1 (Sakakibara et al., 2016). Six1 knockdown in electroporated TA muscle was able to significantly reduce Myoz1 expression levels by a factor of about 25% (Figure 16B, D), and ChIP analysis demonstrated enrichment of Six1 binding at the Myoz1 binding site as confirmed by qRT-PCR (Figure 16C). The Myogenin promoter was used as a positive control for the ChIP-qPCR experiment, as it has been previously demonstrated to be regulated directly by Six1 (Liu et al., 2010). Taking all the presented data into consideration, positive Myoz1 transcriptional regulation is suggested by direct Six1 binding to the intronic enhancer site.

Due to the fact that Myoz1 inhibits NFAT activity through protein-protein binding inhibition of Calcineurin activity (Frey et al., 2000; Frey et al., 2008), confirming that the transcriptional reduction in Myoz1 levels was accompanied by a protein-level reduction was important. Western blot analysis confirmed that under Six1 knockdown condition mean Myoz1 protein levels are significantly reduced, with a reduction in four of six biological replicates (Figure 17). Comprehensively, while the effects of Six1 on both Utrophin expression and Myoz1 expression were confirmed, the potential for Myoz1 to act as a mediator between Six1 activity and Utrophin expression was the next question to tackle. In order to determine if Myoz1 acted as an intermediary, qRT-PCR analysis was carried out to check gene expression under knockdown conditions with siRNA targeting Myoz1 (Figure 18). While some effects obtained with Six1 knockdown condition were recapitulated, for example increase in Zdbf2 transcript levels and a significant decrease in Mb transcript levels, trends in the expression of other genes, such as Utrophin and the remainder of the NFAT pathway panel, were not significantly affected.

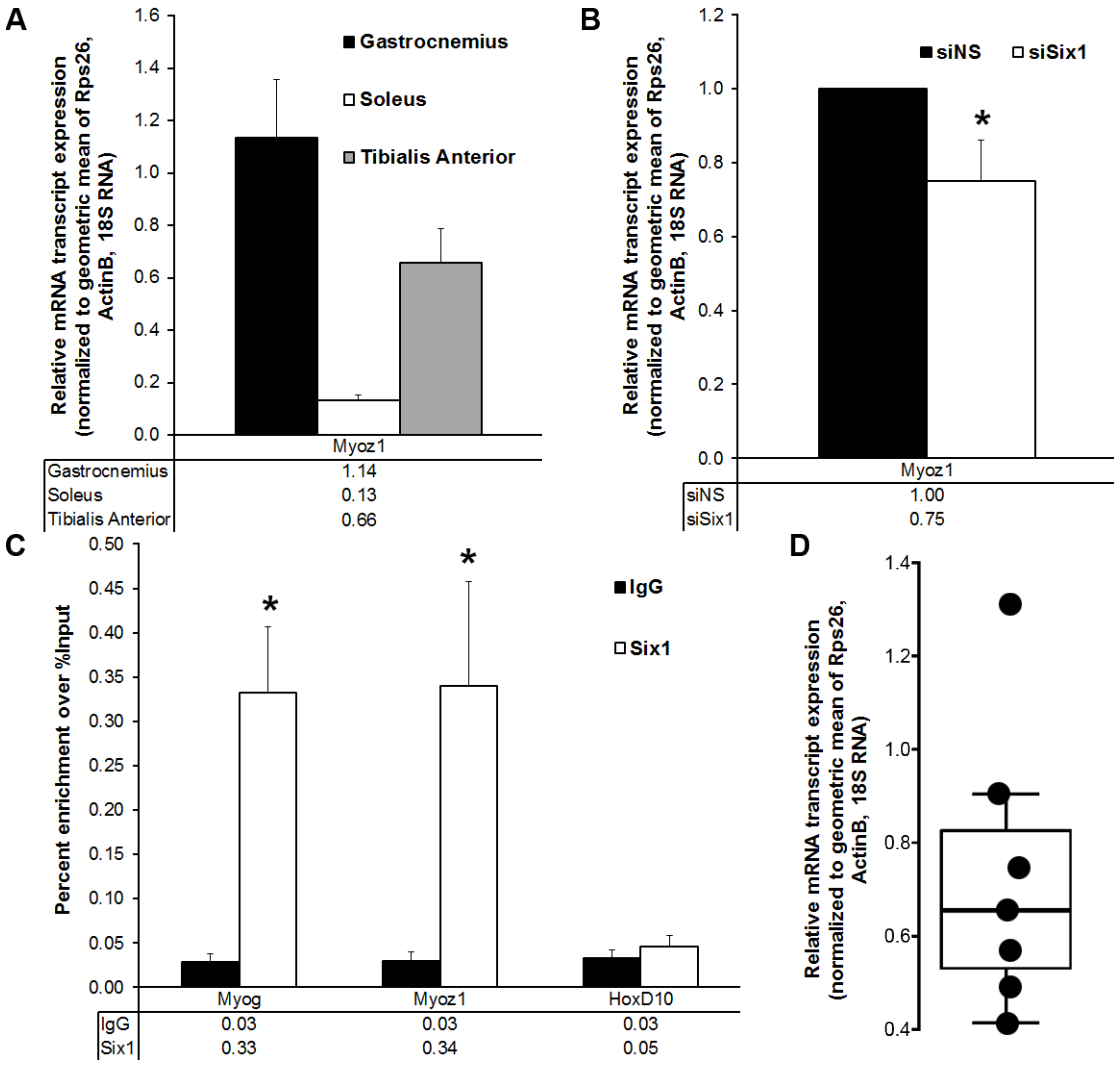

Figure 16: **Myoz1 is a Six1 target *in vivo***
(**A**) Myoz1 mRNA expression levels in unelectroporated mouse slow and fast muscles.
(**B**) Myoz1 mRNA expression levels in electroporated mouse TA muscles under Six1 knockdown condition.
(**C**) Hindlimb muscles from two mice were harvested, fixed and ChIP was carried out using either IgG or Six1 antibody. Results represent qPCR quantification of enrichment of genomic DNA at the Myoz1 locus over a related Input sample. Data represents an average of 4 biological replicates (A + C) and 7 biological replicates (B). siNS represents a control siRNA targeting a non-specific sequence. Error bars indicate the SEM. * Represents statistically significant changes in levels of expression as determined by a one-tailed paired Student's T-Test relative to siNS or IgG control (p-value < 0.05).
(**D**) Boxplot representing Myoz1 mRNA level data distribution and variability under multiple-day Tweezertrodes siSix1 knockdown condition from Panel B.

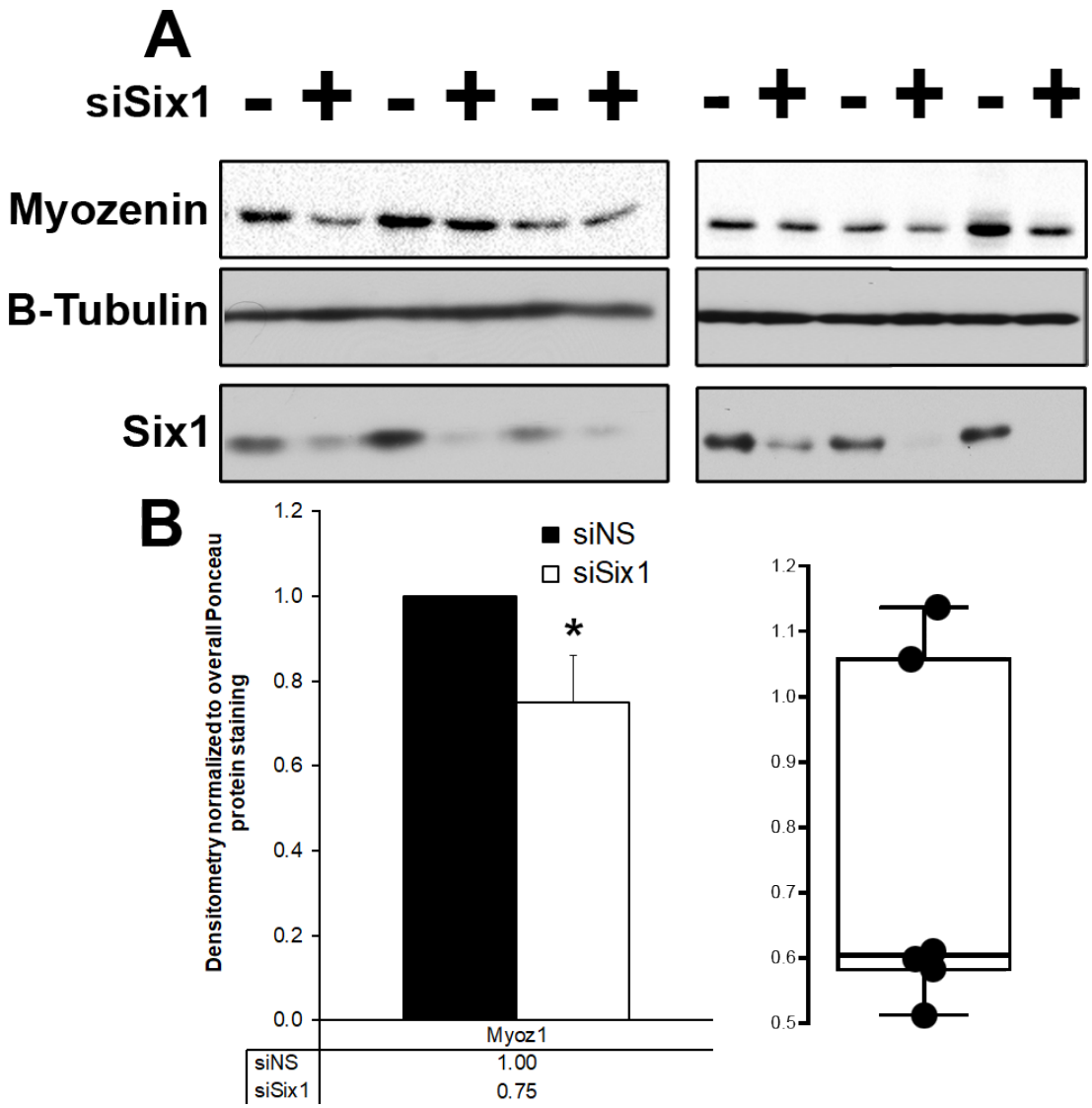

Figure 17: **Six1 knockdown regulates Myoz1 protein levels**
(**A**) Western Blots in order to determine Myoz1 protein expression levels in electroporated mouse TA muscle under Six1 knockdown condition.
(**B**) Densitometric quantification of Western Blots seen in (A), normalized to B-Tubulin levels. Data represents an average of 7 biological replicates. Boxplot represents data distribution and variability of Myoz1 protein levels under multiple-day Tweezertrodes siSix1 knockdown condition. siNS represents a control siRNA targeting a non-specific sequence. Error bars indicate the SEM. * Represents statistically significant changes in levels of expression as determined by a one-tailed paired Student's T-Test relative to siNS (p-value < 0.05).
N.B. siSix1 knockdown effects on both Six1 protein levels are data already represented in Figure 5C.

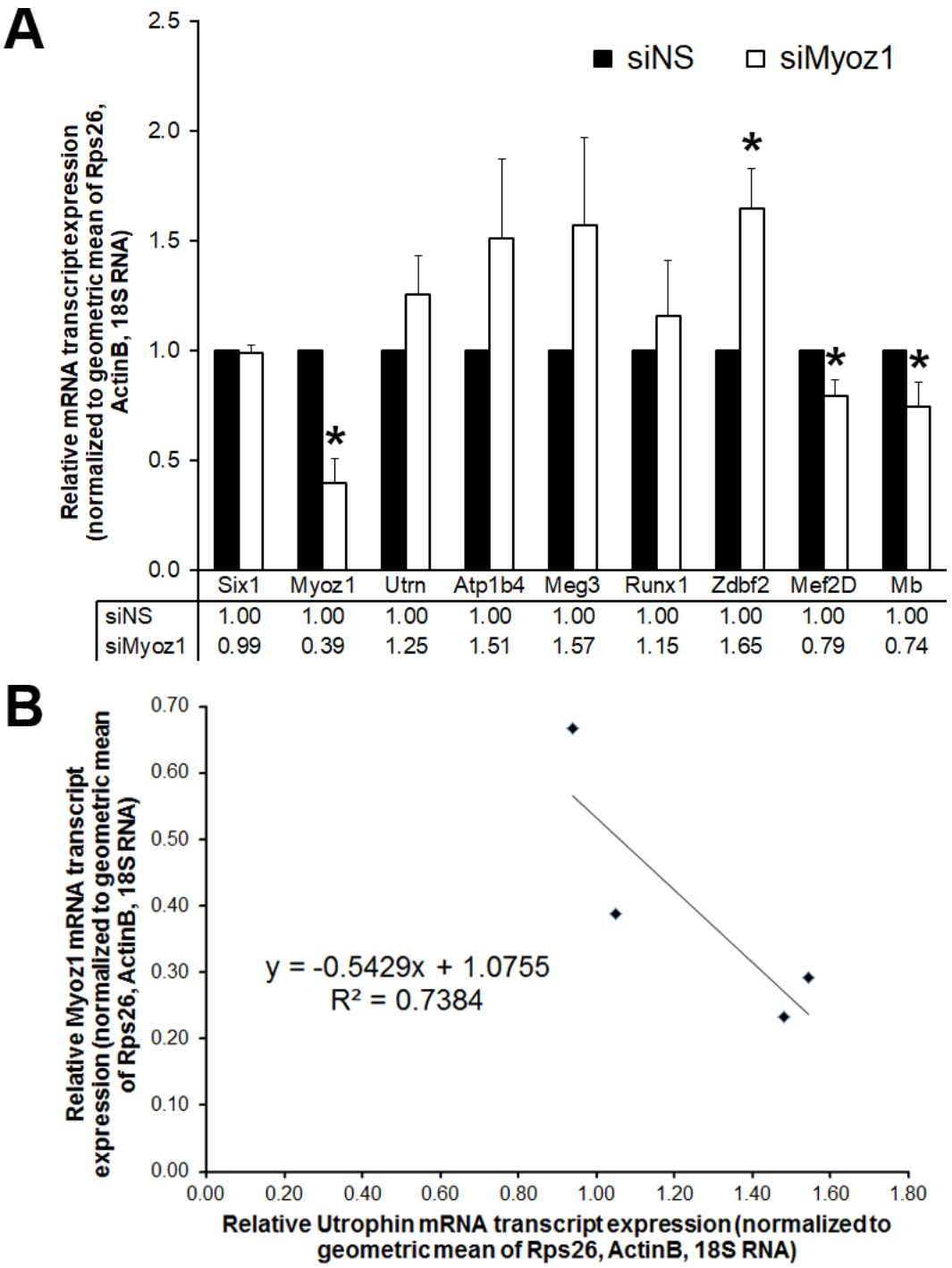

Figure 18: **Recapitulation of NFAT pathway effects with siRNA targeting Myoz1**

(**A**) NFAT target genes mRNA expression levels in mouse electroporated TA muscle under Myoz1 knockdown conditions quantified by qRT-PCR. mRNA levels were normalized to the geometric mean of Rps26, 18S and Beta-Actin. Data represents an average of 4 biological replicates. siNS represents a control siRNA targeting a non-specific sequence. Error bars indicate the SEM. * Represents statistically significant changes in levels of expression as determined by a one-tailed paired Student's T-Test relative to siNS (p-value < 0.05).

(**B**) A scatter plot of Utrophin mRNA expression plotted against Myoz1 mRNA expression under Myoz1 knockdown condition.

3.6 Exploring the Six1 regulome for fiber-type specific targets

A bioinformatics approached was utilized to determine Six1 gene targets that are both dependent and independent of fiber-type. R code used to perform and produce the analyses can be found in section 4.6. Data used to perform the analyses was publicly available from research conducted by other groups (Sakakibara et al., 2014; Sakakibara et al., 2016). To study targets that are fiber-type independent, analysis required a 50% change in expression for the gene between wild-type and Six1 knockout Gastrocnemius (Figure 19). A list of genes identified through this analysis can be found in Table 1. Myoz1 is a significant target identified in this analysis, with a significant decrease in expression with Six1 knockout. To analyze targets that are fiber-type dependent, analysis required the binding of Six1 within 50kb of DNA in an unpublished ChIP-Seq experiment, for a 2-fold change in expression with Six1 knockout, and for the gene to be differentially expressed in either fast-twitch muscle, Gastrocnemius or TA, than the slow-twitch Soleus (Figure 20). A list of genes identified through this analysis can be found in Table 2. A combinatorial analysis of genes found in both analyses yielded high confidence targets of Six1, with many that have been previously reported, such as Myh7, Sln, and the Troponin genes (Sakakibara et al., 2014), suggesting that analyzing the pathways shared between both analyses would yield targets and pathways more likely to be under Six1 regulation. Indeed, while Meg3 and Myoz1 were identified as targets in the fiber-type independent analysis (Table 1), Atp1b4, Runx1 and Zdbf2 were identified as targets in the fiber-type dependent analysis (Table 2).

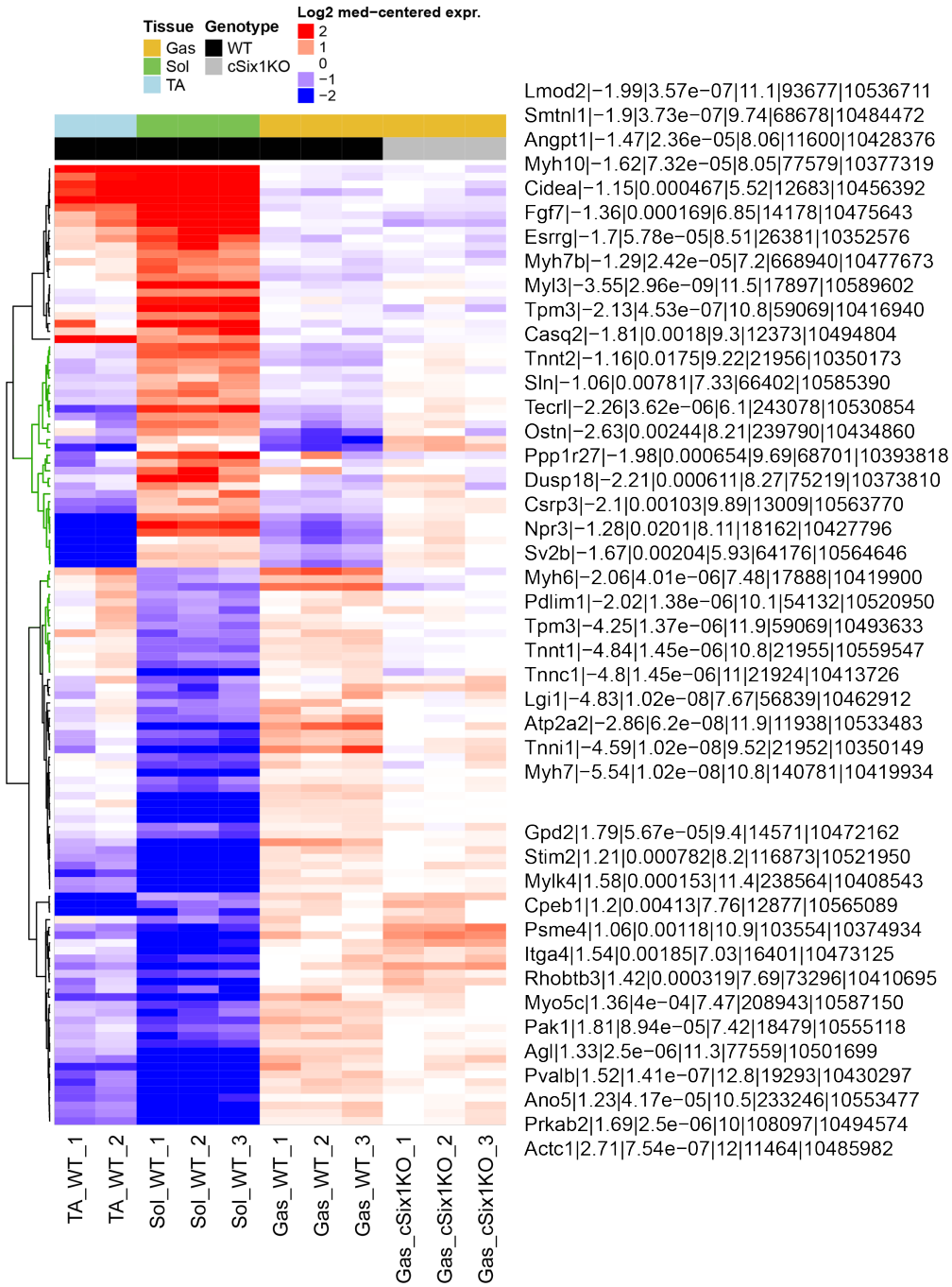

Figure 19: **Fiber-type independent bioinformatics analysis performed to identify Six1 target genes**

Analysis panels from left to right: Box-plot displaying average mRNA expression level, cluster analysis, fold-change expression level heat-map, gene identifying information. The profile analysis used requires genes to be more differentially expressed in knockout Gastrocnemius than wildtype Gastrocnemius by a Log_2 fold-change of 1.5 and a Benjamini-Hochberg corrected P-Value < 0.05. For each gene that satisfies both conditions, and assumes a more slow-twitch phenotype with Six1 knockout (highlighted in green in the cluster analysis), the gene symbol and ID, Log_2 fold-change, adjusted P-Value are plotted in the figure. A list of genes identified through this analysis can be found in Table 1. Data used for analysis was publicly available through previous publications (Sakakibara et al., 2014; Sakakibara et al., 2016).

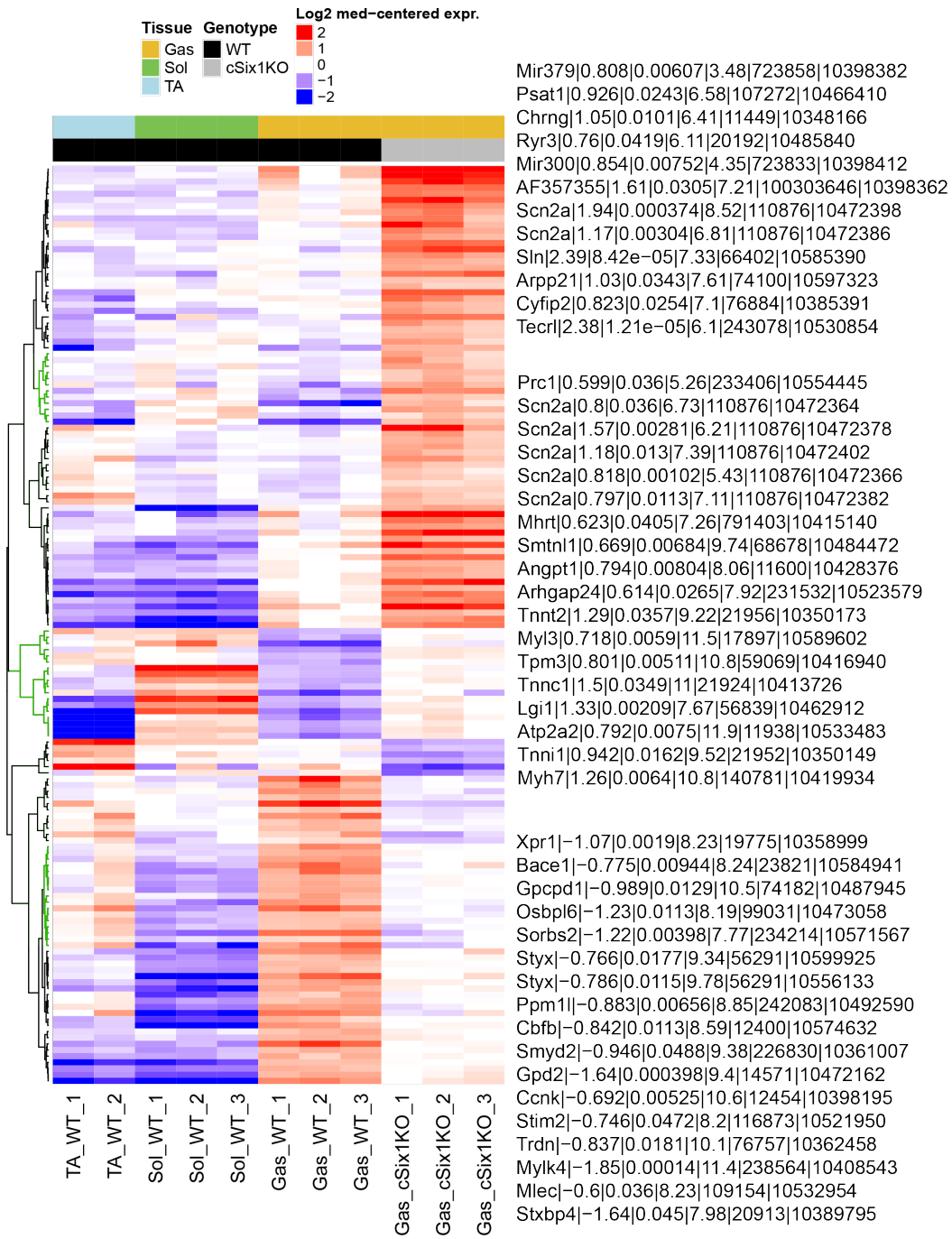

Figure 20: **Fiber-type specific bioinformatics analysis performed to identify Six1 target genes**

Analysis panels from left to right: Cluster analysis, fold-change expression level heat-map, gene information. The profile analysis used requires genes to be bound by Six1 in Myotube conditions in a ChIP-Seq dataset, to be more differentially expressed in wildtype Soleus than wildtype Gastrocnemius or TA by a Log_2 fold-change of 2, and to have a Benjamini-Hochberg corrected P-Value < 0.05. For each gene that satisfies both conditions, and assumes a more slow-twitch phenotype with Six1 knockout (highlighted in green in the cluster analysis), the gene symbol and ID, Log_2 fold-change, adjusted P-Value are plotted in the figure. A complete list of genes identified through this analysis can be found in Table 2. Data used for analysis was publicly available through previous publications (Sakakibara et al., 2014; Sakakibara et al., 2016).

Table 1: Genes affected by Six1 knockout independently of fiber-type

Gene name				
Acss1	Dusp18	Mybph	Pgm2	Sort1
Actc1	Eid1	Myh10	Pip4k2a	Ssr3
Actn3	Esrrg	Myh13	Pla2g16	St3gal6
Acvr1b	Eya4	Myh4	Polr2h	Stim2
Adprhl1	Fbxw7	Myh6	Ppp1r27	Stox2
Agl	Fgf7	Myh7	Ppp1r3c	Sv2b
Angpt1	Gatm	Myh7b	Prkab2	Sypl2
Ano5	Gpd2	Myl1	Prkag3	Tbc1d1
Aqp7	Gpt2	Myl10	Psme4	Tecrl
Atp1b2	Gpx3	Myl3	Pvalb	Tmem184c
Atp2a2	Hmcn1	Mylk4	Pygm	Tmem56
Bag5	Hspb11	Myo5c	Reep1	Tnnc1
BC048679	Ift81	Myom2	Rhobtb3	Tnni1
Cacng1	Igfbp5	Myoz1	Sar1b	Tnnt1
Carhsp1	Itga4	Myoz3	Serinc2	Tnnt2
Casq2	Kcnc4	Npc1	Slc16a3	Tpi1
Ccdc12	Ky	Npr3	Slc25a30	Tpm3
Cd74	Ldha	Nr4a1	Slc38a4	Txnip
Cdkn2aipnl	Lgi1	Nt5dc3	Slc7a2	Ucp3
Ces5a	Lmod2	Nuak1	Slc7a8	Utp3
Chad	Lsm3	Ostn	Slc8a3	Vamp8
Cidea	Man2a1	Otud1	Sln	Wfikkn2
Cpeb1	Mical2	Pak1	Smox	
Csrp3	Mpp7	Pdlim1	Smtnl1	
Ctsc	Mybpc2	Pfkfb3	Socs2	

One pathway that seemed to be common to both analyses was the thyroid hormone pathway. Both analyses identified Atp2a2 as a Six1 target, with fiber-type independent analysis highlighting UCP3, and fiber-type dependent analysis highlighting Slc16a10 as genes regulated by Six1 knockout. All three of these genes are thyroid pathway implicated (Hartong et al., 1994; Solanes et al., 2005; Mebis et al., 2009). Slc16a10, or MCT10, is one of two thyroid hormone transporters expressed in skeletal muscle (Mebis et al., 2009). Lack of MCT8, the other thyroid hormone transporter, is not known to cause any adverse effects in skeletal muscle (Di Cosmo et al., 2013). However not much is known about MCT10, so we investigated the significance of potential MCT10 regulation by Six1.

Table 2: Genes affected by Six1 knockout dependent on fiber-type

Gene name				
Acvr1b	Dmd	Lrrc20	Mylk2	Smyd2
AF357355	Dnase2a	Lrrc38	Mylk4	Sntb1
Ak4	DQ267102	Lsmem1	Nnmt	Sorbs2
Ampd3	Ehd3	Mafb	Nt5c2	Spsb1
Anapc5	Emp2	Map2k6	Nt5dc2	St8sia5
Angpt1	Enpep	Meg3	Osbpl6	Stim2
Aox1	Esr1	Mhrt	Park2	Stom
Arhgap24	Eya4	Mir300	Pde10a	Stxbp4
Arpp21	Frzb	Mir323	Peg10	Styx
Asb4	Gabrr2	Mir337	Plekhh1	Tbc1d19
Asb5	Gadd45a	Mir341	Ppfibp2	Tecrl
Atp1b4	Gadd45b	Mir377	Ppm1l	Tm6sf1
Atp2a2	Gadl1	Mir379	Prc1	Tmem56
Bace1	Gatm	Mir380	Prkag3	Tnnc1
BC067074	Gdap1	Mir382	Psat1	Tnni1
Blnk	Gdf11	Mir412	Rasd2	Tnnt2
Bpgm	Glo1	Mir487b	Rps6ka2	Tpm3
Casr	Gm7265	Mir543	Runx1	Trdn
Cbfb	Gpcpd1	Mir665	Rxrg	Trim16
Ccnk	Gpd2	Mki67	Ryr3	Tspan8
Chrnd	Gstt1	Mlec	Scn2a	Ugcg
Chrng	Hs6st2	Mospd1	Serpina3n	Wfdc1
Cilp	Igdcc4	Mss51	Shisa4	Xpr1
Cks2	Igf2	Mstn	Slc16a10	Xylt1
Cntnap2	Inpp5j	Myh7	Slc43a2	Zdbf2
Cyfip2	Kcng4	Myh8	Sln	Zfp385a
Dlk1	Lgi1	Myl3	Smtnl1	

3.7 MCT10, a thyroid transporter, is under Six1 regulatory control

To confirm the regulatory role of Six1 on MCT10 gene expression is direct, analysis for Six TFs binding was conducted in both unpublished and published ChIP-Seq datasets (Figure 21) (Chakroun et al., 2015). Peaks for binding of both Six1 and Six4 were identified surrounding the locus at different stages of myogenesis, with the redundancy and persistence suggesting a significant importance of the regulation of MCT10 by the Six TFs. In a manner similar to the Myoz1 analysis, a peak was identified 46kb upstream of the MCT10 promoter that is more significantly bound by Six1 in primary myotubes (T48) than in primary myoblasts, which is a significant criteria considering our analysis is dependent on adult skeletal muscle. In order to determine if this Six1 binding to the MCT10 locus was functionally relevant, mRNA expression was studied using qRT-PCR methodology. Expression of MCT10 was determined to be higher in fast-twitch Gastrocnemius and TA muscles than in slow-twitch Soleus muscle, in agreement with previously published data (Mebis et al., 2009) (Figure 22A). Six1 knockdown was capable of significantly reducing MCT10 mRNA expression (Figure 22B), and *in vivo* confirmation of Six1 binding to the 46kb upstream enhancer sequence was confirmed by ChIP-qPCR, demonstrating that Six1 directly positively regulates MCT10 gene expression (Figure 22C).

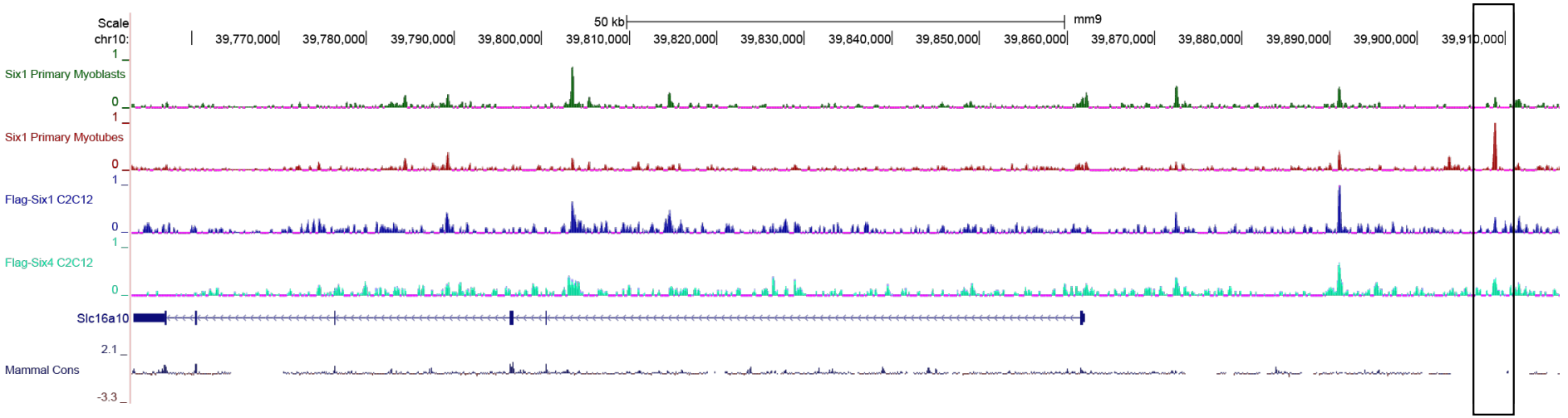

Figure 21: **ChIP-sequencing of Six TFs binding at Slc16a10/MCT10 locus**
Peaks represent binding likelihood for Six1 in primary myoblasts (green), Six1 in primary myotubes (T48) (maroon), Flag-Six1 in growing C2C12 (navy) and Flag-Six4 in growing C2C12 (light blue). A black box highlights putative Six1 binding peak. Signals shown have an input ChIP-Seq sample subtracted.

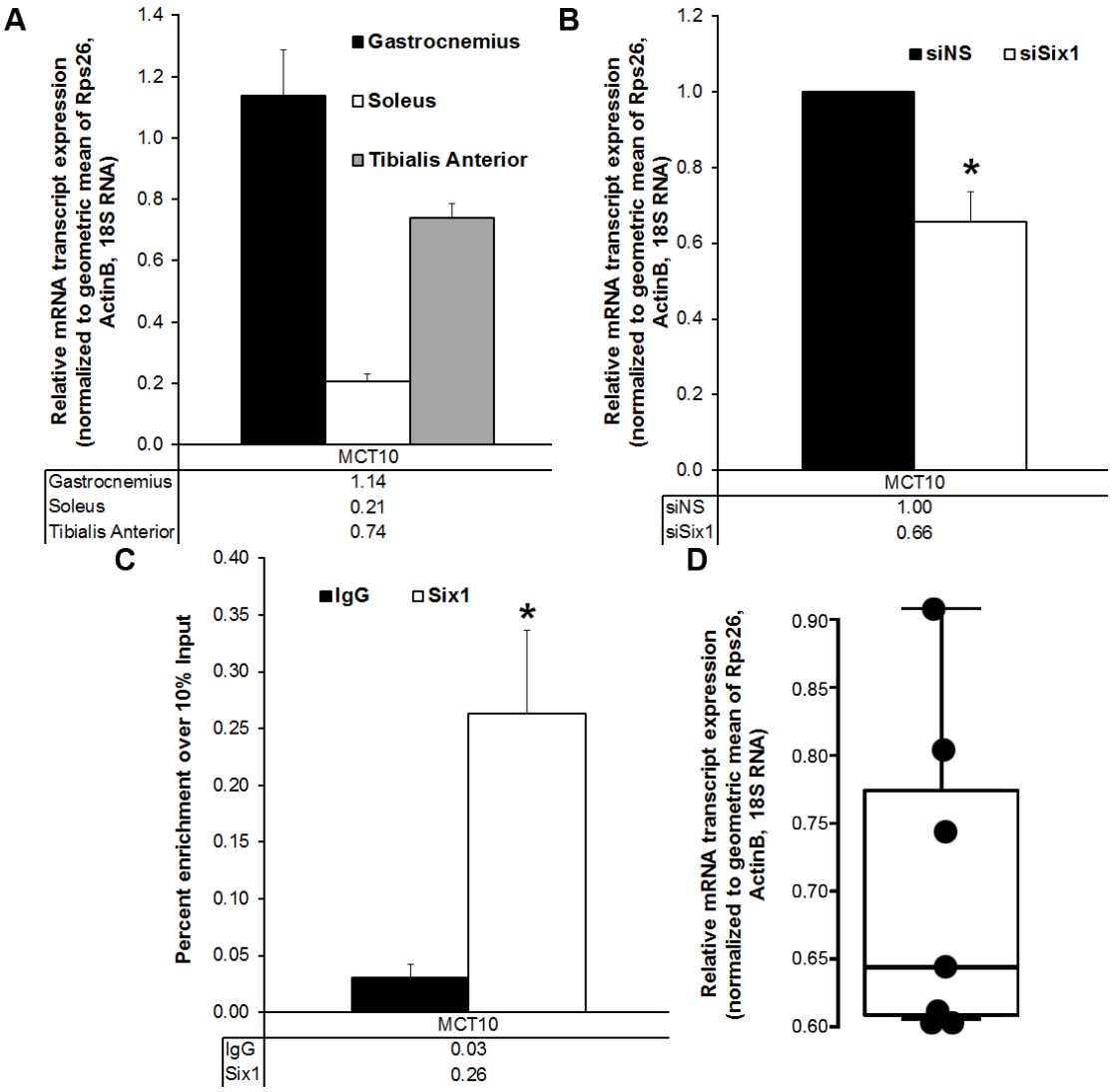

Figure 22: **Slc16a10/MCT10 is a Six1 target *in vivo***
(**A**) Slc16a10/MCT10 mRNA expression levels in unelectroporated mouse slow and fast muscles.
(**B**) Slc16a10/MCT10 mRNA expression levels in electroporated mouse TA muscles under Six1 knockdown condition.
(**C**) Hindlimb muscles from two mice were harvested, fixed and ChIP was carried out using either IgG or Six1 antibody. Results represent qPCR quantification of enrichment of genomic DNA at the 46kb binding site upstream of the Slc16a10/MCT10 locus over a related Input sample. Data represents an average of 4 biological replicates (A + C) and 7 biological replicates (B). siNS represents a control siRNA targeting a non-specific sequence. Error bars indicate the SEM. * Represents statistically significant changes in levels of expression as determined by a one-tailed paired Student's T-Test relative to siNS or IgG control (p-value $<$ 0.05).
(**D**) Boxplot representing MCT10 mRNA level data distribution and variability under multiple-day Tweezertrodes siSix1 knockdown condition from Panel B.
N. B. ChIP DNA samples used were the same found in Figure 16C, where positive and negative control loci binding can be seen.

3.8 Thyroid pathway is impacted negatively in Six1 knockdown conditions

In order to determine the extent of the effects of Six1 knockdown on the thyroid pathway, a panel of thyroid-target genes was selected for qRT-PCR analysis based on previously published data. The thyroid-target genes Atp2a1, encoding a calcium ATPase (Simonides et al., 1996), Glut4, encoding the main glucose transporter in muscle, (Zorzano et al., 2005), Me1, encoding malate dehydrogenase (Desvergne et al., 1991), and UCP3, encoding Uncoupling Protein 3 (Solanes et al., 2005), were selected for the analysis, as they are the most well characterized targets of thyroid hormone signaling in skeletal muscles (Salvatore et al., 2014). Additional genes analyzed included the thyroid-regulatory network of the skeletal muscle specific deiodinases, Dio2 and Dio3 (Ambrosio et al., 2013), MCT8, and the thyroid nuclear receptors Thra and Thrb.

Under Six1 knockdown condition all thyroid hormone target genes trended towards lowered mRNA expression, with Atp2a1 and UCP3 decreasing significantly in expression (Figure 23A). Dio3, a deiodinase that deactivates T_3 intracellularly was significantly transcriptionally induced with Six1 knockdown. No changes were detected in Dio2, a thyroid activating deiodinase or MCT8 mRNA expression levels. Significant reduction in the mRNA expression for both Thra and Thrb was detected. Considering Thra and Thrb mRNA expression levels usually correlate with thyroid hormone responsiveness (Bahi et al., 2005), the data suggested a switch away from thyroid program activity and responsiveness. Analysis of this same panel of genes in unelectroporated fast-twitch and slow-twitch muscles demonstrated higher expression of Thra and Thrb in slow-twitch muscle, as expected with the higher sensitivity of the Soleus to thyroid hormone signaling (Bahi et al., 2005). mRNA expression levels of Atp2a1, Me1 and UCP3 were lower in

slow-twitch Soleus when compared to the fast-twitch Gastrocnemius or TA, in agreement with previous research that thyroid hormone activity promotes fast-twitch energy metabolism programs (Izumo et al., 1986; Mahdavi et al., 1987) (Figure 23B).

Given the potential for Six4 to regulate MCT10 expression based on unpublished ChIP-Seq data and for the identified binding region being exclusively occupied by Six1 (Figures 21 and 22C), it was important to confirm that the effects seen on the thyroid pathway were unique to Six1 regulation of MCT10. qRT-PCR analysis confirmed that neither Six4 knockdown nor double Six1 and Six4 knockdown was incapable of recapitulating the mRNA expression profile of Six1 knockdown experiments (Figure 24).

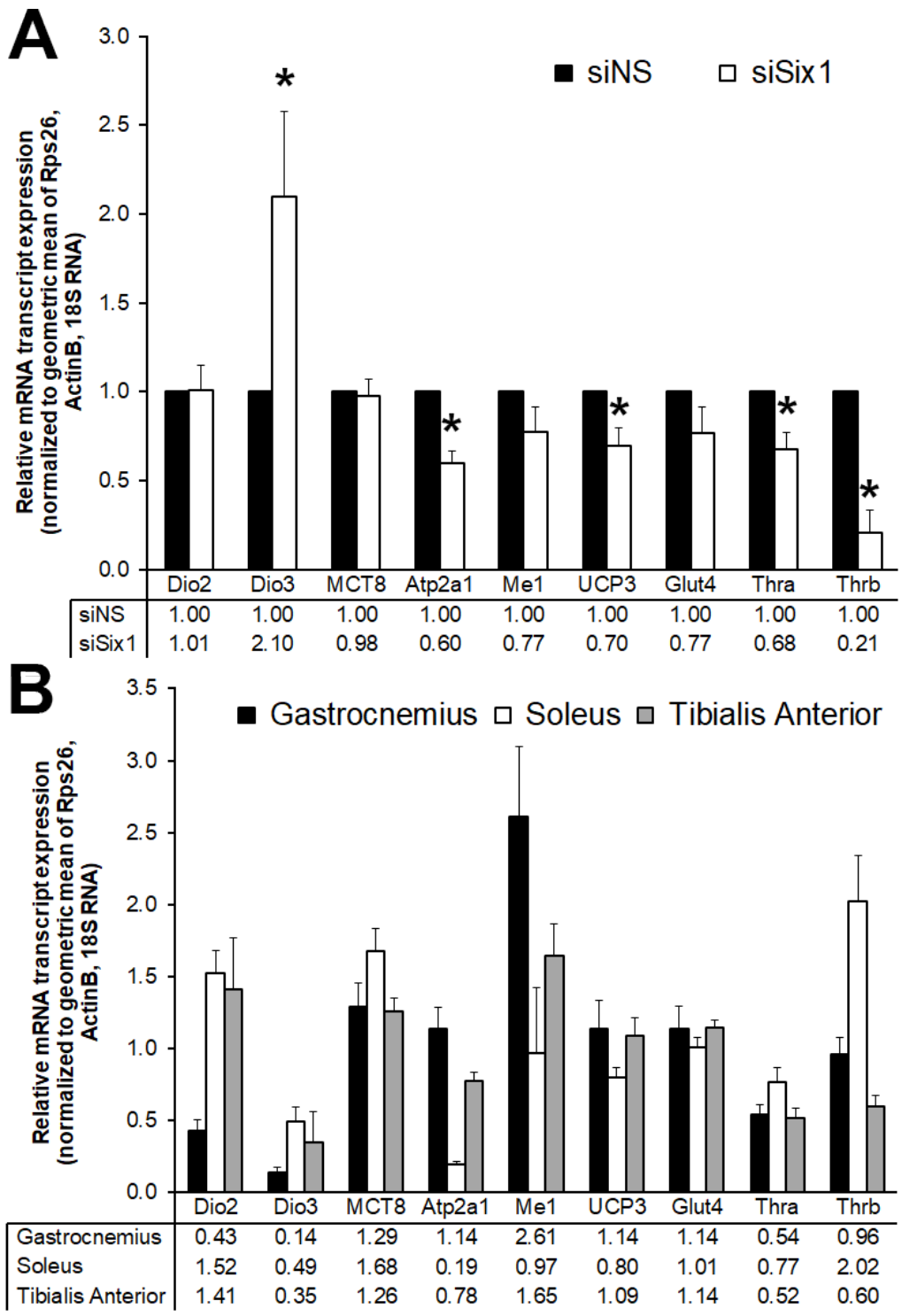

Figure 23: **Effect of Six1 knockdown on Thyroid pathway mRNA**
(**A**) Thyroid target genes mRNA expression levels in electroporated mouse TA muscle under Six1 knockdown condition.
(**B**) Thyroid target genes mRNA expression levels in unelectroporated mouse slow and fast muscles, quantified by qRT-PCR. mRNA levels were normalized to the geometric mean of Rps26, 18S and Beta-Actin. Data represents an average of 7 biological replicates (A) and 4 biological replicates (B). siNS represents a control siRNA targeting a non-specific sequence. Error bars indicate the SEM. * Represents statistically significant changes in levels of expression as determined by a one-tailed paired Student's T-Test relative to siNS (p-value < 0.05).

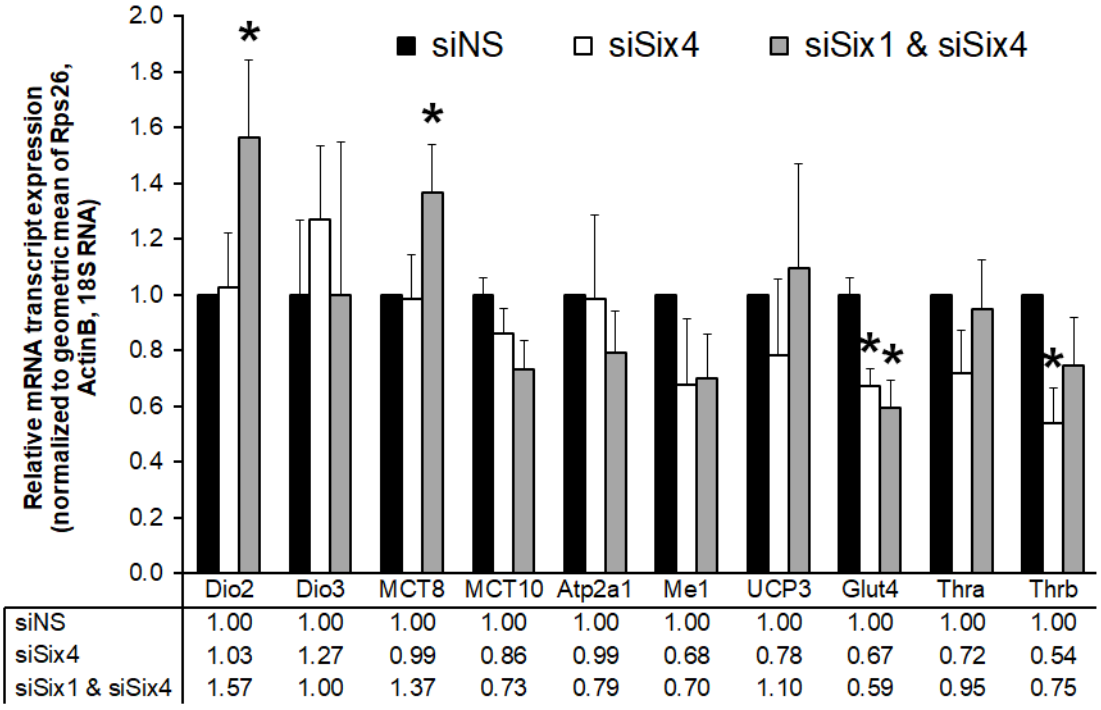

	Dio2	Dio3	MCT8	MCT10	Atp2a1	Me1	UCP3	Glut4	Thra	Thrb
siNS	1.00	1.00	1.00	1.00	1.00	1.00	1.00	1.00	1.00	1.00
siSix4	1.03	1.27	0.99	0.86	0.99	0.68	0.78	0.67	0.72	0.54
siSix1 & siSix4	1.57	1.00	1.37	0.73	0.79	0.70	1.10	0.59	0.95	0.75

Figure 24: **Effect of Six4 and Double knockdown on Thyroid pathway mRNA**

Thyroid target genes mRNA expression levels in mouse electroporated TA muscle under Six4 and double Six1 and Six4 knockdown conditions quantified by qRT-PCR. mRNA levels were normalized to the geometric mean of Rps26, 18S and Beta-Actin. Data represents an average of 7 biological replicates. siNS represents a control siRNA targeting a non-specific sequence. All conditions were normalized to their corresponding contralateral siNS muscles. Error bars indicate the SEM. * Represents statistically significant changes in levels of expression as determined by a one-tailed paired Student's T-Test relative to siNS (p-value < 0.05).

Confirmation that effects seen on the thyroid gene program by Six1 knockdown are mediated through MCT10 was analyzed by studying the activity of a Luciferase-reporter with multiple TREs, and by qRT-PCR analysis of thyroid hormone target genes under siRNA-mediated knockdown conditions targeting MCT10 (Figure 25). MCT10 knockdown was able to cause a significant reduction in the activity of a thyroid-responsive Luciferase plasmid (Figure 25A), indicating protein-level changes in the thyroid hormone signaling pathway. MCT10 also recapitulated gene expression patterns seen by Six1 knockdown, and was able to reduce, albeit not significantly, Six1 gene expression, raising the possibility of feedback loops across pathways (Figure 25B).

Given the seeming inter-regulation between the Six1 regulatory pathways and the thyroid signaling pathway - both Six1 and MCT10 knockdown are capable of inducing reductions in expression of the other gene - analysis of the thyroid-regulated genes in the unpublished ChIP-Seq was carried out. Indeed, of five target genes, Six1 had binding sites found at or near the loci of three of the genes, hinting that cooperative or even synergestic effects of regulation of these genes could be possible (Figure 26). Finally, given inter-connectedness of gene regulatory pathways, analysis of thyroid-regulated genes that could affect the NFAT pathway was carried out. The RCAN proteins are negative regulators of the NFAT pathway (Davies et al., 2007), and are under thyroid program regulation (Gürgen et al., 2011). qRT-PCR ensured that inter-pathway cross-talk was not responsible for the observed effects on the NFAT pathway (Figure 27).

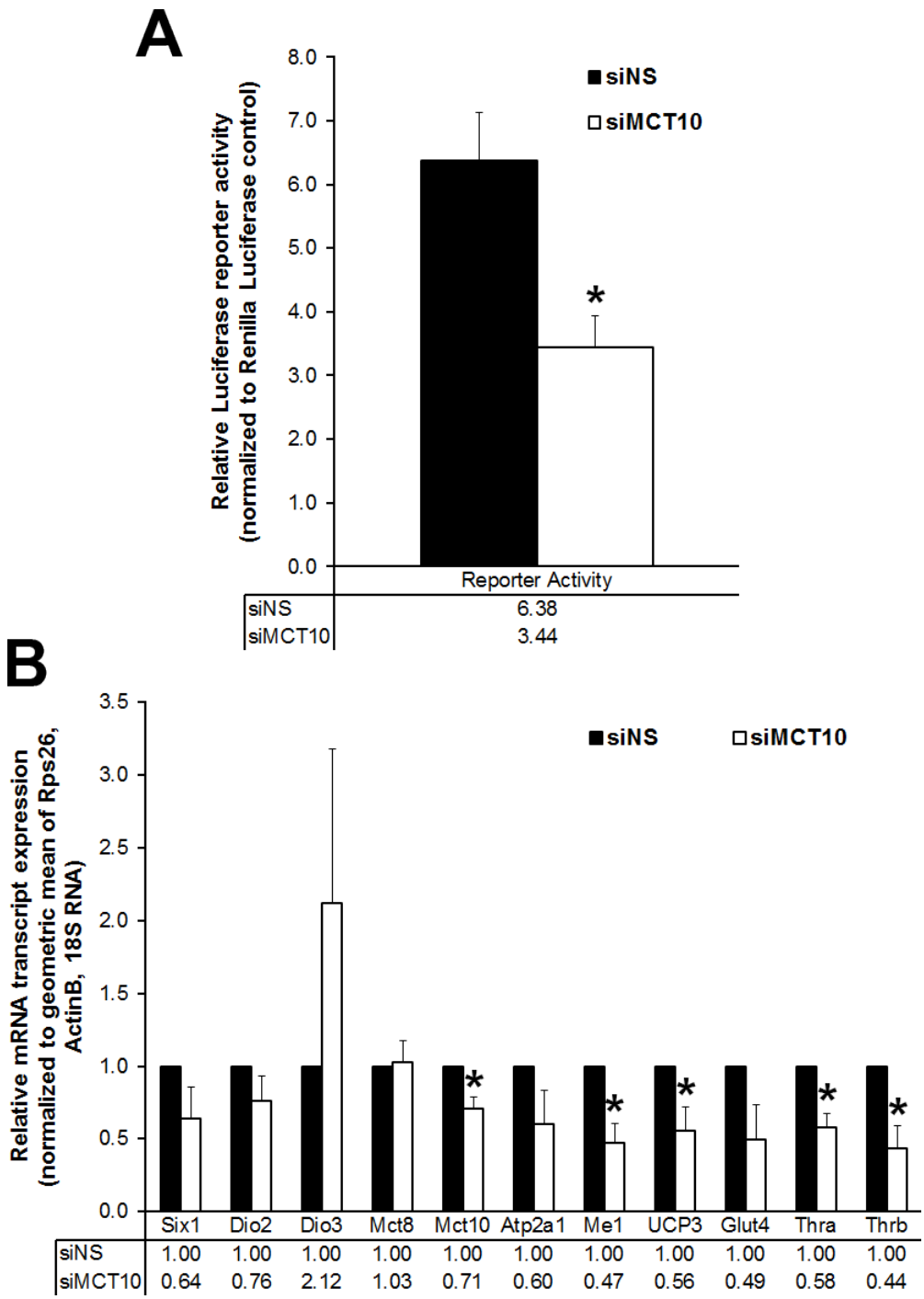

Figure 25: **Recapitulation of Thyroid pathway effects with siRNA targeting MCT10**

(A) Relative Luciferase activity in mouse electroporated TA muscle under MCT10 knockdown condition.

(B) Thyroid target genes mRNA expression levels in mouse electroporated TA muscle under MCT10 knockdown conditions quantified by qRT-PCR. mRNA levels were normalized to the geometric mean of Rps26, 18S and Beta-Actin. Data represents an average of 8 biological replicates (A) and 5 biological replicates (B). siNS represents a control siRNA targeting a non-specific sequence. Error bars indicate the SEM. * Represents statistically significant changes in levels of expression as determined by a Wilcoxon Rank-Sum test (A) or a one-tailed paired Student's T-Test (B) relative to siNS (p-value < 0.05).

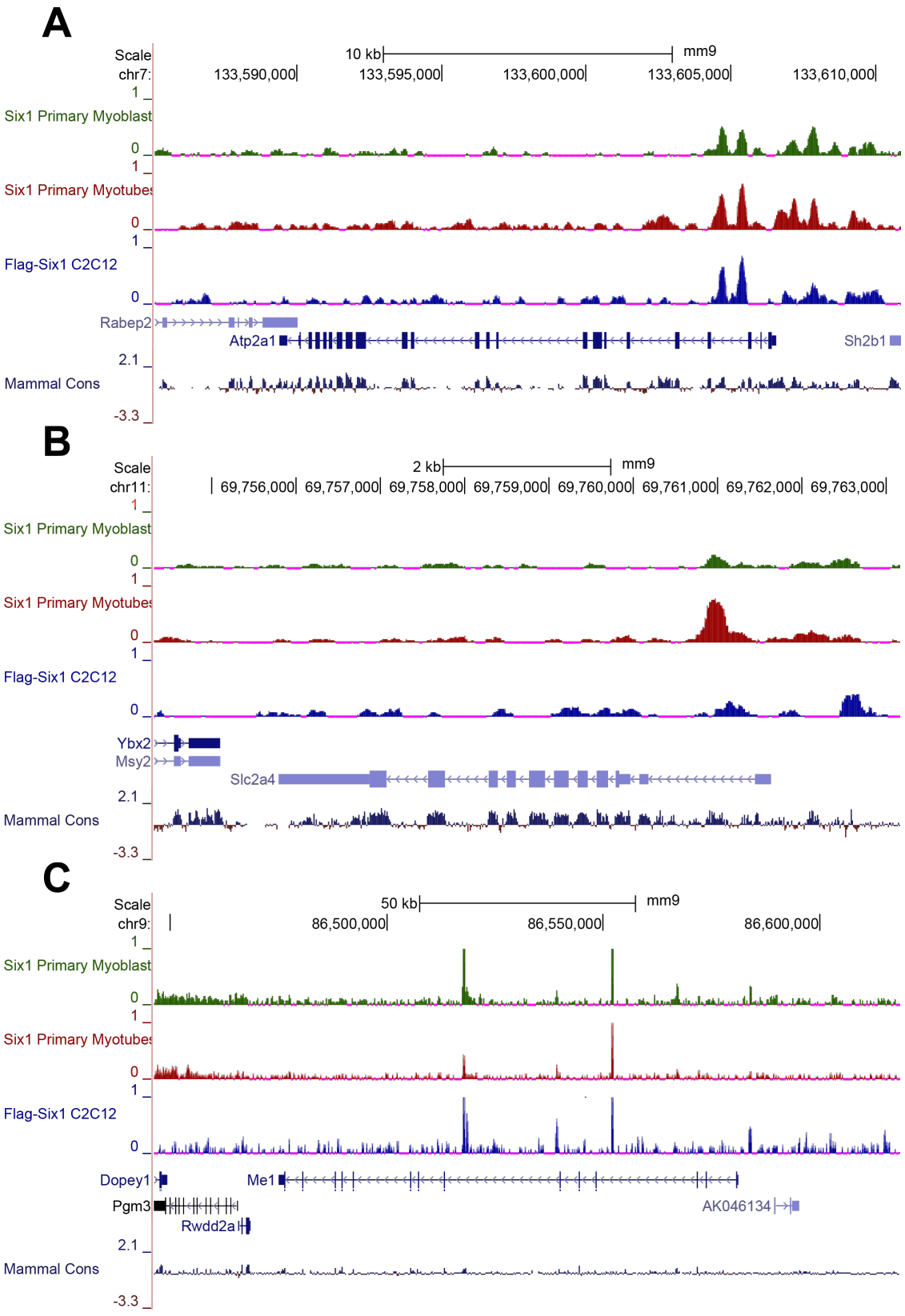

Figure 26: **Thyroid signaling pathway overlaps with Six1 regulome**
Peaks represent binding likelihood for Six1 in primary myoblasts (green), Six1 in primary myotubes (maroon), Flag-Six1 in growing C2C12 (navy). Analysis genes include (**A**) *Atp2a1*, (**B**) *Glut4*, also known as *Slc2a4*, and (**C**) *Me1*. Signals shown have an input ChIP-Seq sample subtracted.

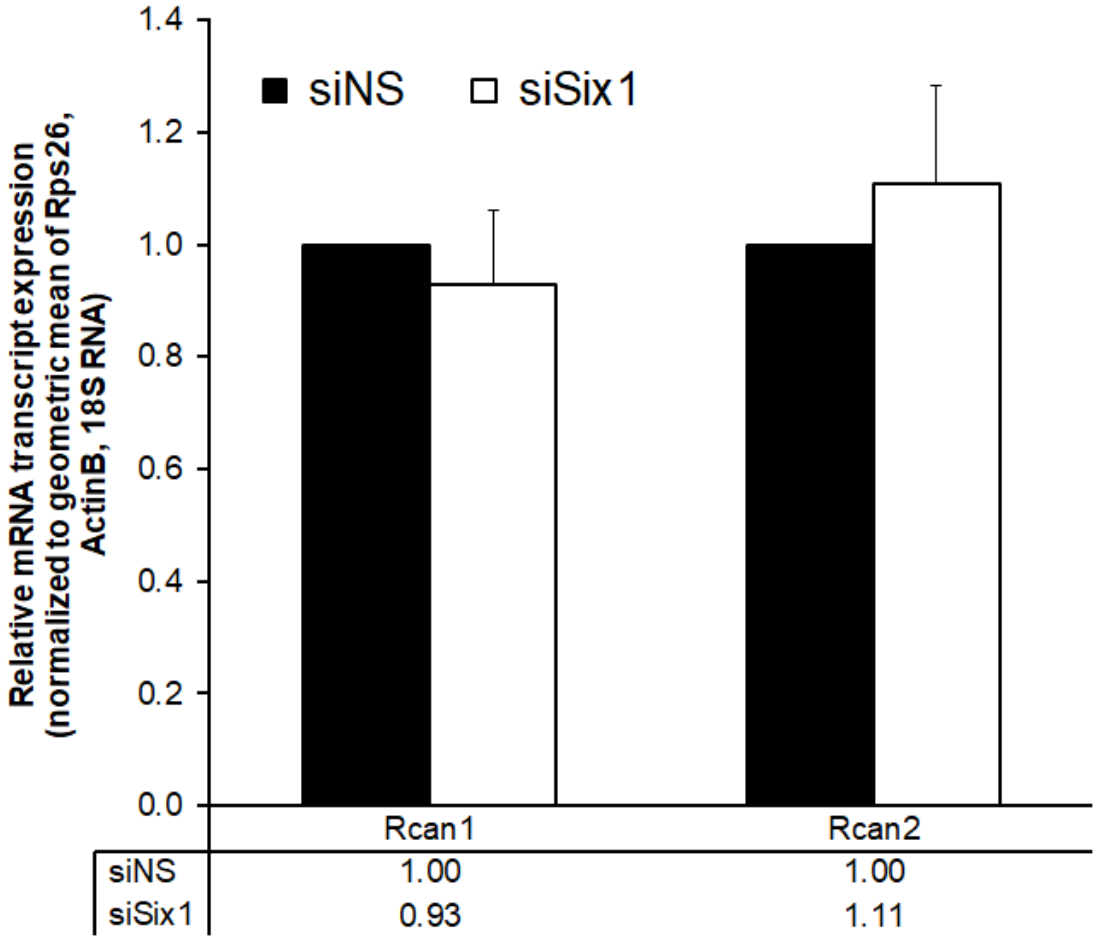

Figure 27: **Thyroid-regulated Rcan proteins are not affected by Six1 knockdown**
RCAN1/RCAN2 expression levels in electroporated mouse TA muscle, quantified by qRT-PCR. mRNA levels were normalized to the geometric mean of Rps26, 18S and Beta-Actin. Data represents an average of 7 biological replicates. siNS represents a control siRNA targeting a non-specific sequence. Error bars indicate the SEM.

Chapter 4

Discussion

In the research presented herein reliable methodology for the knockdown of the Six1 and Six4 TFs was achieved using electroporation-mediated siRNA interference, resulting in 80% Six1 protein level reduction, and 50% Six4 protein level reduction. Reduction of Six1, but not Six4, expression levels resulted in elevated Utrophin levels, with 28% mRNA upregulation and 2.5-fold protein upregulation. While elevated Utrophin expression is typical of slow-twitch muscle fibers, and antagonism of the Six TFs can induce a fiber-type switch towards slow-twitch muscle, analysis of Myosin isoform expression did not demonstrate an induction of Myosin type I expression at the mRNA or protein levels, but a reduction in Myosin type IIa, IIb, and IIx mRNA was detected. Investigation of alternative mechanisms responsible for the Utrophin level induction resulted in the discovery that Six1 regulates Myoz1 expression, an NFAT activity inhibitor, a known pathway that promotes Utrophin expression. Six1 knockdown reduced Myoz1 expression levels by 25% at both the mRNA and protein levels, and resulted in upregulation of four of six NFAT pathway target genes. Myoz1 knockdown was capable of recapitulating some, but not all, effects of Six1 knockdown, suggesting that it is downstream of some of the effects demonstrated. Finally, the regulatory role of Six1 on the thyroid hormone signaling pathway was investigated, with Six1 being

demonstrated to regulate MCT10 expression, a thyroid hormone transporter. Six1 knockdown reduced MCT10 mRNA expression by 35%, along with significant reduction of the expression of thyroid hormone regulated genes and thyroid receptors, and a significant upregulation of Dio3, a T_3 deactivating deiodinase. Six4 knockdown was incapable of recapitulating effects observed with Six1 knockdown, but MCT10 knockdown was able to recapitulate most effects observed suggesting its intermediary role between Six1 activity and the thyroid hormone signaling pathway in adult skeletal muscles. A schematic of the suggested regulatory networks involved can be found in Figure 28.

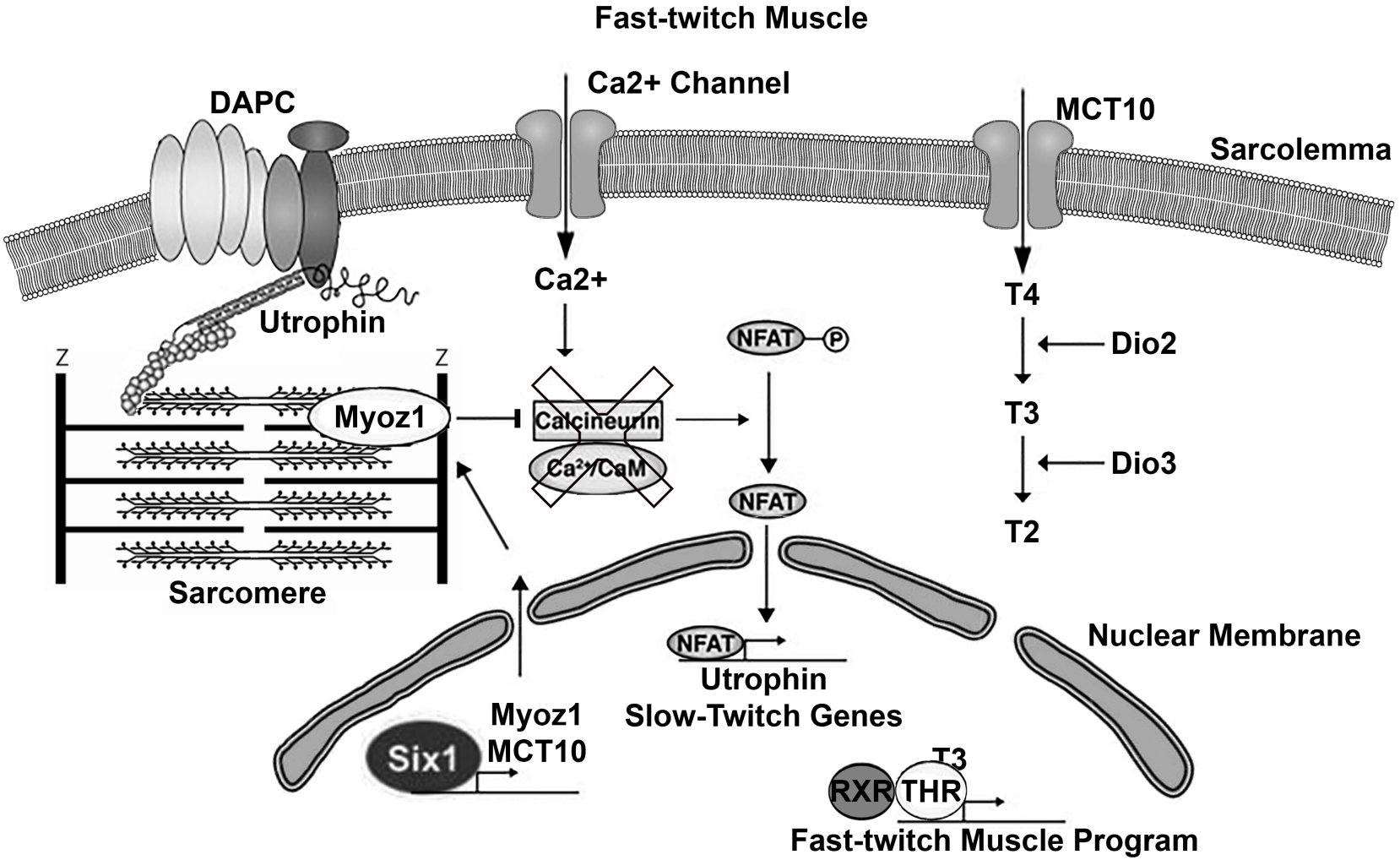

Figure 28: **Model of Six1 action in adult skeletal muscle homeostasis**
Representative methods of Six1 activity that drive phenotypes demonstrated within this research. Image adapted from (Frey et al., 2008; Batters et al., 2014).

4.1 Achieving Six TFs knockdown in skeletal muscle

Attempts to study the effects of Six TFs knockdown *in vitro* were unsuccessful, as in the absence of the Six TFs late differentiation and maturation of C2C12 Myotubes is inhibited (Figure 30). As such, the development of *in vivo* analysis methodologies was attempted. Three distinct electroporation methodologies were investigated for their potential to achieve Six TFs knockdown, with a timeline of the different methodologies listed in (Figure 3A). The electroporation timeline using Needle Array technology was capable of the highest transfection efficiency of a GFP encoding plasmid (Figure 3B), but resulted in an increased Six1 mRNA and protein expression level (Figure 4A, 5A). One explanation for this, is that the Needle Array electroporation condition expressed the highest amount of eMHC mRNA (Figure 4C), a regeneration marker, suggesting significant induction of muscle damage with this technology, a known disadvantage of electroporation methodologies in adult skeletal muscles (Collins et al., 2007). Considering Six1 expression is induced during the muscle regeneration process (Liu et al., 2010), this could explain why Needle Array electroporation knockdowns produced a contrary result to the experimental intent.

Tweertrodes electroporations (Figure 3A). While both experimental timelines, with either single-day electroporation or repeated multiple-day electroporations, induced much lower levels of eMHC mRNA expression when compared to Needle Array technology (Figure 4C), and were both capable of significantly reducing Six1 mRNA expression (27% and 40%, respectively) ((Figure 4A). More importantly, Six1 protein levels were significantly reduced (by over 80% of siNS electroporations) in the multiple-day Tweezertrodes electroporation condition, that relies on a second electroporation of siRNA on the third day of the experiment (Figure 4B & C). This could be due to the significantly lower transfection potential of single-day Tweezertrodes electroporations - with only about 30% of fibers successfully electroporated

with a plasmid using this methodology when compared to the 70% transfection efficiency of multiple-day Tweezertrodes electroporations (Figure 3B). This is an agreement with previous research that demonstrated increased transfection efficiency with repeated electroporations (Manthorpe et al., 1993). Additionally, Six1 mRNA may be expressed in excess, requiring a specific threshold of knockdown before protein levels are affected by the treatment, as previous research demonstrated Six1 protein knockdown at a similar level of 40% mRNA expression knockdown (Hetzler et al., 2014).

The data presented describes a methodology for consistent and successful knockdown of the Six TFs at both the mRNA and protein levels without the reliance on knockout models as previously described in the study of these TFs (Sakakibara et al., 2014; Sakakibara et al., 2016), and the resultant methodology was used for all subsequent experiments carried out in our research.

4.2 Six1 knockdown promotes Utrophin upregulation

qRT-PCR analysis of Utrophin mRNA expression levels demonstrated a significant 28% upregulation in Utrophin transcript levels (Figure 6A). This effect was seen with Multiple-day but not Single-day Tweezertrodes electroporation methodology, which is in agreement with the fact that this is the only knockdown methodology capable of reducing protein level expression of the Six TFs (Figure 5). Significant variability was present in the experimental results, with two samples not demonstrating Utrophin upregulation. Attempts to correlate magnitude of effect with magnitude of Six1 knockdown or damage induced as detected by eMHC expression were unsuccessful, raising the possibility of additional unknown confounding variables. Utrophin mRNA upregulation was not detected under Six4 knockdown condition, but was recapitulated under double Six1 and Six4

knockdown condition (Figure 7), suggesting a unique mechanism downstream of Six1, but not Six4, capable of regulating Utrophin mRNA expression.

Given that slow-twitch muscles expression are more resistant to the Dystrophic phenotype (Webster et al., 1988) due to innately increased Utrophin expression (Gramolini et al., 2001), we analyzed Utrophin expression levels in slow-twitch when compared to fast-twitch muscles to investigate the potential biological relevance of the observed Utrophin upregulation under Six1 knockdown condition. qRT-PCR analysis of unelectroporated slow-twitch (Soleus) and fast-twitch muscles (Gastrocnemius, TA) showed a slight 20% higher expression of Utrophin mRNA expression in slow-twitch muscle (Figure 6B). While previous research demonstrated 2-fold or higher expression of Utrophin mRNA in slow-twitch muscle (Gramolini et al., 2001; Chakkalakal et al., 2003), the research was conducted in the Extensor digitorum longus (EDL) muscle, while the TA has been shown to express Utrophin mRNA to about 95% of the Soleus expression levels (Risson et al., 2009). Gastrocnemius muscle is comprised of comparable levels of slow-twitch muscle fibers as TA muscle (Augusto et al., 2004), suggesting that it may express similar levels of Utrophin mRNA. Given the comparable magnitude of effect of Utrophin upregulation under Six1 knockdown condition, 28%, with the inherently higher expression of Utrophin in slow-twitch muscle, 23%, the possibility was raised of biological significance of the effect of Six1 regulatory effects on Utrophin expression.

Analysis of Utrophin protein expression was performed to elucidate the biological significance of the mRNA upregulation. Under Six1 knockdown condition, western blot densitometric analysis demonstrated a 2.5 fold upregulation of Utrophin protein level (Figure 8). While some samples did not demonstrate Utrophin protein change with Six1 knockdown, similar to the data obtained with mRNA analysis, there was a lack of correlation between magnitudes of Six1 knockdown and magnitudes of Utrophin protein

upregulation, again suggesting confounding factors in the analysis. Only one observed sample did not increase in Utrophin protein expression according to densitometric analysis (Figure 8B), with four samples demonstrating 1.5-fold protein expression upregulation, suggesting relative consistency in magnitude of effect. Discordance between magnitudes of Utrophin mRNA and protein upregulation indicates that while Six1 knockdown may indirectly affect Utrophin expression, it is possible that Six1 knockdown may also affect levels of proteins that regulate the translation of Utrophin mRNA and have not been identified yet. Additionally, the discordance between Utrophin mRNA and protein upregulation levels could be due to post-translational regulation of Utrophin, and is commonly seen in literature that attempts to force Utrophin expression upregulation (Ljubicic et al., 2011; Péladeau et al., 2015).

Taken together, our experimental treatment achieved 28% mRNA upregulation and 2.5-fold protein upregulation. Comparatively, AICAR treatment is capable of 25% mRNA upregulation and 2-fold protein upregulation (Ljubicic et al., 2011), Metformin treatment is capable of 1.5-fold protein upregulation (Ljubicic and Jasmin, 2015), SIRT1 treatment is capable of 1.8-fold mRNA overexpression (Chalkiadaki et al., 2014), Arginine Butyrate is capable of 1.5-fold protein upregulation (Vianello et al., 2013), mTOR inhibition is capable of 1.5-fold protein upregulation (Risson et al., 2009), small molecule compounds that target the Utrophin promoter increase mRNA expression by 1.5- to 2-fold (Khurana et al., 2012), and Heparin treatment is capable 1.8-fold protein upregulation but no mRNA upregulation in the TA muscle (Péladeau et al., 2015), hinting that Six1 inhibition is among the most potent targets for Utrophin upregulation strategies.

It is crucial to note, however, that a majority of referenced studies were carried out in the context of the *mdx* Dystrophic model mouse, which exhibits muscles in a state of constant regeneration. Effects observed with Six1 knockdown may be reduced when attempted in contexts with fewer expressed

adult muscle fibers. The possibility for differences between therapy potential between healthy and Dystrophic muscle is further highlighted by the fact that Utrophin upregulation in the literature is usually seen between 2 and 4 weeks post-treatment in *mdx* mice (Chakkalakal et al., 2003; Ljubicic et al., 2011; Péladeau et al., 2015), however, our aggressive experimental timeline displays Utrophin sarcolemmal localization 7 days post-electroporation. This alludes to the possibility that degenerating and regenerating muscle may require longer treatment timelines, and future experiments should study the potential for Six1 to regulate Utrophin expression in *mdx* mice, with analysis of force output and resistance to repeated contractions, as is the standard in the field to confirm functional benefits in the context of DMD (Tinsley et al., 1996).

Immunofluorescent analysis demonstrated localization of Utrophin protein to the sarcolemma of fibers in the TA muscle (Figure 9), with a staining pattern consistent with previously published research with therapeutically relevant Utrophin upregulation (Tinsley et al., 1998; Chakkalakal et al., 2003; Stupka et al., 2006). A 5-fold increase in sarcolemmal Utrophin was seen between Six1 knockdown and siNS conditions. While three of four analyzed samples demonstrated about a 3-fold increase in sarcolemmal Utrophin expression, one sample expressed a 10-fold increase, due to increased damaged area on the knockdown-treated leg causing a reduction in area of muscle analyzed, and inflating normalized numbers. The analyzed area of the injured muscle spanned 117μm^2 and contained 70 fibers expressing sarcolemmal Utrophin that fit the selection criteria, however, the control muscle spanned 942μm^2 and contained 50 fibers that satisfied the criteria. The overall discordance between immunofluorescent fold-change and western blot fold change could be explained due to a sampling difference. Western blots demonstrate the overall protein level changes in a whole muscle, while immunofluorescent sections represent local changes, suggesting that there may be regions of the experimentally treated muscles that display lower Utrophin

upregulation. While in healthy adult muscle Dystrophin occupies most DAPCs, and sarcolemmal Utrophin suggests some amount of displacement, both can coexist in one muscle sample under Utrophin upregulation (Tjondrokoesoemo et al., 2016), and crucially, Dystrophin immunofluorescence was not carried out so its status in our experimental samples is unknown. An important consideration is that the sarcolemmal localization of Utrophin was not demonstrated to overlap with α-Dystrobrevin, a known interactor with Utrophin within the DAPC (Figure 9A). Future work should aim to confirm this colocalization to further confirm the functional integration of Utrophin into the DAPC and the therapeutic potential of Utrophin upregulation in context of Six1 knockdown.

While the research presented herein demonstrates exciting potential for the use of Six1 antagonism in the context of Utrophin upregulation, it is important to note that a few important questions have yet to be addressed. One factor that remains unexplored is the potential for the Six1 knockdown methodology used here to allow for Six1 knockdown in satellite cells. Six1 is expressed in satellite cells and drives the expression of MRFs (Liu et al., 2013). Dystrophic muscle satellite cells are already susceptible to reduction in the frequency of asymmetrical division (Dumont et al., 2015) and expression of differentiation genes (Chang et al., 2018), so a chance exists that Six1 antagonism that is not myofiber-targeted could aggravate the Dystrophic phenotype in the context of muscle regeneration, by inhibiting the differentiation process. Methodologies to target adult fibers specifically during electroporations exist (Wong et al., 2005) and further studies on the differences within interaction patterns between the role of Six1 in myogenesis and in adult skeletal muscle homeostasis could shed light on drug-targetable interactions that could be disrupted in order to achieve targeted effects in adult skeletal muscles exclusively.

4.3 Six1 knockdown effect on Myosin expression

Given that Six1 antagonism has been demonstrated to promote a fiber-type switch from fast to slow (Niro et al., 2010; Sakakibara et al., 2014), and given that Utrophin is more highly expressed in slow-twitch than in fast-twitch muscle (Gramolini et al., 2001), the data suggested the possibility that a fiber-type switch may have occurred in our Six1 knockdown condition.

qRT-PCR analysis demonstrated the expected reduction in fast-twitch Myosin isoform IIb (Myh4) and Myosin isoforms IIa and IIx (Myh2 and Myh1, respectively) mRNA expression (Figure 10A). However, Myosin type I mRNA expression was unchanged between experimental and siNS conditions, refuting the possibility that a fiber-type switch towards a slow-twitch muscle phenotype had occurred. This is concordant with previous research that attempted to study Myosin isoform distribution with acute Six1 knockdown in adult muscle and concluded that Myosin type I was not induced 2 days post-electroporation (Hetzler et al., 2014). While our experimental timeline, with muscle harvest performed 7 days post-electroporation, studies the effects of Six1 knockdown at a latter timepoint, our employed aggressive experimental timeline could still being too short for Myosin isoform turnover. Research that concluded Six1 antagonism promotes Myosin type I expression typically used conditional knockout mice with a minimum 2-week period before harvest (Le Grand et al., 2012; Sakakibara et al., 2014).

Significantly, this downregulation of the fast Myosin Type IIa was not seen with immunofluorescent staining (Figure 11). This could be due to multiple factors. The most obvious is that the half-life of Myosin protein is estimated around 30 days (Kay, 1978), and the experimental timeline as explored wasn't sufficiently long, or a threshold of Myosin mRNA may exist, below which the protein levels also become significantly reduced. Notably, adult skeletal muscle fibers can express multiple simultaneous intracellular isoforms of Myosin (Banas et al., 2011). A significant reduction at the mRNA

level but not at the Myosin localization level may suggest an increase in fibers that exclusively express singular Myosin isoforms. In order to confirm if this is the case, western blot analysis or Myosin isoform co-staining could elucidate cases in which protein expression can align with the obtained mRNA results, with the relative proportion of fiber-types remaining unchanged. Myosin Type I expressing fibers were not differentially expressed between Six1 knockdown and siNS conditions (Figure 11), in agreement with results obtained in the qRT-PCR analysis, confirming the lack of a fiber-type switch.

This is not the first such case of fiber-type independent Utrophin upregulation, as the pharmaceutical drug SMT C1100 is capable of upregulating Utrophin expression in all skeletal muscles by increasing activity of its promoter (Tinsley et al., 2011). Similarly, all fibers express Utrophin during their regenerative process (Wilson et al., 1994) after which it is degraded and replaced by Dystrophin in late differentiation and healthy muscle, and some protease inhibitors have been shown to be capable of delaying or inhibiting this switch (Tjondrokoesoemo et al., 2016). One advantage of fiber type independent Utrophin upregulation is the clinical significance of not necessitating that patients over-express slow twitch skeletal muscle to supranatural levels, as would be required with fiber type specific treatments (Borders, 2016), suggesting Six1-regulated pathways may present a therapeutic target for Utrophin upregulation without the promotion of non-specific fiber-type modulation pathways.

4.4 Six1 knockdown promotes NFAT pathway activity

Utrophin expression regulation can occur transcriptionally and post-transcriptionally through Calcineurin/NFAT pathway (Chakkalakal et al., 2003; Chakkalakal et al., 2007), while post-translational regulation can occur through Calpain proteolysis (Gokhin et al., 2014) or through

biglycan-dependent localization (Amenta et al., 2011). Given that our data suggested mRNA involvement in Utrophin upregulation (Figure 6A), effects of Six1 knockdown on the NFAT pathway were investigated.

Six1 knockdown was capable of upregulating the expression of four of six genes in a panel of NFAT targets, suggesting increased pathway activity (Figure 12A). Six4 knockdown conditions were incapable of recapitulating the effects of Six1 knockdown on the panel of genes (Figure 13), suggesting the uniqueness of Six1 activity on the NFAT pathway. This is concordant with the previously observed result where Six1 knockdown conditions were uniquely capable of effecting Utrophin upregulation at the mRNA level (Figure 7), and suggest that the unique effects of Six1 knockdown on Utrophin expression may be mediated through NFAT pathway activity. Similarly, and in agreement, with Figure 7, double knockdown of both Six1 and Six4 was capable of inducing a trend towards increased NFAT pathway gene expression, with Zdbf2 being the only significantly upregulated gene with this condition. The inability to recapitulate the effects of Six1 knockdown could be due to sample variability being too large a confounding factor with the reduced number of replicates between double knockdown and Six1 knockdown conditions (5 biological replicates and 7 biological replicates, respectively). Myoglobin, or Mb, gene expression was significantly downregulated with both Six1 and Six4 single knockdown experiments, and trended towards lower expression in double knockdown conditions, suggesting that its regulation in fast-twitch skeletal muscle may be downstream of the Six TFs gene program, independent of the effects Six1 enacts on the NFAT pathway.

Given that the Six TFs are preferentially active in fast-twitch muscle (Sakakibara et al., 2016), and the NFAT TFs are more active in slow-twitch muscle (Calabria et al., 2009), inhibitors of the NFAT that are potential Six1 targets were investigated. Due to the lack of a fiber-type switch, and due to previous research demonstrating that the Calsarcin family of

inhibitors are the main elements regulating NFAT activity in fast-twitch muscle (Frey et al., 2000; Frey et al., 2004; Frey et al., 2008), an analysis of potential effects of Six1 knockdown on this family of inhibitors was conducted. A potential binding site for Six1 was found within the Calsarcin2 or Myoz1 locus (Figure 15), and consultation of microarray datasets demonstrated potential for the increased binding of Six1 to the Myoz1 locus upon differentiation to be transcriptionally functional (Figure 14). We demonstrate here that Six1 is capable of regulating the Calcineurin/NFAT inhibitor (Frey et al., 2008), Myoz1, expression *in vivo* (Figure 16, 17) at both the mRNA and protein levels. Myoz1 itself was shown to be expressed to higher levels in fast-twitch muscle (Figure 16A) in agreement with previous literature (Wang et al., 2006). This direct regulatory behavior of Myoz1 by Six1 is supported by the fact that in Six1 conditional knockout mice, Myoz1 is among the most downregulated genes in a microarray experiment (Sakakibara et al., 2016). While Myoz1 knockout mice have been demonstrated to express a higher proportion of slow-twitch muscle (Frey et al., 2008), we report here that Myoz1 level reduction is insufficient to recapitulate this phenotype. A longer experimental timeline may be necessary to confirm the effects of Myoz1 knockdown on fiber-type, however, as Six1 knockdown itself was similarly incapable of inducing a fiber-type switch in our experimental conditions.

Concordant with its potential action as a mediator between the Six TFs and the NFAT pathway, siRNA knockdown targeting Myoz1 is sufficient to recapitulate some effects of Six1 knockdown according to mRNA expression levels of targets determined through bioinformatic methods (Figures 12A and 18). Zdbf2 mRNA expression increases significantly, while Mef2D mRNA expression decreases significantly. Statistically significant effects were not observed with Atp1b4, Meg3 or Runx1, even though a trend could be seen towards an increase, suggesting that the current statistical resolution of the experiment may not be sufficient to tease out effects of the knockdown,

especially considering the use of only 4 biological replicates for this experiment, when compared to the 7 examined under Six1 knockdown conditions. Utrophin mRNA levels similarly did not increase, however, a negative correlation was observed with magnitude of Myoz1 knockdown when compared to magnitude of Utrophin mRNA expression, with an R^2 value of -0.74, and with the lowest Utrophin mRNA expression recorded with the sample demonstrating lowest magnitude of Myoz1 knockdown (Figure 18B).

It is interesting to note that while Six1 inhibits the NFAT pathway through Myoz1, published literature highlights an antagonistic relationship between MyoD and NFAT TFs in adult skeletal muscle (Ehlers et al., 2014). MyoD itself is in turn under Six1 regulation in certain contexts (Liu et al., 2010; Liu et al., 2013), suggesting multiple levels of regulation with which Six1 can inhibit NFAT pathway activity. Supporting this suggestion is the fact that a MyoD ChIP-Seq binding peak is observed neighboring the Six1 binding site in a publicly available dataset (Cao et al., 2010), highlighting the potential for cooperation of multiple TFs to suppress the slow-twitch phenotype. A future experiment could attempt a combinatorial approach of knockdown against both Six1 and MyoD in order to fully recapitulate effects seen in Myoz1 knockout mice (Frey et al., 2008).

4.5 Six1 effect on Thyroid hormone signaling pathway

A bioinformatics analysis (Figures 19 and 20) suggested that MCT10, a thyroid transporter expressed in skeletal muscle, may be a Six1 target. The ChIP-Seq profile near the gene locus contains multiple potential binding locations of the Six TFs across growing and differentiating cells highlighting the potential importance of regulating the expression of the transporter, especially in fast-twitch skeletal muscle (Figure 21, 22A). Adult skeletal muscles express two separate thyroid transporters, MCT8 and MCT10 (Mebis et al., 2009), but MCT8

knockout mice present with a relatively normal phenotype (Di Cosmo et al., 2013), suggesting that MCT10 may be the critical thyroid transporter in skeletal muscle. The full effects of antagonism of MCT10 is an open research question, considering its status as a thyroid hormone transporter. Given that both the Six and thyroid signaling pathways are required during development, raising the possibility that synchrony between the pathways may exist (Laclef et al., 2003a; Grifone et al., 2005; Xu et al., 2003; Weil, 1941), and suggesting biological significance of the regulation of MCT10 by Six1.

qRT-PCR and ChIP-qPCR confirmed positive *in vivo* regulation of MCT10 by Six1 (Figure 22B, C), implicating Six1 in thyroid pathway signaling. The proposed regulatory binding site for Six1 near the MCT10 locus *in vivo* is approximately 46kb upstream of the gene. While this is a significant distance away, enhancer sequences can exist upto a megabase away (Amano et al., 2009). Experiments to confirm the potential of the binding site to act as an enhancer could include chromosome conformation capture techniques, and even Clustered Regularly Interspaced Short Palindromic Repeats (CRISPR)-mediated mutagenesis of the binding site with subsequent qRT-PCR analysis.

Downstream of the transporter, the entire thyroid pathway seems to be negatively affected in Six1 knockdown condition. Dio3, a T_3 deactivating deiodonase, mRNA levels significantly increase (Figure 23A), indicating increased intracellular deactivation of thyroid hormone. Thyroid signaling targets in skeletal muscle responsible for calcium storage (Atp2a1) (Murphy et al., 2009), glucose transporter-mediated import (Glut4) (Goodyear et al., 1991), fatty acid biosynthesis (Me1) (Desvergne et al., 1991), and resting metabolic rate (UCP3) (Gong et al., 1997) decrease in expression. While these combined changes on genes downstream of thyroid hormone signaling represent a move towards a more slow-twitch representative expression profile for the thyroid signaling pathway (Figure 23B), two genes behave in an opposing fashion. Signficant decreases in thyroid receptor levels, associated

with thyroid responsiveness (Thra/Thrb) (Bahi et al., 2005), combined with the shift towards lower thyroid pathway activity, implies a broad negative impact on thyroid hormone signaling under Six1 knockdown conditions. It is also worthwhile to note that our obtained Myosin isoform expression profile at the mRNA level, with reduction in fast and intermediary forms of Myosin isoforms, but no change in slow-twitch Myosin type I expression (Figure 10) agrees with the expected distribution profile in hypothyroid conditions, with ablation of fast and intermediate Myosin isoforms but persistence of slow-twitch Myosin type I (Butler-Browne et al., 1984). While other targets such as MyoD and myogenin exist and can be studied, they are direct Six1 targets as well (Liu et al., 2013), complicating the potential for determining differences between thyroid-mediated effects and Six1-mediated gene expression changes.

qRT-PCR analysis of Six4 and double knockdown samples revealed conflicting results. Six4 knockdown was only capable of significantly downregulating Glut4 and Thrb gene expression levels, but not MCT10 levels (Figure 24A). This suggested that effects seen on Dio3, Atp2a1, UCP3, and Thra were unique to Six1 knockdown conditions. Double Six1 and Six4 knockdown meanwhile increased Dio2 and MCT8 expression significantly (Figure 24A). Considering the levels of Dio2 are induced in conditions of low serum T_4 levels (Mebis et al., 2007) and with excess insulin infusion (Mills et al., 1987). The upregulation of MCT8 but not MCT10 has been noted in chronically ill patients (Mebis et al., 2009). Taken together, the obtained profile of gene upregulation suggests aberrant intracellular signaling in the context of double Six1 and Six4 knockdown. The downregulation of Glut4 by Six4 and double knockdowns attempted suggests that glucose uptake regulation maybe a unique downstream of Six4, but not Six1, in adult fast-twitch skeletal muscle, independent of effects the TFs exert on the thyroid hormone signaling pathway.

In order to ensure that remaining effects are due to regulation of MCT10

by Six1, a knockdown experiment with siRNA targeting MCT10 was attempted. MCT10 knockdown was capable of recapitulating most effects of Six1 knockdown, with significant downregulation of Me1, UCP3, Thra, and Thrb (Figure 25B). Upregulation of Dio3 was not observed, but this is due to high variability across experimental samples and a lower number of biological replicates used in this experiment when compared to Six1 knockdown experiments (5 replicates as compared to 7, respectively). This experiment also represents the first suggestion that impacting MCT10 levels affects thyroid hormone signaling at the protein level. Crucially, MCT10 knockdown was capable of significantly downregulating the activity of a thyroid responsive luciferase reporter (Figure 25A), indicating that pathway activity may additionally be negatively regulated at the protein level, and highlighting the importance of MCT10 expression for thyroid hormone signaling.

A few key future experiments remain outstanding to confirm the effects of Six1 regulation of the thyroid hormone signaling pathway through MCT10. First and foremost, future experiments should aim to confirm protein expression modulation of targets in the thyroid pathway to affirm pathway downregulation. Additionally, future work should leverage available technologies to determine intracellular T_3 levels to confirm functional significance of the upregulation of Dio3 in conditions of Six1 knockdown (Bárez-López et al., 2014; Dentice et al., 2014). Fiber-type specific gene regulation downstream of thyroid hormone signaling, including Myosin isoform regulation, have been demonstrated to be mediated through miR-133a1 regulation by thyroid hormone (Zhang et al., 2014), and future studies can attempt to study the effect of Six1 knockdown on this micro-RNA.

It has been hypothesized that due to their distribution and size, changing the profile of skeletal muscle sensitivity or uptake of thyroid hormone can contribute to therapeutic research in hypo- or hyper-thyroidism by affecting serum hormone levels (Maia et al., 2005). This is supported by data showing

that global knockout of Dio2 is capable of increasing serum T_4 levels (Schneider et al., 2001), but is countered by data showing no changes in serum levels of thyroid hormone in skeletal muscle specific Dio2 knockout (Werneck-de Castro et al., 2015). The regulatory network elucidated here showing MCT10 as being a key transporter in the thyroid signaling pathway (Figure 25), and Six1 being a potent regulator (Figure 22), presents a new opportunity to study potential therapeutic modulators of serum thyroid levels. While it was demonstrated skeletal muscles may have difficulty in activating thyroid hormone intracellularly and present with a hypothyroid phenotype when lacking Dio2 (Bárez-López et al., 2014), the research did not take into account thyroid transporter, receptor or Dio3 expression levels. Our work demonstrates that thyroid regulation at all three levels is impacted in Six1 and MCT10 knockdown conditions (Figure 23).

4.6 Conclusion

In the research presented herein, two pathways acting downstream of Six1 were demonstrated to simultaneously suppress the slow-twitch gene program, through positive regulation of a repressor Myoz1, and promote the fast-twitch program, through positive regulation of a transporter, MCT10. These are two novel targets of Six1 described herein for the first time. While the effects of Six1 and Myoz1 knockout mice are well known and studied (Sakakibara et al., 2014; Sakakibara et al., 2016; Frey et al., 2008), the effects of their acute knockdown in adult skeletal muscle are reported here uniquely for the first time, demonstrating canonically slow-twitch gene program expression without an accompanying slow-twitch fiber-type switch, with potential for therapeutic relevance in DMD. MCT10 knockdown and an accompanying gene expression profile is reported here for the first time, demonstrating critical significance of its expression for thyroid hormone responsiveness, and its regulation by Six1.

Bibliography

Abitua, P. B., Gainous, T. B., Kaczmarczyk, A. N., Winchell, C. J., Hudson, C., Kamata, K., Nakagawa, M., Tsuda, M., Kusakabe, T. G. and Levine, M. (2015). The pre-vertebrate origins of neurogenic placodes. Nature *524*, 462–465. 14

Abmayr, S., Gregorevic, P., Allen, J. M. and Chamberlain, J. S. (2005). Phenotypic improvement of dystrophic muscles by rAAV/microdystrophin vectors is augmented by Igf1 codelivery. Molecular Therapy *12*, 441–450. 11

Amano, T., Sagai, T., Tanabe, H., Mizushina, Y., Nakazawa, H. and Shiroishi, T. (2009). Chromosomal dynamics at the Shh locus: limb bud-specific differential regulation of competence and active transcription. Developmental cell *16*, 47–57. 94

Amat, R., Planavila, A., Chen, S. L., Iglesias, R., Giralt, M. and Villarroya, F. (2009). SIRT1 controls the transcription of the peroxisome proliferator-activated receptor-γ co-activator-1α (PGC-1α) gene in skeletal muscle through the PGC-1α autoregulatory loop and interaction with MyoD. Journal of Biological Chemistry *284*, 21872–21880. 22

Ambrosio, R., Damiano, V., Sibilio, A., De Stefano, M. A., Avvedimento, V. E., Salvatore, D. and Dentice, M. (2013). Epigenetic control of type 2 and 3 deiodinases in myogenesis: role of Lysine-specific Demethylase enzyme and FoxO3. Nucleic acids research *41*, 3551–3562. 72

Amenta, A. R., Yilmaz, A., Bogdanovich, S., McKechnie, B. A., Abedi, M., Khurana, T. S. and Fallon, J. R. (2011). Biglycan recruits utrophin to the sarcolemma and counters dystrophic pathology in mdx mice. Proceedings of the National Academy of Sciences *108*, 762–767. 91

Ameziane-Le Hir, S., Paboeuf, G., Tascon, C., Hubert, J.-F., Le Rumeur, E., Vié, V. and Raguénès-Nicol, C. (2016). Dystrophin hot-spot mutants leading to Becker muscular dystrophy insert more deeply into membrane models than the native protein. Biochemistry *55*, 4018–4026. 6

Anderson, J. E., McIntosh, L. M., Moor, A. N. and Yablonka-Reuveni, Z. (1998). Levels of MyoD protein expression following injury of mdx and normal limb muscle are modified by thyroid hormone. Journal of Histochemistry & Cytochemistry *46*, 59–67. 23

Angus, L. M., Chakkalakal, J. V., Méjat, A., Eibl, J. K., Bélanger, G., Megeney, L. A., Chin, E. R., Schaeffer, L., Michel, R. N. and Jasmin, B. J. (2005).

Calcineurin-NFAT signaling, together with GABP and peroxisome PGC-1α, drives utrophin gene expression at the neuromuscular junction. American Journal of Physiology-Cell Physiology *289*, C908–C917. 12

Arechavala-Gomeza, V., Kinali, M., Feng, L., Guglieri, M., Edge, G., Main, M., Hunt, D., Lehovsky, J., Straub, V., Bushby, K. et al. (2010). Revertant fibres and dystrophin traces in Duchenne muscular dystrophy: implication for clinical trials. Neuromuscular Disorders *20*, 295–301. 9

Armand, A.-S., Bourajjaj, M., Martínez-Martínez, S., el Azzouzi, H., da Costa Martins, P. A., Hatzis, P., Seidler, T., Redondo, J. M. and De Windt, L. J. (2008). Cooperative synergy between NFAT and MyoD regulates myogenin expression and myogenesis. Journal of Biological Chemistry *283*, 29004–29010. 22

Asakura, A. (2012). Skeletal Muscle-derived Hematopoietic Stem Cells: Muscular Dystrophy Therapy by Bone Marrow Transplantation. Journal of stem cell research & therapy *Suppl 11*. 10

Augusto, V., Padovani, C. R. and Campos, G. R. (2004). Skeletal muscle fiber types in C57BL6J mice. Braz J Morphol Sci *21*, 89–94. 47, 50, 85

Bahi, L., Garnier, A., Fortin, D., Serrurier, B., Veksler, V., Bigard, A. and Ventura-Clapier, R. (2005). Differential effects of thyroid hormones on energy metabolism of rat slow-and fast-twitch muscles. Journal of cellular physiology *203*, 589–598. 72, 95

Banas, K., Clow, C., Jasmin, B. J. and Renaud, J.-M. (2011). The KATP channel Kir6. 2 subunit content is higher in glycolytic than oxidative skeletal muscle fibers. American Journal of Physiology-Regulatory, Integrative and Comparative Physiology *301*, R916–R925. 2, 89

Bárez-López, S., Bosch-García, D., Gómez-Andrés, D., Pulido-Valdeolivas, I., Montero-Pedrazuela, A., Obregon, M. J. and Guadaño-Ferraz, A. (2014). Abnormal motor phenotype at adult stages in mice lacking type 2 deiodinase. PloS one *9*, e103857. 96, 97

Batters, C., Veigel, C., Homsher, E. and Sellers, J. R. (2014). To understand muscle you must take it apart. Frontiers in physiology *5*. 26, 82

Belanto, J. J., Olthoff, J. T., Mader, T. L., Chamberlain, C. M., McCourt, P. M., Talsness, D. M., Gundersen, G. G., Lowe, D. A., Ervasti, J. M. et al. (2016). Independent variability of microtubule perturbations associated with dystrophinopathy. Human molecular genetics *25*, 4951–4961. 6

Bhat, H. F., Mir, S. S., Dar, K. B., Bhat, Z. F., Shah, R. A. and Ganai, N. A. (2017). ABC of multifaceted Dystrophin glycoprotein complex (DGC). Journal of Cellular Physiology *232*. 6

Bianco, A. C., Salvatore, D., Gereben, B., Berry, M. J. and Larsen, P. R. (2002). Biochemistry, cellular and molecular biology, and physiological roles of the iodothyronine selenodeiodinases. Endocrine reviews *23*, 38–89. 23

Biggar, W. D., Gingras, M., Fehlings, D. L., Harris, V. A. and Steele, C. A. (2001). Deflazacort treatment of Duchenne muscular dystrophy. The Journal of pediatrics *138*, 45–50. 8

Bione, S., Maestrini, E., Rivella, S., Mancini, M., Regis, S., Romeo, G. and Toniolo, D. (1994). Identification of a novel X-linked gene responsible for Emery-Dreifuss muscular dystrophy. Nature genetics *8*, 323. 4

Blaauw, B., Mammucari, C., Toniolo, L., Agatea, L., Abraham, R., Sandri, M., Reggiani, C. and Schiaffino, S. (2008). Akt activation prevents the force drop induced by eccentric contractions in dystrophin-deficient skeletal muscle. Human molecular genetics *17*, 3686–3696. 5

Bladen, C. L., Salgado, D., Monges, S., Foncuberta, M. E., Kekou, K., Kosma, K., Dawkins, H., Lamont, L., Roy, A. J., Chamova, T., Guergueltcheva, V., Chan, S., Korngut, L., Campbell, C., Dai, Y., Wang, J., Bariši , N., Brabec, P., Lahdetie, J., Walter, M. C., Schreiber-Katz, O., Karcagi, V., Garami, M., Viswanathan, V., Bayat, F., Buccella, F., Kimura, E., Koeks, Z., van den Bergen, J. C., Rodrigues, M., Roxburgh, R., Lusakowska, A., Kostera-Pruszczyk, A., Zimowski, J., Santos, R., Neagu, E., Artemieva, S., Rasic, V. M., Vojinovic, D., Posada, M., Bloetzer, C., Jeannet, P.-Y., Joncourt, F., Díaz-Manera, J., Gallardo, E., Karaduman, A. A., Topaloğlu, H., El Sherif, R., Stringer, A., Shatillo, A. V., Martin, A. S., Peay, H. L., Bellgard, M. I., Kirschner, J., Flanigan, K. M., Straub, V., Bushby, K., Verschuuren, J., Aartsma-Rus, A., Béroud, C. and Lochmüller, H. (2015). The TREAT-NMD DMD Global Database: analysis of more than 7,000 Duchenne muscular dystrophy mutations. Human mutation *36*, 395–402. 8, 9

Blais, A., Tsikitis, M., Acosta-Alvear, D., Sharan, R., Kluger, Y. and Dynlacht, B. D. (2005). An initial blueprint for myogenic differentiation. Genes & development *19*, 553–569. 18

Boelen, A., van der Spek, A. H., Bloise, F., de Vries, E. M., Surovtseva, O. V., van Beeren, M., Ackermans, M. T., Kwakkel, J. and Fliers, E. (2017). Tissue thyroid hormone metabolism is differentially regulated during illness in mice. Journal of Endocrinology *233*, 25–36. 23

Bonuccelli, G., Sotgia, F., Schubert, W., Park, D. S., Frank, P. G., Woodman, S. E., Insabato, L., Cammer, M., Minetti, C. and Lisanti, M. P. (2003). Proteasome inhibitor (MG-132) treatment of mdx mice rescues the expression and membrane localization of dystrophin and dystrophin-associated proteins. The American journal of pathology *163*, 1663–1675. 11

Borders, L. F. (2016). Electrical Stimulation Use in Duchenne Muscular Dystrophy-An Evidence Based Analysis. University of New Mexico Digital Repository *1*. 90

Bridge, A. J., Pebernard, S., Ducraux, A., Nicoulaz, A.-L. and Iggo, R. (2003). Induction of an interferon response by RNAi vectors in mammalian cells. Nature genetics *34*, 263. 40

Briggs, D. and Morgan, J. E. (2013). Recent progress in satellite cell/myoblast engraftment – relevance for therapy. The FEBS journal *280*, 4281–4293. 10

Bryson-Richardson, R. J. and Currie, P. D. (2008). The genetics of vertebrate myogenesis. Nature Reviews Genetics *9*, 632–646. 18

Buckingham, M. and Relaix, F. (2007). The role of Pax genes in the development of tissues and organs: Pax3 and Pax7 regulate muscle progenitor cell functions. Annu. Rev. Cell Dev. Biol. *23*, 645–673. 16

Buckingham, M. and Rigby, P. W. (2014). Gene regulatory networks and transcriptional mechanisms that control myogenesis. Developmental cell *28*, 225–238. 18

Buller, A., Eccles, J. C. and Eccles, R. M. (1960). Interactions between motoneurones and muscles in respect of the characteristic speeds of their responses. The Journal of physiology *150*, 417–439. 19

Bushby, K., Finkel, R., Wong, B., Barohn, R., Campbell, C., Comi, G. P., Connolly, A. M., Day, J. W., Flanigan, K. M., Goemans, N. et al. (2014). Ataluren treatment of patients with nonsense mutation dystrophinopathy. Muscle & nerve *50*, 477–487. 10

Butler-Browne, G. S., Herlicoviez, D. and Whalen, R. G. (1984). Effects of hypothyroidism on myosin isozyme transitions in developing rat muscle. FEBS letters *166*, 71–75. 95

Calabria, E., Ciciliot, S., Moretti, I., Garcia, M., Picard, A., Dyar, K. A., Pallafacchina, G., Tothova, J., Schiaffino, S. and Murgia, M. (2009). NFAT isoforms control activity-dependent muscle fiber type specification. Proceedings of the National Academy of Sciences *106*, 13335–13340. 21, 91

Cao, Y., Kumar, R. M., Penn, B. H., Berkes, C. A., Kooperberg, C., Boyer, L. A., Young, R. A. and Tapscott, S. J. (2006). Global and gene-specific analyses show distinct roles for Myod and Myog at a common set of promoters. The EMBO journal *25*, 502–511. 18

Cao, Y., Yao, Z., Sarkar, D., Lawrence, M., Sanchez, G. J., Parker, M. H., MacQuarrie, K. L., Davison, J., Morgan, M. T., Ruzzo, W. L. et al. (2010). Genome-wide MyoD binding in skeletal muscle cells: a potential for broad cellular reprogramming. Developmental cell *18*, 662–674. 93

Carmignac, V., Quéré, R. and Durbeej, M. (2011). Proteasome inhibition improves the muscle of laminin 2 chain-deficient mice. Human molecular genetics *20*, 541–552. 11

Carnac, G., Albagli-Curiel, O., Vandromme, M., Pinset, C., Montarras, D., Laudet, V. and Bonnieu, A. (1992). 3, 5, 3'-Triiodothyronine positively regulates both MyoD1 gene transcription and terminal differentiation in C2 myoblasts. Molecular Endocrinology *6*, 1185–1194. 23

Carr, S. J., Zahedi, R. P., Lochmüller, H. and Roos, A. (2017). Mass spectrometry-based protein analysis to unravel the tissue pathophysiology in Duchenne muscular dystrophy. Proteomics. Clinical applications *12*. 7

Chakkalakal, J. V., Harrison, M.-A., Carbonetto, S., Chin, E., Michel, R. N. and Jasmin, B. J. (2003). Stimulation of calcineurin signaling attenuates the dystrophic pathology in mdx mice. Human molecular genetics *13*, 379–388. 13, 14

Chakkalakal, J. V., Miura, P., Belanger, G., Michel, R. N. and Jasmin, B. J. (2007). Modulation of utrophin A mRNA stability in fast versus slow muscles via an AU-rich element and calcineurin signaling. Nucleic acids research *36*, 826–838. 90

Chakkalakal, J. V., Stocksley, M. A., Harrison, M.-A., Angus, L. M., Deschênes-Furry, J., St-Pierre, S., Megeney, L. A., Chin, E. R., Michel, R. N. and Jasmin, B. J. (2003). Expression of utrophin A mRNA correlates with the oxidative capacity of skeletal muscle fiber types and is regulated by calcineurin/NFAT signaling. Proceedings of the National Academy of Sciences *100*, 7791–7796. 12, 21, 25, 47, 50, 53, 85, 87, 90

Chakroun, I., Yang, D., Girgis, J., Gunasekharan, A., Phenix, H., Kærn, M. and Blais, A. (2015). Genome-wide association between Six4, MyoD, and the histone demethylase Utx during myogenesis. FASEB journal : official publication of the Federation of American Societies for Experimental Biology *29*, 4738–4755. 18, 69

Chalkiadaki, A., Igarashi, M., Nasamu, A. S., Knezevic, J. and Guarente, L. (2014). Muscle-specific SIRT1 gain-of-function increases slow-twitch fibers and ameliorates pathophysiology in a mouse model of duchenne muscular dystrophy. PLoS genetics *10*, e1004490. 86

Chan, M. C., Rowe, G. C., Raghuram, S., Patten, I. S., Farrell, C. and Arany, Z. (2014). Post-natal induction of PGC-1α protects against severe muscle dystrophy independently of utrophin. Skeletal muscle *4*, 2. 12

Chang, N. C., Sincennes, M.-C., Chevalier, F. P., Brun, C. E., Lacaria, M., Segalés, J., Muñoz-Cánovez, P., Ming, H. and Rudnicki, M. A. (2018). The Dystrophin Glycoprotein Complex Regulates the Epigenetic Activation of Muscle Stem Cell Commitment. Cell Stem Cell *23*. 7, 88

Chen, L., Glover, J. M., Hogan, P. G., Rao, A. and Harrison, S. C. (1998). Structure of the DNA-binding domains from NFAT, Fos and Jun bound specifically to DNA. Nature *392*, 42–48. 21

Chen, R., Amoui, M., Zhang, Z. and Mardon, G. (1997). Dachshund and eyes absent proteins form a complex and function synergistically to induce ectopic eye development in Drosophila. Cell *91*, 893–903. 15

Chiappalupi, S., Luca, G., Mancuso, F., Madaro, L., Fallarino, F., Nicoletti, C., Calvitti, M., Arato, I., Falabella, G., Salvadori, L., Di Meo, A., Bufalari, A., Giovagnoli, S., Calafiore, R., Donato, R. and Sorci, G. (2016). Intraperitoneal injection of microencapsulated Sertoli cells restores muscle morphology and performance in dystrophic mice. Biomaterials *75*, 313–326. 13

Chin, E. R., Olson, E. N., Richardson, J. A., Yang, Q., Humphries, C., Shelton, J. M., Wu, H., Zhu, W., Bassel-Duby, R. and Williams, R. S. (1998). A calcineurin-dependent transcriptional pathway controls skeletal muscle fiber type. Genes & development *12*, 2499–2509. 19, 53

Cho, C.-H., Choi, J.-H., Kang, S.-G., Yoon, H.-K., Park, Y.-M., Moon, J.-H., Jung, K.-Y., Han, J.-K., Shin, H.-B., Noh, H. J., Koo, Y. S., Kim, L., Woo, H. G. and Lee, H.-J. (2017). A Genome-Wide Association Study Identifies UTRN Gene Polymorphism for Restless Legs Syndrome in a Korean Population. Psychiatry Investigation *14*, 830. 12

Chow, C.-W. and Davis, R. J. (2000). Integration of calcium and cyclic AMP signaling pathways by 14-3-3. Molecular and cellular biology *20*, 702–712. 21

Collins, J. M., Despa, F. and Lee, R. C. (2007). Structural and functional recovery of electropermeabilized skeletal muscle in-vivo after treatment with surfactant poloxamer 188. Biochimica et Biophysica Acta (BBA)-Biomembranes *1768*, 1238–1246. 83

Condon, K., Silberstein, L., Blau, H. M. and Thompson, W. J. (1990). Differentiation of fiber types in aneural musculature of the prenatal rat hindlimb. Developmental biology *138*, 275–295. 19

Cossu, G., Previtali, S. C., Napolitano, S., Cicalese, M. P., Tedesco, F. S., Nicastro, F., Noviello, M., Roostalu, U., Natali Sora, M. G., Scarlato, M., De Pellegrin, M., Godi, C., Giuliani, S., Ciotti, F., Tonlorenzi, R., Lorenzetti, I., Rivellini, C., Benedetti, S., Gatti, R., Marktel, S., Mazzi, B., Tettamanti, A., Ragazzi, M., Imro, M. A., Marano, G., Ambrosi, A., Fiori, R., Sormani, M. P., Bonini, C., Venturini, M., Politi, L. S., Torrente, Y. and Ciceri, F. (2015). Intra-arterial transplantation of HLA-matched donor mesoangioblasts in Duchenne muscular dystrophy. EMBO molecular medicine *7*, 1513–1528. 10

Davies, K. J., Ermak, G., Rothermel, B. A., Pritchard, M., Heitman, J., Ahnn, J., Henrique-Silva, F., Crawford, D., Canaider, S., Strippoli, P. et al. (2007). Renaming the DSCR1/Adapt78 gene family as RCAN: regulators of calcineurin. The FASEB Journal *21*, 3023–3028. 21, 76

Dellavalle, A., Sampaolesi, M., Tonlorenzi, R., Tagliafico, E., Sacchetti, B., Perani, L., Innocenzi, A., Galvez, B. G., Messina, G., Morosetti, R. et al. (2007). Pericytes of human skeletal muscle are myogenic precursors distinct from satellite cells. Nature cell biology *9*, 255–267. 18

Dentice, M., Ambrosio, R., Damiano, V., Sibilio, A., Luongo, C., Guardiola, O., Yennek, S., Zordan, P., Minchiotti, G., Colao, A. et al. (2014). Intracellular inactivation of thyroid hormone is a survival mechanism for muscle stem cell proliferation and lineage progression. Cell metabolism *20*, 1038–1048. 23, 96

Dentice, M., Marsili, A., Ambrosio, R., Guardiola, O., Sibilio, A., Paik, J.-H., Minchiotti, G., DePinho, R. A., Fenzi, G., Larsen, P. R. et al. (2010). The FoxO3/type 2 deiodinase pathway is required for normal mouse myogenesis and muscle regeneration. The Journal of clinical investigation *120*, 4021. 23

Desvergne, B., Petty, K. J. and Nikodem, V. M. (1991). Functional characterization and receptor binding studies of the malic enzyme thyroid hormone response element. Journal of Biological Chemistry *266*, 1008–1013. *72*, 94

Di Cosmo, C., Liao, X.-H., Ye, H., Ferrara, A. M., Weiss, R. E., Refetoff, S. and Dumitrescu, A. M. (2013). Mct8-deficient mice have increased energy expenditure and reduced fat mass that is abrogated by normalization of serum T3 levels. Endocrinology *154*, 4885–4895. *67*, 94

Downes, M., Griggs, R., Atkins, A., Olson, E. and Muscat, G. (1993). Identification of a thyroid hormone response element in the mouse myogenin gene: characterization of the thyroid hormone and retinoid X receptor heterodimeric binding site. Cell growth and differentiation *4*, 901–901. *23*

Drachman, D., Toyka, K. and Myer, E. (1974). Prednisone in Duchenne muscular dystrophy. The Lancet *304*, 1409–1412. 8

Dubowitz, V. (1965). Intellectual impairment in muscular dystrophy. Archives of disease in childhood *40*, 296. *7*

Dumont, N. A., Wang, Y. X., von Maltzahn, J., Pasut, A., Bentzinger, C. F., Brun, C. E. and Rudnicki, M. A. (2015). Dystrophin expression in muscle stem cells regulates their polarity and asymmetric division. Nature medicine *21*, 1455–1463. *7*, 88

Dupont, J.-B. (2016). Restriction Factors Against Recombinant Adeno-associated Virus Vectormediated Gene Transfer in Dystrophin-deficient Muscles. Current gene therapy *16*, 168–183. 9

Ehlers, M. L., Celona, B. and Black, B. L. (2014). NFATc1 controls skeletal muscle fiber type and is a negative regulator of MyoD activity. Cell reports *8*, 1639–1648. *22*, 93

Ervasti, J. M., Ohlendieck, K., Kahl, S. D., Gaver, M. G. and Campbell, K. P. (1990). Deficiency of a glycoprotein component of the dystrophin complex in dystrophic muscle. Nature *345*, 315. 5

Fallon, J. R. and McNally, E. M. (2018). Biglycan and LTBP4: Leveraging the extracellular matrix for Duchenne Muscular Dystrophy therapeutics. Matrix Biology *67*. 13

Feng, X., Jiang, Y., Meltzer, P. and Yen, P. M. (2000). Thyroid hormone regulation of hepatic genes in vivo detected by complementary DNA microarray. Molecular Endocrinology *14*, 947–955. *23*

Ferrari, G., Angelis, D., Coletta, M., Paolucci, E., Stornaiuolo, A., Cossu, G., Mavilio, F. et al. (1998). Muscle regeneration by bone marrow-derived myogenic progenitors. Science *279*, 1528–1530. 18

Filareto, A., Rinaldi, F., Arpke, R. W., Darabi, R., Belanto, J. J., Toso, E. A., Miller, A. Z., Ervasti, J. M., McIvor, R. S., Kyba, M. and Perlingeiro, R. C. (2015). Pax3-induced expansion enables the genetic correction of dystrophic satellite cells. Skeletal muscle *5*, 36. 10

Finkel, R. S., Flanigan, K. M., Wong, B., Bönnemann, C., Sampson, J., Sweeney, H. L., Reha, A., Northcutt, V. J., Elfring, G., Barth, J. et al. (2013). Phase 2a study of ataluren-mediated dystrophin production in patients with nonsense mutation Duchenne muscular dystrophy. PloS one *8*, e81302. 10

Frey, N., Barrientos, T., Shelton, J. M., Frank, D., Rütten, H., Gehring, D., Kuhn, C., Lutz, M., Rothermel, B., Bassel-Duby, R. et al. (2004). Mice lacking calsarcin-1 are sensitized to calcineurin signaling and show accelerated cardiomyopathy in response to pathological biomechanical stress. Nature medicine *10*, 1336–1343. 92

Frey, N., Frank, D., Lippl, S., Kuhn, C., Kögler, H., Barrientos, T., Rohr, C., Will, R., Müller, O. J., Weiler, H. et al. (2008). Calsarcin-2 deficiency increases exercise capacity in mice through calcineurin/NFAT activation. The Journal of clinical investigation *118*, 3598. 21, 26, 60, 82, 92, 93, 97

Frey, N., Richardson, J. A. and Olson, E. N. (2000). Calsarcins, a novel family of sarcomeric calcineurin-binding proteins. Proceedings of the National Academy of Sciences *97*, 14632–14637. 21, 57, 60, 92

Frontera, W. R. and Ochala, J. (2015). Skeletal muscle: a brief review of structure and function. Calcified tissue international *96*, 183–195. 2

Fujimoto, Y., Tanaka, S. S., Yamaguchi, Y. L., Kobayashi, H., Kuroki, S., Tachibana, M., Shinomura, M., Kanai, Y., Morohashi, K.-i., Kawakami, K. et al. (2013). Homeoproteins Six1 and Six4 regulate male sex determination and mouse gonadal development. Developmental cell *26*, 416–430. 15

Fulle, S., Protasi, F., Di Tano, G., Pietrangelo, T., Beltramin, A., Boncompagni, S., Vecchiet, L. and Fanò, G. (2004). The contribution of reactive oxygen species to sarcopenia and muscle ageing. Experimental gerontology *39*, 17–24. 2

Ghahramani Seno, M. M., Graham, I. R., Athanasopoulos, T., Trollet, C., Pohlschmidt, M., Crompton, M. R. and Dickson, G. (2008). RNAi-mediated knockdown of dystrophin expression in adult mice does not lead to overt muscular dystrophy pathology. Human molecular genetics *17*, 2622–2632. 6, 10

Gloss, D., Moxley, R. T., Ashwal, S. and Oskoui, M. (2016). Practice guideline update summary: Corticosteroid treatment of Duchenne muscular dystrophy Report of the Guideline Development Subcommittee of the American Academy of Neurology. Neurology *86*, 465–472. 8

Gokhin, D. S., Tierney, M. T., Sui, Z., Sacco, A. and Fowler, V. M. (2014). Calpain-mediated proteolysis of tropomodulin isoforms leads to thin filament elongation in dystrophic skeletal muscle. Molecular biology of the cell *25*, 852–865. 90

Gollnick, P., Armstrong, R., Saubert 4th, C., Piehl, K. and Saltin, B. (1972). Enzyme activity and fiber composition in skeletal muscle of untrained and trained men. Journal of applied physiology *33*, 312–319. 19

Gong, D.-W., He, Y., Karas, M. and Reitman, M. (1997). Uncoupling protein-3 is a mediator of thermogenesis regulated by thyroid hormone, β3-adrenergic agonists, and leptin. Journal of Biological Chemistry *272*, 24129–24132. 94

Gonzalez, J. P., Kyrychenko, S., Kyrychenko, V., Schneider, J. S., Granier, C. J., Himelman, E., Lahey, K. C., Zhao, Q., Yehia, G., Tao, Y.-X. et al. (2017). Small Fractions of Muscular Dystrophy Embryonic Stem Cells Yield Severe Cardiac and Skeletal Muscle Defects in Adult Mouse Chimeras. STEM CELLS *35*, 597–610. 7

Goodyear, L. J., Hirshman, M. F., Smith, R. J. and Horton, E. S. (1991). Glucose transporter number, activity, and isoform content in plasma membranes of red and white skeletal muscle. American Journal of Physiology-Endocrinology And Metabolism *261*, E556–E561. 94

Gordon, B. S., Díaz, D. C. D. and Kostek, M. C. (2013). Resveratrol decreases inflammation and increases utrophin gene expression in the mdx mouse model of Duchenne muscular dystrophy. Clinical nutrition *32*, 104–111. 13

Goyenvalle, A., Vulin, A., Fougerousse, F., Leturcq, F., Kaplan, J.-C., Garcia, L. and Danos, O. (2004). Rescue of dystrophic muscle through U7 snRNA-mediated exon skipping. Science *306*, 1796–1799. 10

Graef, I. A., Wang, F., Charron, F., Chen, L., Neilson, J., Tessier-Lavigne, M. and Crabtree, G. R. (2003). Neurotrophins and netrins require calcineurin/NFAT signaling to stimulate outgrowth of embryonic axons. Cell *113*, 657–670. 20

Gramolini, A. O., Angus, L. M., Schaeffer, L., Burton, E. A., Tinsley, J. M., Davies, K. E., Changeux, J.-P. and Jasmin, B. J. (1999). Induction of utrophin gene expression by heregulin in skeletal muscle cells: role of the N-box motif and GA binding protein. Proceedings of the National Academy of Sciences *96*, 3223–3227. 12

Gramolini, A. O., Bélanger, G., Thompson, J. M., Chakkalakal, J. V. and Jasmin, B. J. (2001). Increased expression of utrophin in a slow vs. a fast muscle involves posttranscriptional events. American journal of physiology. Cell physiology *281*, C1300–C1309. 13, 44, 85, 89

Grifone, R., Demignon, J., Houbron, C., Souil, E., Niro, C., Seller, M. J., Hamard, G. and Maire, P. (2005). Six1 and Six4 homeoproteins are required for Pax3 and Mrf expression during myogenesis in the mouse embryo. Development *132*, 2235–2249. 15, 17, 22, 94

Grifone, R., Laclef, C., Spitz, F., Lopez, S., Demignon, J., Guidotti, J.-E., Kawakami, K., Xu, P.-X., Kelly, R., Petrof, B. J. et al. (2004). Six1 and Eya1 expression can reprogram adult muscle from the slow-twitch phenotype into the fast-twitch phenotype. Molecular and cellular biology *24*, 6253–6267. 19, 25

Gros, J., Manceau, M., Thomé, V. and Marcelle, C. (2005). A common somitic origin for embryonic muscle progenitors and satellite cells. Nature *435*, 954–958. 16, 18

Gumerson, J. D. and Michele, D. E. (2011). The dystrophin-glycoprotein complex in the prevention of muscle damage. Journal of biomedicine & biotechnology *2011*, 210797. 6

Gürgen, D., Hegner, B., Kusch, A., Catar, R., Chaykovska, L., Hoff, U., Gross, V., Slowinski, T., da Costa Goncalves, A. C., Kintscher, U. et al. (2011). Estrogen receptor-β signals left ventricular hypertrophy sex differences in normotensive deoxycorticosterone acetate-salt mice. Hypertension *57*, 648–654. 76

Hackman, P., Marchand, S., Sarparanta, J., Vihola, A., Pénisson-Besnier, I., Eymard, B., Pardal-Fernández, J. M., Hammouda, E.-H., Richard, I., Illa, I. et al. (2008). Truncating mutations in C-terminal titin may cause more severe tibial muscular dystrophy (TMD). Neuromuscular Disorders *18*, 922–928. 4

Handschin, C., Kobayashi, Y. M., Chin, S., Seale, P., Campbell, K. P. and Spiegelman, B. M. (2007). PGC-1α regulates the neuromuscular junction program and ameliorates Duchenne muscular dystrophy. Genes & development *21*, 770–783. 13

Harper, S. Q., Hauser, M. A., DelloRusso, C., Duan, D., Crawford, R. W., Phelps, S. F., Harper, H. A., Robinson, A. S., Engelhardt, J. F., Brooks, S. V. et al. (2002). Modular flexibility of dystrophin: implications for gene therapy of Duchenne muscular dystrophy. Nature medicine *8*, 253–261. 9

Hartong, R., Wang, N., Kurokawa, R., Lazar, M. A., Glass, C. K., Apriletti, J. W. and Dillmann, W. H. (1994). Delineation of three different thyroid hormone-response elements in promoter of rat sarcoplasmic reticulum Ca2+ ATPase gene. Demonstration that retinoid X receptor binds 5'to thyroid hormone receptor in response element 1. Journal of Biological Chemistry *269*, 13021–13029. 67

Heanue, T. A., Reshef, R., Davis, R. J., Mardon, G., Oliver, G., Tomarev, S., Lassar, A. B. and Tabin, C. J. (1999). Synergistic regulation of vertebrate muscle development by Dach2, Eya2, and Six1, homologs of genes required for Drosophila eye formation. Genes & development *13*, 3231–3243. 17, 22

Heller, K. N., Mendell, J. T., Mendell, J. R. and Rodino-Klapac, L. R. (2017). MicroRNA-29 overexpression by adeno-associated virus suppresses fibrosis and restores muscle function in combination with micro-dystrophin. JCI insight *2*. 11

Hetzler, K. L., Collins, B. C., Shanely, R. A., Sue, H. and Kostek, M. C. (2014). The homoeobox gene SIX1 alters myosin heavy chain isoform expression in mouse skeletal muscle. Acta physiologica (Oxford, England) *210*, 415–428. 20, 50, 84, 89

Hollinger, K. and Selsby, J. (2013). The physiological response of protease inhibition in dystrophic muscle. Acta Physiologica *208*, 234–244. 6

Hoogerwaard, E., Van der Wouw, P., Wilde, A., Bakker, E., Ippel, P., Oosterwijk, J., Majoor-Krakauer, D., van Essen, A., Leschot, N. and de Visser, M. (1999). Cardiac involvement in carriers of Duchenne and Becker muscular dystrophy. Neuromuscular Disorders *9*, 347–351. 7

Hoskins, B. E., Cramer, C. H., Silvius, D., Zou, D., Raymond, R. M., Orten, D. J., Kimberling, W. J., Smith, R. J., Weil, D., Petit, C. et al. (2007). Transcription factor SIX5 is mutated in patients with branchio-oto-renal syndrome. The American Journal of Human Genetics *80*, 800–804. 16

Hughes, D. C., Marcotte, G. R., Marshall, A. G., West, D. W., Baehr, L. M., Wallace, M. A., Saleh, P. M., Bodine, S. C. and Baar, K. (2016). Age-related Differences in Dystrophin: Impact on Force Transfer Proteins, Membrane Integrity, and Neuromuscular Junction Stability. Journals of Gerontology Series A: Biomedical Sciences and Medical Sciences *72*, 640–648. 11

Hutcheson, D. A., Zhao, J., Merrell, A., Haldar, M. and Kardon, G. (2009). Embryonic and fetal limb myogenic cells are derived from developmentally distinct progenitors and have different requirements for β-catenin. Genes & development *23*, 997–1013. 16

Ikeda, K., Watanabe, Y., Ohto, H. and Kawakami, K. (2002). Molecular interaction and synergistic activation of a promoter by Six, Eya, and Dach proteins mediated through CREB binding protein. Molecular and cellular biology *22*, 6759–6766. 15

Ito, N., Kii, I., Shimizu, N., Tanaka, H. and Shin'ichi, T. (2017). Direct reprogramming of fibroblasts into skeletal muscle progenitor cells by transcription factors enriched in undifferentiated subpopulation of satellite cells. Scientific Reports *7*. 18

Izumo, S., Nadal-Ginard, B. and Mahdavi, V. (1986). All members of the MHC multigene family respond to thyroid hormone in a highly tissue-specific manner. Science *231*, 597–600. 73

Jacobs, S., Bär, P. and Bootsma, A. (1996). Effect of hypothyroidism on satellite cells and postnatal fiber development in the soleus muscle of rat. Cell and tissue research *286*, 137–144. 23

Jansson, E., Sjödin, B. and Tesch, P. (1978). Changes in muscle fibre type distribution in man after physical training: a sign of fibre type transformation? Acta Physiologica *104*, 235–237. 19

Juretic , N., Díaz, J., Romero, F., González, G., Jaimovich, E. and Riveros, N. (2017). Interleukin-6 and neuregulin-1 as regulators of utrophin expression via the activation of NRG-1/ErbB signaling pathway in mdx cells. Biochimica et Biophysica Acta (BBA)-Molecular Basis of Disease *1863*, 770–780. 12

Kassar-Duchossoy, L., Gayraud-Morel, B., Gomès, D., Rocancourt, D., Buckingham, M., Shinin, V. and Tajbakhsh, S. (2004). Mrf4 determines skeletal muscle identity in Myf5: Myod double-mutant mice. Nature *431*, 466–471. 17

Kawakami, K., Ohto, H., Ikeda, K. and Roeder, R. G. (1996a). Structure, function and expression of a murine homeobox protein AREC3, a homologue of Drosophila sine oculis gene product, and implication in development. Nucleic acids research *24*, 303–310. 14, 15

Kawakami, K., Ohto, H., Takizawa, T. and Saito, T. (1996b). Identification and expression of six family genes in mouse retina. FEBS letters *393*, 259–263. 14

Kawakami, K., Sato, S., Ozaki, H. and Ikeda, K. (2000). Six family genes–structure and function as transcription factors and their roles in development. BioEssays : news and reviews in molecular, cellular and developmental biology *22*, 616–626. 3

Kay, J. (1978). Intracellular Protein Degradation. Biochemical Society Transactions *6*, 789–797. 89

Kendall, G. C., Mokhonova, E. I., Moran, M., Sejbuk, N. E., Wang, D. W., Silva, O., Wang, R. T., Martinez, L., Lu, Q. L., Damoiseaux, R. et al. (2012). Dantrolene enhances antisense-mediated exon skipping in human and mouse models of Duchenne muscular dystrophy. Science translational medicine *4*, 164ra160–164ra160. 11

Khurana, T. S., Diamond, S. L., Moorwood, C., Lozynska, O., Napper, A. D., Pistilli, E. and Suri, N. (2012). Utrophin promoter activity upregulation for the treatment of muscular dystrophy. US Patent App. 13/129,074. 13, 86

Khurana, T. S., Rosmarin, A. G., Shang, J., Krag, T. O., Das, S. and Gammeltoft, S. (1999). Activation of Utrophin Promoter by Heregulin via theets-related Transcription Factor Complex GA-binding Protein α/β. Molecular Biology of the Cell *10*, 2075–2086. 12

Khurana, T. S., Watkins, S. C., Chafey, P., Chelly, J., Tomé, F. M., Fardeau, M., Kaplan, J.-C. and Kunkel, L. M. (1991). Immunolocalization and developmental expression of dystrophin related protein in skeletal muscle. Neuromuscular Disorders *1*, 185–194. 12

Kitajima, Y., Tashiro, Y., Suzuki, N., Warita, H., Kato, M., Tateyama, M., Ando, R., Izumi, R., Yamazaki, M., Abe, M., Sakimura, K., Ito, H., Urushitani, M., Nagatomi, R., Takahashi, R. and Aoki, M. (2014). Proteasome dysfunction induces muscle growth defects and protein aggregation. Journal of cell science *127*, 5204–5217. 11

Kobayashi, M., Nishikawa, K., Suzuki, T. and Yamamoto, M. (2001). The homeobox protein Six3 interacts with the Groucho corepressor and acts as a transcriptional repressor in eye and forebrain formation. Developmental biology *232*, 315–326. 15

Kochhar, A., Orten, D. J., Sorensen, J. L., Fischer, S. M., Cremers, C. W., Kimberling, W. J. and Smith, R. J. (2008). SIX1 mutation screening in 247 branchio-oto-renal syndrome families: A recurrent missense mutation associated with BOR. Human mutation *29*, 565–565. 16

Kuang, S., Kuroda, K., Le Grand, F. and Rudnicki, M. A. (2007). Asymmetric self-renewal and commitment of satellite stem cells in muscle. Cell *129*, 999–1010. 18

Kumar, J. (2009). The sine oculis homeobox (SIX) family of transcription factors as regulators of development and disease. Cellular and molecular life sciences *66*, 565–583. 14

Laclef, C., Hamard, G., Demignon, J., Souil, E., Houbron, C. and Maire, P. (2003a). Altered myogenesis in Six1-deficient mice. Development (Cambridge, England) *130*, 2239–2252. 17, 19, 94

Laclef, C., Souil, E., Demignon, J. and Maire, P. (2003b). Thymus, kidney and craniofacial abnormalities in Six1 deficient mice. Mechanisms of development *120*, 669–679. 17

Le Grand, F., Grifone, R., Mourikis, P., Houbron, C., Gigaud, C., Pujol, J., Maillet, M., Pagès, G., Rudnicki, M., Tajbakhsh, S. and Maire, P. (2012). Six1 regulates stem cell repair potential and self-renewal during skeletal muscle regeneration. The Journal of cell biology *198*, 815–832. 17, 89

Lepper, C., Partridge, T. A. and Fan, C.-M. (2011). An absolute requirement for Pax7-positive satellite cells in acute injury-induced skeletal muscle regeneration. Development *138*, 3639–3646. 18

Li, X., Oghi, K. A., Zhang, J., Krones, A., Bush, K. T., Glass, C. K., Nigam, S. K., Aggarwal, A. K., Maas, R., Rose, D. W. and Rosenfeld, M. G. (2003). Eya protein phosphatase activity regulates Six1-Dach-Eya transcriptional effects in mammalian organogenesis. Nature *426*, 247–254. 15, 18

Lin, K.-H., Shieh, H.-Y., Chen, S.-L. and Hsu, H.-C. (1999). Expression of mutant thyroid hormone nuclear receptors in human hepatocellular carcinoma cells. Molecular carcinogenesis *26*, 53–61. 24

Lin, S. and Burgunder, J.-M. (2000). Utrophin may be a precursor of dystrophin during skeletal muscle development. Developmental Brain Research *119*, 289–295. 12

Lin, S., Gaschen, F. and Burgunder, J. (1998). Utrophin is a regeneration-associated protein transiently present at the sarcolemma of regenerating skeletal muscle fibers in dystrophin-deficient hypertrophic feline muscular dystrophy. Journal of Neuropathology & Experimental Neurology *57*, 780–790. 47

Liu, Y., Chakroun, I., Yang, D., Horner, E., Liang, J., Aziz, A., Chu, A., De Repentigny, Y., Dilworth, F. J., Kothary, R. and Blais, A. (2013). Six1 regulates MyoD expression in adult muscle progenitor cells. PloS one *8*, e67762. 17, 18, 88, 93, 95

Liu, Y., Chu, A., Chakroun, I., Islam, U. and Blais, A. (2010). Cooperation between myogenic regulatory factors and SIX family transcription factors is important for myoblast differentiation. Nucleic acids research *38*, 6857–6871. 18, 39, 57, 60, 83, 93

Liu, Y., Cseresnyés, Z., Randall, W. R. and Schneider, M. F. (2001). Activity-dependent nuclear translocation and intranuclear distribution of NFATc in adult skeletal muscle fibers. J Cell Biol *155*, 27–40. 21

Liu, Y., Nandi, S., Martel, A., Antoun, A., Ioshikhes, I. and Blais, A. (2012). Discovery, optimization and validation of an optimal DNA-binding sequence for the Six1 homeodomain transcription factor. Nucleic acids research *40*, 8227–8239. 15

Ljubicic, V. and Jasmin, B. J. (2015). Metformin increases peroxisome proliferator–activated receptor γ Co-activator-1α and utrophin a expression in dystrophic skeletal muscle. Muscle & nerve *52*, 139–142. 13, 86

Ljubicic, V., Miura, P., Burt, M., Boudreault, L., Khogali, S., Lunde, J. A., Renaud, J.-M. and Jasmin, B. J. (2011). Chronic AMPK activation evokes the slow, oxidative myogenic program and triggers beneficial adaptations in mdx mouse skeletal muscle. Human molecular genetics *20*, 3478–3493. 13, 14, 86, 87

Long, C., Amoasii, L., Mireault, A. A., McAnally, J. R., Li, H., Sanchez-Ortiz, E., Bhattacharyya, S., Shelton, J. M., Bassel-Duby, R. and Olson, E. N. (2016). Postnatal genome editing partially restores dystrophin expression in a mouse model of muscular dystrophy. Science *351*, 400–403. 10

Love, D. R., Hill, D. F., Dickson, G., Spurr, N. K., Byth, B. C., Marsden, R. F., Walsh, F. S., Edwards, Y. H. and Davies, K. E. (1989). An autosomal transcript in skeletal muscle with homology to dystrophin. Nature *339*, 55–58. 11

Lu, A., Poddar, M., Tang, Y., Proto, J. D., Sohn, J., Mu, X., Oyster, N., Wang, B. and Huard, J. (2014). Rapid depletion of muscle progenitor cells in dystrophic mdx/utrophin-/- mice. Human molecular genetics *23*, 4786–4800. 12

Lu, Q.-L., Yokota, T., Takeda, S., Garcia, L., Muntoni, F. and Partridge, T. (2011). The status of exon skipping as a therapeutic approach to duchenne muscular dystrophy. Molecular Therapy *19*, 9–15. 10

Macian, F. (2005). NFAT proteins: key regulators of T-cell development and function. Nature Reviews Immunology *5*, 472–484. 20

Mahdavi, V., Izumo, S. and Nadal-Ginard, B. (1987). Developmental and hormonal regulation of sarcomeric myosin heavy chain gene family. Circulation Research *60*, 804–814. 73

Maia, A. L., Kim, B. W., Huang, S. A., Harney, J. W. and Larsen, P. R. (2005). Type 2 iodothyronine deiodinase is the major source of plasma T3 in euthyroid humans. Journal of Clinical Investigation *115*, 2524. 96

Mâncio, R. D., de Almeida Hermes, T., Macedo, A. B., Mizobuti, D. S., Valduga, A. H., Rupcic, I. F. and Minatel, E. (2017). Vitamin E treatment decreases muscle injury in mdx mice. Nutrition *43*, 39–46. 11

Manthorpe, M., Cornefert-Jensen, F., Hartikka, J., Felgner, J., Rundell, A., Margalith, M. and Dwarki, V. (1993). Gene therapy by intramuscular injection of plasmid DNA: studies on firefly luciferase gene expression in mice. Human gene therapy *4*, 419–431. 40, 84

Mauro, A. (1961). Satellite cell of skeletal muscle fibers. The Journal of biophysical and biochemical cytology *9*, 493. 18

Maves, L., Waskiewicz, A. J., Paul, B., Cao, Y., Tyler, A., Moens, C. B. and Tapscott, S. J. (2007). Pbx homeodomain proteins direct Myod activity to promote fast-muscle differentiation. Development *134*, 3371–3382. 22

McArdle, A., Helliwell, T. R., Beckett, G. J., Catapano, M., Davis, A. and Jackson, M. J. (1998). Effect of propylthiouracil-induced hypothyroidism on the onset of skeletal muscle necrosis in dystrophin-deficient mdx mice. Clinical Science *95*, 83–89. 24

McCaffrey, P. G., Luo, C., Kerppola, T. K., Jain, J., Badalian, T. M., Ho, A. M., Burgeon, E., Lane, W. S., Lambert, J. N., Curran, T. et al. (1993). Isolation of the cyclosporin-sensitive T cell transcription factor NFATp. SCIENCE-NEW YORK THEN WASHINGTON- *262*, 750–750. 20

McCarter, G. and Steinhardt, R. (2000). Increased activity of calcium leak channels caused by proteolysis near sarcolemmal ruptures. The Journal of membrane biology *176*, 169–174. 6

McCullagh, K. J., Calabria, E., Pallafacchina, G., Ciciliot, S., Serrano, A. L., Argentini, C., Kalhovde, J. M., Lømo, T. and Schiaffino, S. (2004). NFAT is a nerve activity sensor in skeletal muscle and controls activity-dependent myosin switching. Proceedings of the National Academy of Sciences of the United States of America *101*, 10590–10595. 21

McIntosh, L., Pernitsky, A. and Anderson, J. E. (1994). The effects of altered metabolism (hypothyroidism) on muscle repair in the mdx dystrophic mouse. Muscle & nerve *17*, 444–453. 24

McMahon, J., Signori, E., Wells, K., Fazio, V. and Wells, D. (2001). Optimisation of electrotransfer of plasmid into skeletal muscle by pretreatment with hyaluronidase-increased expression with reduced muscle damage. Gene therapy *8*, 1264. 29

McRae, N., Forgan, L., McNeill, B., Addinsall, A., McCulloch, D., Van der Poel, C. and Stupka, N. (2017). Glucocorticoids Improve Myogenic Differentiation In Vitro by Suppressing the Synthesis of Versican, a Transitional Matrix Protein Overexpressed in Dystrophic Skeletal Muscles. International Journal of Molecular Sciences *18*, 2629. 8

Mebis, L., Langouche, L., Visser, T. J. and Van den Berghe, G. (2007). The type II iodothyronine deiodinase is up-regulated in skeletal muscle during prolonged critical illness. The Journal of Clinical Endocrinology & Metabolism *92*, 3330–3333. 95

Mebis, L., Paletta, D., Debaveye, Y., Ellger, B., Langouche, L., D'Hoore, A., Darras, V. M., Visser, T. J. and Van den Berghe, G. (2009). Expression of thyroid hormone transporters during critical illness. European journal of endocrinology *161*, 243–250. 23, 67, 69, 93, 95

Meißner, J. D., Gros, G., Scheibe, R. J., Scholz, M. and Kubis, H.-P. (2001). Calcineurin regulates slow myosin, but not fast myosin or metabolic enzymes,

during fast-to-slow transformation in rabbit skeletal muscle cell culture. The Journal of physiology *533*, 215–226. 21

Mendell, J. R., Campbell, K., Rodino-Klapac, L., Sahenk, Z., Shilling, C., Lewis, S., Bowles, D., Gray, S., Li, C., Galloway, G. et al. (2010). Dystrophin immunity in Duchenne's muscular dystrophy. New England Journal of Medicine *363*, 1429–1437. 9

Mendell, J. R., Moxley, R. T., Griggs, R. C., Brooke, M. H., Fenichel, G. M., Miller, J. P., King, W., Signore, L., Pandya, S. and Florence, J. (1989). Randomized, double-blind six-month trial of prednisone in Duchenne's muscular dystrophy. The New England journal of medicine *320*, 1592–1597. 8

Mendell, J. R., Rodino-Klapac, L. R., Sahenk, Z., Roush, K., Bird, L., Lowes, L. P., Alfano, L., Gomez, A. M., Lewis, S., Kota, J. et al. (2013). Eteplirsen for the treatment of Duchenne muscular dystrophy. Annals of neurology *74*, 637–647. 9

Millay, D. P., Goonasekera, S. A., Sargent, M. A., Maillet, M., Aronow, B. J. and Molkentin, J. D. (2009). Calcium influx is sufficient to induce muscular dystrophy through a TRPC-dependent mechanism. Proceedings of the National Academy of Sciences *106*, 19023–19028. 6

Mills, I., Barge, R. M., Silva, J. E. and Larsen, P. R. (1987). Insulin stimulation of iodothyronine 5 -deiodinase in rat brown adipocytes. Biochemical and biophysical research communications *143*, 81–86. 95

Mitchell, K. J., Pannérec, A., Cadot, B., Parlakian, A., Besson, V., Gomes, E. R., Marazzi, G. and Sassoon, D. A. (2010). Identification and characterization of a non-satellite cell muscle resident progenitor during postnatal development. Nature cell biology *12*, 257–266. 18

Miura, P., Thompson, J., Chakkalakal, J. V., Holcik, M. and Jasmin, B. J. (2005). The utrophin A 5 -untranslated region confers internal ribosome entry site-mediated translational control during regeneration of skeletal muscle fibers. Journal of Biological Chemistry *280*, 32997–33005. 44

Moens, P., Baatsen, P. and Maréchal, G. (1993). Increased susceptibility of EDL muscles from mdx mice to damage induced by contractions with stretch. Journal of Muscle Research & Cell Motility *14*, 446–451. 5

Mu, X., Tang, Y., Takayama, K., Chen, W., Lu, A., Wang, B., Weiss, K. and Huard, J. (2017). RhoA/ROCK inhibition improves the beneficial effects of glucocorticoid treatment in dystrophic muscle: implications for stem cell depletion. Human Molecular Genetics *26*, ddx117. 8

Muntoni, F., Gobbi, P., Sewry, C., Sherratt, T., Taylor, J., Sandhu, S. K., Abbs, S., Roberts, R., Hodgson, S. V. and Bobrow, M. (1994). Deletions in the 59 region of dystrophin and resulting phenotypes. Journal of medical genetics *31*, 843–847. 9

Murphy, M. M., Lawson, J. A., Mathew, S. J., Hutcheson, D. A. and Kardon, G. (2011). Satellite cells, connective tissue fibroblasts and their interactions are crucial for muscle regeneration. Development *138*, 3625–3637. 18

Murphy, R. M., Larkins, N. T., Mollica, J. P., Beard, N. A. and Lamb, G. D. (2009). Calsequestrin content and SERCA determine normal and maximal Ca2+ storage levels in sarcoplasmic reticulum of fast-and slow-twitch fibres of rat. The Journal of physiology *587*, 443–460. 94

Murphy, S., Brinkmeier, H., Krautwald, M., Henry, M., Meleady, P. and Ohlendieck, K. (2017). Proteomic profiling of the dystrophin complex and membrane fraction from dystrophic mdx muscle reveals decreases in the cytolinker desmoglein and increases in the extracellular matrix stabilizers biglycan and fibronectin. Journal of Muscle Research and Cell Motility *37*, 1–18. 5

Muscat, G. E., Downes, M. and Dowhan, D. H. (1995). Regulation of vertebrate muscle differentiation by thyroid hormone: the role of the myoD gene family. Bioessays *17*, 211–218. 24

Nguyen, T. M., Ellis, J. M., Love, D. R., Davies, K. E., Gatter, K. C., Dickson, G. and Morris, G. E. (1991). Localization of the DMDL gene-encoded dystrophin-related protein using a panel of nineteen monoclonal antibodies: presence at neuromuscular junctions, in the sarcolemma of dystrophic skeletal muscle, in vascular and other smooth muscles, and in proliferating brain cell lines. The Journal of cell biology *115*, 1695–1700. 47

Nico, B., Nicchia, G. P., Frigeri, A., Corsi, P., Mangieri, D., Ribatti, D., Svelto, M. and Roncali, L. (2004). Altered blood–brain barrier development in dystrophic MDX mice. Neuroscience *125*, 921–935. 5

Nielsen, C., Potter, R. M., Borowy, C., Jacinto, K., Kumar, R. and Carlson, C. G. (2017). Postnatal Hyperplasic Effects of ActRIIB Blockade in a Severely Dystrophic Muscle. Journal of cellular physiology *232*, 1774–1793. *7*

Niro, C., Demignon, J., Vincent, S., Liu, Y., Giordani, J., Sgarioto, N., Favier, M., Guillet-Deniau, I., Blais, A. and Maire, P. (2010). Six1 and Six4 gene expression is necessary to activate the fast-type muscle gene program in the mouse primary myotome. Developmental biology *338*, 168–182. 19, 89

Noyes, M. B., Christensen, R. G., Wakabayashi, A., Stormo, G. D., Brodsky, M. H. and Wolfe, S. A. (2008). Analysis of homeodomain specificities allows the family-wide prediction of preferred recognition sites. Cell *133*, 1277–1289. 15

Ohlendieck, K., Ervasti, J. M., Matsumura, K., Kahl, S. D., Leveille, C. J. and Campbell, K. P. (1991). Dystrophin-related protein is localized to neuromuscular junctions of adult skeletal muscle. Neuron *7*, 499–508. 12

Ohto, H., Kamada, S., Tago, K., Tominaga, S.-I., Ozaki, H., Sato, S. and Kawakami, K. (1999). Cooperation of six and eya in activation of their target genes through nuclear translocation of Eya. Molecular and cellular biology *19*, 6815–6824. 15

Ohto, H., Takizawa, T., Saito, T., Kobayashi, M., Ikeda, K. and Kawakami, K. (2002). Tissue and developmental distribution of Six family gene products. International Journal of Developmental Biology *42*, 141–148. 15

Olguín, H. C. and Pisconti, A. (2012). Marking the tempo for myogenesis: Pax7 and the regulation of muscle stem cell fate decisions. Journal of cellular and molecular medicine *16*, 1013–1025. 3

Oliver, G., Mailhos, A., Wehr, R., Copeland, N. G., Jenkins, N. A. and Gruss, P. (1995a). Six3, a murine homologue of the sine oculis gene, demarcates the most anterior border of the developing neural plate and is expressed during eye development. Development *121*, 4045–4055. 14

Oliver, G., Wehr, R., Jenkins, N. A., Copeland, N. G., Cheyette, B., Hartenstein, V., Zipursky, S. L. and Gruss, P. (1995b). Homeobox genes and connective tissue patterning. Development *121*, 693–705. 15

Olson, E. N. and Klein, W. H. (1994). bHLH factors in muscle development: dead lines and commitments, what to leave in and what to leave out. Genes & development *8*, 1–8. 17

Ordahl, C. and Le Douarin, N. (1992). Two myogenic lineages within the developing somite. Development *114*, 339–353. 16

Ousterout, D. G., Kabadi, A. M., Thakore, P. I., Majoros, W. H., Reddy, T. E. and Gersbach, C. A. (2015). Multiplex CRISPR/Cas9-based genome editing for correction of dystrophin mutations that cause Duchenne muscular dystrophy. Nature communications *6*, 6244. 10

Ozaki, H., Watanabe, Y., Takahashi, K., Kitamura, K., Tanaka, A., Urase, K., Momoi, T., Sudo, K., Sakagami, J., Asano, M. et al. (2001). Six4, a Putative myogeninGene Regulator, Is Not Essential for Mouse Embryonal Development. Molecular and cellular biology *21*, 3343–3350. 17

Patrick, A. N., Cabrera, J. H., Smith, A. L., Chen, X. S., Ford, H. L. and Zhao, R. (2013). Structure-function analyses of the human SIX1–EYA2 complex reveal insights into metastasis and BOR syndrome. Nature Structural and Molecular Biology *20*, 447. 15

Péladeau, C., Ahmed, A., Amirouche, A., Crawford Parks, T. E., Bronicki, L. M., Ljubicic, V., Renaud, J.-M. and Jasmin, B. J. (2015). Combinatorial therapeutic activation with heparin and AICAR stimulates additive effects on utrophin A expression in dystrophic muscles. Human molecular genetics *25*, 24–43. 13, 86, 87

Petrof, B. J., Shrager, J. B., Stedman, H. H., Kelly, A. M. and Sweeney, H. L. (1993). Dystrophin protects the sarcolemma from stresses developed during muscle contraction. Proceedings of the National Academy of Sciences *90*, 3710–3714. 5

Pette, D. and Staron, R. S. (1997). Mammalian skeletal muscle fiber type transitions. International review of cytology *170*, 143–223. 24

Pierre, S. J. S., Chakkalakal, J. V., Kolodziejczyk, S. M., Knudson, J. C., Jasmin, B. J. and Megeney, L. A. (2004). Glucocorticoid treatment alleviates dystrophic myofiber pathology by activation of the calcineurin/NF-AT pathway. The FASEB journal *18*, 1937–1939. 8

Poortmans, J., Carpentier, A., Pereira-Lancha, L. and Lancha Jr, A. (2012). Protein turnover, amino acid requirements and recommendations for athletes and active populations. Brazilian Journal of Medical and Biological Research *45*, 875–890. 50

Rando, T. A. (2001). The dystrophin–glycoprotein complex, cellular signaling, and the regulation of cell survival in the muscular dystrophies. Muscle & nerve *24*, 1575–1594. 5

Ranger, A. M., Oukka, M., Rengarajan, J. and Glimcher, L. H. (1998). Inhibitory function of two NFAT family members in lymphoid homeostasis and Th2 development. Immunity *9*, 627–635. 20

Relaix, F. and Buckingham, M. (1999). From insect eye to vertebrate muscle: redeployment of a regulatory network. Genes & development *13*, 3171–3178. 15

Relaix, F., Rocancourt, D., Mansouri, A. and Buckingham, M. (2005). A Pax3/Pax7-dependent population of skeletal muscle progenitor cells. Nature *435*, 948–953. 17

Reza, M., Laval, S. H., Roos, A., Carr, S. and Lochmüller, H. (2016). Optimization of Internally Deleted Dystrophin Constructs. Human gene therapy methods *27*, 174–186. 6

Ricotti, V., Spinty, S., Roper, H., Hughes, I., Tejura, B., Robinson, N., Layton, G., Davies, K., Muntoni, F. and Tinsley, J. (2016). Safety, tolerability, and pharmacokinetics of SMT C1100, a 2-Arylbenzoxazole utrophin modulator, following single-and multiple-dose administration to pediatric patients with Duchenne muscular dystrophy. PloS one *11*, e0152840. 13

Risson, V., Mazelin, L., Roceri, M., Sanchez, H., Moncollin, V., Corneloup, C., Richard-Bulteau, H., Vignaud, A., Baas, D., Defour, A. et al. (2009). Muscle inactivation of mTOR causes metabolic and dystrophin defects leading to severe myopathy. The Journal of cell biology *187*, 859–874. 85, 86

Röckl, K. S., Hirshman, M. F., Brandauer, J., Fujii, N., Witters, L. A. and Goodyear, L. J. (2007). Skeletal muscle adaptation to exercise training. Diabetes *56*, 2062–2069. 19

Romitti, P. A., Zhu, Y., Puzhankara, S., James, K. A., Nabukera, S. K., Zamba, G. K. D., Ciafaloni, E., Cunniff, C., Druschel, C. M., Mathews, K. D., Matthews, D. J., Meaney, F. J., Andrews, J. G., Conway, K. M. C., Fox, D. J., Street, N., Adams, M. M., Bolen, J. and STARnet, M. (2015). Prevalence of Duchenne and Becker muscular dystrophies in the United States. Pediatrics *135*, 513–521. 4

Roy, P., Rau, F., Ochala, J., Messéant, J., Fraysse, B., Lainé, J., Agbulut, O., Butler-Browne, G., Furling, D. and Ferry, A. (2016). Dystrophin restoration therapy improves both the reduced excitability and the force drop induced by lengthening contractions in dystrophic mdx skeletal muscle. Skeletal muscle *6*, 23. 5

Ruf, R. G., Xu, P.-X., Silvius, D., Otto, E. A., Beekmann, F., Muerb, U. T., Kumar, S., Neuhaus, T. J., Kemper, M. J., Raymond, R. M. et al. (2004). SIX1 mutations cause branchio-oto-renal syndrome by disruption of EYA1–SIX1–DNA complexes. Proceedings of the National Academy of Sciences of the United States of America *101*, 8090–8095. 16

Ryu, D., Zhang, H., Ropelle, E. R., Sorrentino, V., Mázala, D. A., Mouchiroud, L., Marshall, P. L., Campbell, M. D., Ali, A. S., Knowels, G. M. et al. (2016). NAD+ repletion improves muscle function in muscular dystrophy and counters global PARylation. Science translational medicine *8*, 361ra139–361ra139. 11, 12

Sacco, A., Mourkioti, F., Tran, R., Choi, J., Llewellyn, M., Kraft, P., Shkreli, M., Delp, S., Pomerantz, J. H., Artandi, S. E. et al. (2010). Short telomeres and stem cell exhaustion model Duchenne muscular dystrophy in mdx/mTR mice. Cell *143*, 1059–1071. 7

Sakakibara, I., Santolini, M., Ferry, A., Hakim, V. and Maire, P. (2014). Six homeoproteins and a Iinc-RNA at the fast MYH locus lock fast myofiber terminal phenotype. PLoS genetics *10*, e1004386. 20, 37, 50, 64, 65, 66, 84, 89, 97, 124

Sakakibara, I., Wurmser, M., Dos Santos, M., Santolini, M., Ducommun, S., Davaze, R., Guernec, A., Sakamoto, K. and Maire, P. (2016). Six1 homeoprotein drives myofiber type IIA specialization in soleus muscle. Skeletal muscle *6*, 30. 20, 37, 60, 64, 65, 66, 84, 91, 92, 97, 124

Salmons, S. and Vrbova, G. (1969). The influence of activity on some contractile characteristics of mammalian fast and slow muscles. The Journal of physiology *201*, 535–549. 19

Salvatore, D., Simonides, W. S., Dentice, M., Zavacki, A. M. and Larsen, P. R. (2014). Thyroid hormones and skeletal muscle–new insights and potential implications. Nature Reviews Endocrinology *10*, 206. 72

Sambasivan, R., Yao, R., Kissenpfennig, A., Van Wittenberghe, L., Paldi, A., Gayraud-Morel, B., Guenou, H., Malissen, B., Tajbakhsh, S. and Galy, A. (2011). Pax7-expressing satellite cells are indispensable for adult skeletal muscle regeneration. Development *138*, 3647–3656. 18

Santaluci a, T., Moreno, H., Palaci n, M., Yacoub, M. H., Brand, N. J. and Zorzano, A. (2001). A novel functional co-operation between MyoD, MEF2 and TRα1 is sufficient for the induction of GLUT4 gene transcription. Journal of molecular biology *314*, 195–204. 22, 24

Santos, R., Gonçalves, A., Oliveira, J., Vieira, E., Vieira, J. P., Evangelista, T., Moreno, T., Santos, M., Fineza, I. and Bronze-da Rocha, E. (2014). New

variants, challenges and pitfalls in DMD genotyping: implications in diagnosis, prognosis and therapy. Journal of human genetics *59*, 454–464. 8

Sartorelli, V. and Fulco, M. (2004). Molecular and cellular determinants of skeletal muscle atrophy and hypertrophy. Sci. STKE *2004*, re11–re11. 2

Sassoon, D., Lyons, G., Wright, W. E., Lin, V., Lassar, A., Weintraub, H. and Buckingham, M. (1989). Expression of two myogenic regulatory factors myogenin and MyoDl during mouse embryogenesis. Nature *341*, 303–307. 17

Schiaffino, S. and Reggiani, C. (1994). Myosin isoforms in mammalian skeletal muscle. Journal of Applied Physiology *77*, 493–501. 50

Schienda, J., Engleka, K. A., Jun, S., Hansen, M. S., Epstein, J. A., Tabin, C. J., Kunkel, L. M. and Kardon, G. (2006). Somitic origin of limb muscle satellite and side population cells. Proceedings of the National Academy of Sciences of the United States of America *103*, 945–950. 16, 18

Schneider, M. J., Fiering, S. N., Pallud, S. E., Parlow, A. F., St. Germain, D. L. and Galton, V. A. (2001). Targeted disruption of the type 2 selenodeiodinase gene (DIO 2) results in a phenotype of pituitary resistance to T4. Molecular Endocrinology *15*, 2137–2148. 97

Seale, P., Sabourin, L. A., Girgis-Gabardo, A., Mansouri, A., Gruss, P. and Rudnicki, M. A. (2000). Pax7 is required for the specification of myogenic satellite cells. Cell *102*, 777–786. 18

Sekulic-Jablanovic, M., Ullrich, N. D., Goldblum, D., Palmowski-Wolfe, A., Zorzato, F. and Treves, S. (2016). Functional characterization of orbicularis oculi and extraocular muscles. The Journal of general physiology *147*, jgp–201511542. 13

Seo, H.-C., Curtiss, J., Mlodzik, M. and Fjose, A. (1999). Six class homeobox genes in Drosophila belong to three distinct families and are involved in head development. Mechanisms of development *83*, 127–139. 14

Serikaku, M. A. and O'Tousa, J. E. (1994). sine oculis is a homeobox gene required for Drosophila visual system development. Genetics *138*, 1137–1150. 14

Shaw, J.-P., Utz, P. J., Durand, D. B., Toole, J. J., Emmel, E. A. and Crabtree, G. R. (1988). Idetification of a Putative Regulator of Early T Cell Activation Genes. Science *241*, 202. 20

Simonides, W. S., Brent, G. A., Thelen, M. H., van der Linden, C. G., Larsen, P. R. and van Hardeveld, C. (1996). Characterization of the promoter of the rat sarcoplasmic endoplasmic reticulum Ca2+-ATPase 1 gene and analysis of thyroid hormone responsiveness. Journal of Biological Chemistry *271*, 32048–32056. 72

Simonides, W. S. and van Hardeveld, C. (2008). Thyroid hormone as a determinant of metabolic and contractile phenotype of skeletal muscle. Thyroid *18*, 205–216. 23

Sitzia, C., Farini, A., Jardim, L., Razini, P., Belicchi, M., Cassinelli, L., Villa, C., Erratico, S., Parolini, D., Bella, P. et al. (2016). Adaptive immune response impairs the efficacy of autologous transplantation of engineered stem cells in dystrophic dogs. Molecular Therapy *24*, 1949–1964. 10

Sledz, C. A., Holko, M., De Veer, M. J., Silverman, R. H. and Williams, B. R. (2003). Activation of the interferon system by short-interfering RNAs. Nature cell biology *5*, 834–839. 40

Solanes, G., Pedraza, N., Calvo, V., Vidal-Puig, A., Lowell, B. B. and Villarroya, F. (2005). Thyroid hormones directly activate the expression of the human and mouse uncoupling protein-3 genes through a thyroid response element in the proximal promoter region. Biochemical Journal *386*, 505–513. 67, 72

Spitz, F., Demignon, J., Porteu, A., Kahn, A., Concordet, J.-P., Daegelen, D. and Maire, P. (1998). Expression of myogenin during embryogenesis is controlled by Six/sine oculis homeoproteins through a conserved MEF3 binding site. Proceedings of the National Academy of Sciences *95*, 14220–14225. 22

Spitz, F., Salminen, M., Demignon, J., Kahn, A., Daegelen, D. and Maire, P. (1997). A combination of MEF3 and NFI proteins activates transcription in a subset of fast-twitch muscles. Molecular and cellular biology *17*, 656–666. 22

Studitsky, A. (1965). free auto-and homografts of muscle tissue in experiments on animals. Annals of the New York Academy of Sciences *120*, 789–801. 18

Stupka, N., Plant, D. R., Schertzer, J. D., Emerson, T. M., Bassel-Duby, R., Olson, E. N. and Lynch, G. S. (2006). Activated calcineurin ameliorates contraction-induced injury to skeletal muscles of mdx dystrophic mice. The Journal of physiology *575*, 645–656. 87

Syed, Y. Y. (2016). Eteplirsen: first global approval. Drugs *76*, 1699–1704. 9

Tadayoni, R., Rendon, A., Soria-Jasso, L. E. and Cisneros, B. (2012). Dystrophin Dp71: the smallest but multifunctional product of the Duchenne muscular dystrophy gene. Molecular neurobiology *45*, 43–60. 12

Tian, T., Li, A., Lu, H., Luo, R., Zhang, M. and Li, Z. (2015). Six1 promotes glioblastoma cell proliferation and invasion by upregulation of connective tissue growth factor. American journal of cancer research *5*, 1823–1830. 17

Timpani, C. A., Trewin, A. J., Stojanovska, V., Robinson, A., Goodman, C. A., Nurgali, K., Betik, A. C., Stepto, N., Hayes, A., McConell, G. K. et al. (2017). Attempting to compensate for reduced neuronal nitric oxide synthase protein with nitrate supplementation cannot overcome metabolic dysfunction but rather Has detrimental effects in dystrophin-deficient mdx muscle. Neurotherapeutics *14*, 429–446. 11

Tinsley, J., Deconinck, N., Fisher, R., Kahn, D., Phelps, S., Gillis, J. M. and Davies, K. (1998). Expression of full-length utrophin prevents muscular dystrophy in mdx mice. Nature medicine *4*, 1441–1444. 12, 87

Tinsley, J. M., Fairclough, R. J., Storer, R., Wilkes, F. J., Potter, A. C., Squire, S. E., Powell, D. S., Cozzoli, A., Capogrosso, R. F., Lambert, A., Wilson, F. X., Wren, S. P., De Luca, A. and Davies, K. E. (2011). Daily treatment with SMTC1100, a novel small molecule utrophin upregulator, dramatically reduces the dystrophic symptoms in the mdx mouse. PloS one *6*, e19189. 90

Tinsley, J. M., Potter, A. C., Phelps, S. R., Fisher, R., Trickett, J. I. and Davies, K. E. (1996). Amelioration of the dystrophic phenotype of mdx mice using a truncated utrophin transgene. Nature *384*, 349–353. 12, 25, 87

Tjondrokoesoemo, A., Schips, T., Kanisicak, O., Sargent, M. A. and Molkentin, J. D. (2016). Genetic overexpression of Serpina3n attenuates muscular dystrophy in mice. Human molecular genetics *25*, 1192–1202. 88, 90

Tomczak, K. K., Marinescu, V. D., Ramoni, M. F., Sanoudou, D., Montanaro, F., Han, M., Kunkel, L. M., Kohane, I. S. and Beggs, A. H. (2004). Expression profiling and identification of novel genes involved in myogenic differentiation. The FASEB journal *18*, 403–405. 18

Tremblay, P., Dietrich, S., Mericskay, M., Schubert, F. R., Li, Z. and Paulin, D. (1998). A Crucial Role forPax3in the Development of the Hypaxial Musculature and the Long-Range Migration of Muscle Precursors. Developmental biology *203*, 49–61. 17

Vandebrouck, C., Martin, D., Colson-Van Schoor, M., Debaix, H. and Gailly, P. (2002). Involvement of TRPC in the abnormal calcium influx observed in dystrophic (mdx) mouse skeletal muscle fibers. The Journal of cell biology *158*, 1089–1096. 6

Ventura-Holman, T., Mamoon, A., Subauste, M. C. and Subauste, J. S. (2011). The effect of oncoprotein v-erbA on thyroid hormone-regulated genes in hepatocytes and their potential role in hepatocellular carcinoma. Molecular biology reports *38*, 1137–1144. 24

Vianello, S., Yu, H., Voisin, V., Haddad, H., He, X., Foutz, A. S., Sebrié, C., Gillet, B., Roulot, M., Fougerousse, F. et al. (2013). Arginine butyrate: a therapeutic candidate for Duchenne muscular dystrophy. The FASEB Journal *27*, 2256–2269. 86

Vila, M. C., Rayavarapu, S., Hogarth, M. W., Van der Meulen, J. H., Horn, A., Defour, A., Takeda, S., Brown, K. J., Hathout, Y., Nagaraju, K. et al. (2017). Mitochondria mediate cell membrane repair and contribute to Duchenne muscular dystrophy. Cell death and differentiation *24*, 330. 6

Voit, T., Topaloglu, H., Straub, V., Muntoni, F., Deconinck, N., Campion, G., De Kimpe, S. J., Eagle, M., Guglieri, M., Hood, S. et al. (2014). Safety and efficacy of drisapersen for the treatment of Duchenne muscular dystrophy (DEMAND II): an exploratory, randomised, placebo-controlled phase 2 study. The Lancet Neurology *13*, 987–996. 10

Wang, H., Xu, Y., Liu, X., Wang, L., Jiang, W., Xiao, B., Wei, W., Chen, Y., Ye, W. and Ji, X. (2017). Prenatal diagnosis of Duchenne muscular dystrophy in 131 Chinese families with dystrophinopathy. Prenatal Diagnosis *37*, 356–364. 8

Wang, H., Zhu, Z., Wang, H., Yang, S., Mo, D. and Li, K. (2006). Characterization of different expression patterns of calsarcin-1 and calsarcin-2 in porcine muscle. Gene *374*, 104–111. 92

Wang, J., Chen, T., Feng, F., Wei, H., Pang, W., Yang, G. and Shen, Q. W. (2014). KLF15 regulates slow myosin heavy chain expression through NFATc1 in C2C12 myotubes. Biochemical and biophysical research communications *446*, 1231–1236. 21

Webster, C., Silberstein, L., Hays, A. P. and Blau, H. M. (1988). Fast muscle fibers are preferentially affected in Duchenne muscular dystrophy. Cell *52*, 503–513. 13, 25, 85

Weil, A. (1941). The chemical constitution of brain, kidneys and heart of white rats in experimental hypothyroidism. Endocrinology *29*, 919–926. 24, 94

Werneck-de Castro, J. P., Fonseca, T. L., Ignacio, D. L., Fernandes, G. W., Andrade-Feraud, C. M., Lartey, L. J., Ribeiro, M. B., Ribeiro, M. O., Gereben, B. and Bianco, A. C. (2015). Thyroid hormone signaling in male mouse skeletal muscle is largely independent of D2 in myocytes. Endocrinology *156*, 3842–3852. 97

Whitehead, N. P., Pham, C., Gervasio, O. L. and Allen, D. G. (2008). N-Acetylcysteine ameliorates skeletal muscle pathophysiology in mdx mice. The Journal of physiology *586*, 2003–2014. 6

Whitehead, N. P., Streamer, M., Lusambili, L. I., Sachs, F. and Allen, D. G. (2006). Streptomycin reduces stretch-induced membrane permeability in muscles from mdx mice. Neuromuscular Disorders *16*, 845–854. 6

Wilson, L., Cooper, B., Dux, L., Dubowitz, V. and Sewry, C. (1994). Expression of utrophin (dystrophin–related protein) during regeneration and maturation of skeletal muscle in canine X–linked muscular dystrophy. Neuropathology and applied neurobiology *20*, 359–367. 90

Winder, S. J., Lipscomb, L., Angela Parkin, C. and Juusola, M. (2011). The proteasomal inhibitor MG132 prevents muscular dystrophy in zebrafish. PLoS currents *3*, RRN1286. 11

Wong, S. H., Lowes, K. N., Quigley, A. F., Marotta, R., Kita, M., Byrne, E., Kornberg, A. J., Cook, M. J. and Kapsa, R. M. (2005). DNA electroporation in vivo targets mature fibres in dystrophic mdx muscle. Neuromuscular Disorders *15*, 630–641. 88

Wu, H., Rothermel, B., Kanatous, S., Rosenberg, P., Naya, F. J., Shelton, J. M., Hutcheson, K. A., DiMaio, J. M., Olson, E. N., Bassel-Duby, R. et al. (2001). Activation of MEF2 by muscle activity is mediated through a calcineurin-dependent pathway. The EMBO journal *20*, 6414–6423. 22, 53

Wu, W., Huang, R., Wu, Q., Li, P., Chen, J., Li, B. and Liu, H. (2014). The role of Six1 in the genesis of muscle cell and skeletal muscle development. International journal of biological sciences *10*, 983–989. 17

Wuebbles, R. D., Sarathy, A., Kornegay, J. N. and Burkin, D. J. (2013). Levels of 7 integrin and laminin- 2 are increased following prednisone treatment in the mdx mouse and GRMD dog models of Duchenne muscular dystrophy. Disease models & mechanisms *6*, 1175–1184. 8

Xu, P.-X., Zheng, W., Huang, L., Maire, P., Laclef, C. and Silvius, D. (2003). Six1 is required for the early organogenesis of mammalian kidney. Development *130*, 3085–3094. 24, 94

Xu, P.-X., Zheng, W., Laclef, C., Maire, P., Maas, R. L., Peters, H. and Xu, X. (2002). Eya1 is required for the morphogenesis of mammalian thymus, parathyroid and thyroid. Development *129*, 3033–3044. 24

Yaffe, D. and Saxel, O. (1977). A myogenic cell line with altered serum requirements for differentiation. Differentiation *7*, 159–166. 27

Yajima, H. and Kawakami, K. (2016). Low Six4 and Six5 gene dosage improves dystrophic phenotype and prolongs life span of mdx mice. Development, growth & differentiation *58*, 546–561. 16

Yajima, H., Motohashi, N., Ono, Y., Sato, S., Ikeda, K., Masuda, S., Yada, E., Kanesaki, H., Miyagoe-Suzuki, Y., Takeda, S. et al. (2010). Six family genes control the proliferation and differentiation of muscle satellite cells. Experimental cell research *316*, 2932–2944. 16

Yoshida, M. and Ozawa, E. (1990). Glycoprotein complex anchoring dystrophin to sarcolemma. The Journal of Biochemistry *108*, 748–752. 5

Young, C. S. and Pyle, A. D. (2016). Exon skipping therapy. Cell *167*, 1144. 9

Yuan, Y., Shi, X.-e., Liu, Y.-g. and Yang, G.-s. (2011). FoxO1 regulates muscle fiber-type specification and inhibits calcineurin signaling during C2C12 myoblast differentiation. Molecular and cellular biochemistry *348*, 77–87. 21

Zammit, P. S., Relaix, F., Nagata, Y., Ruiz, A. P., Collins, C. A., Partridge, T. A. and Beauchamp, J. R. (2006). Pax7 and myogenic progression in skeletal muscle satellite cells. Journal of cell science *119*, 1824–1832. 18

Zhang, D., Wang, X., Li, Y., Zhao, L., Lu, M., Yao, X., Xia, H., Wang, Y.-c., Liu, M.-F., Jiang, J. et al. (2014). Thyroid hormone regulates muscle fiber type conversion via miR-133a1. J Cell Biol *207*, jcb–201406068. 23, 96

Zhang, J. and Lazar, M. A. (2000). The mechanism of action of thyroid hormones. Annual review of physiology *62*. 23

Zhu, C. C., Dyer, M. A., Uchikawa, M., Kondoh, H., Lagutin, O. V. and Oliver, G. (2002). Six3-mediated auto repression and eye development requires its interaction with members of the Groucho-related family of co-repressors. Development *129*, 2835–2849. 15

Zorzano, A., Palacin, M. and Guma, A. (2005). Mechanisms regulating GLUT4 glucose transporter expression and glucose transport in skeletal muscle. Acta Physiologica *183*, 43–58. 72

Zubrzycka-Gaarn, E. E., Bulman, D. E., Karpati, G., Burghes, A. H., Belfall, B., Klamut, H. J., Talbot, J., Hodges, R. S., Ray, P. N. and Worton, R. G. (1988). The Duchenne muscular dystrophy gene product is localized in sarcolemma of human skeletal muscle. Nature *333*, 466. 47

Zybek-Kocik, A., Sawicka-Gutaj, N., Szczepanek-Parulska, E., Andrusiewicz, M., Waligórska-Stachura, J., Bia as, P., Krauze, T., Guzik, P., Skrobisz, J. and Rucha a, M. (2017). The association between irisin and muscle metabolism in different thyroid disorders. Clinical endocrinology *88*. 24

Contributions of Collaborators

John Girgis and Alexandre Blais designed the experiments and performed the bioinformatics analyses. Thesis was written by John Girgis and edited by Alexandre Blais. John Girgis and Dabo Yang performed the animal work. Iman Chakroun performed one of four *in vivo* ChIP replicates. Iman Chakroun performed the ChIP-Seq. Alphonse Chu performed the microarray timecourse and microarray Six TFs knockdown experiments. Data used to produce Figure 19 and Figure 20 was publicly available through publications by the Pascal Maire group (Sakakibara et al., 2014; Sakakibara et al., 2016). Thyroid-responsive Luciferase plasmid used in Figure 25A was donated kindly by Dr. Marcel Meima of the Erasmus University in Rotterdam.

Appendices

Bioinformatics Code

Plotting Heatmaps

```
library("affycoretools")
library("Biobase")
library("limma")
library("knitr")
library(affy)
library(annotate)
library(oligo)
library(pd.mogene.1.0.st.v1)
library("mogene10sttranscriptcluster.db")
library(rgl)
library(gplots)
library("extrafont")
library("ComplexHeatmap")
library("genefilter")


### set working directory
### On Windows machines, remember to use forward slashes in all
   paths

      setwd("D:/Expander/2016-06-07_PMaire_cSix1-KO_Gastroc/R_
         analysis/")

### indicate path with cel files, since it is different

      celpath <- paste("D:/Expander/2016-06-07_PMaire_cSix1-KO_
         Gastroc/cel_files/", sep="")

### read annotation file
### read it twice, will become useful later
```

```
        SDRF <- read.AnnotatedDataFrame("Maire_GAS-sol-ta_SDRF.txt",
           header=TRUE,row.names=1 ,as.is=TRUE)
        SDRFtext <- read.delim("Maire_GAS-sol-ta_SDRF.txt",check.
           names=FALSE,stringsAsFactors=FALSE)

### indicate the cel files to read

        cel_to_read <- paste(celpath, pData(SDRF)$File, sep="")

### read data and use all SDRF to populate phenoData

        mydata <- read.celfiles(filenames=cel_to_read, phenoData=
           SDRF)

### normalize using rma with defaults, Gene level using "core"

        normData <- oligo::rma(mydata, target="core")
        normData

### annotate, before running nsFilter

        annotation(normData) <- "mogene10sttranscriptcluster.db"

### remove probes with no Entrez GeneID annotation
### the reason is that this will improve stats after multiple
   hypothesis correction

        normData.entrez <- nsFilter(normData, require.entrez=TRUE,
           remove.dupEntrez=FALSE, var.filter=FALSE)

### create annotation lookup tables

        # this one has duplicates
                ID <- featureNames(normData.entrez)
                tmp <- select(mogene10sttranscriptcluster.db, ID, c("
                   SYMBOL","GENENAME","ENTREZID"))
        # this one removes all duplicates
                tmp4 <- tmp[!duplicated(tmp$PROBEID),]
        # this one concatenates names for those with duplicates
                tmp2 <- do.call("rbind", lapply(split(tmp, tmp$
                   PROBEID), function(x) apply(x,2,function(y) paste
                   (y[!duplicated(y)], collapse = "␣|␣"))))


##########################################
### Differential expression analysis
### linear model fitting based on genotype
```

```
Type <- factor(SDRFtext$Type, levels = unique(SDRFtext$Type)
    )
design <- model.matrix(~0+Type)

# 3 types of contrasts interest us
cont.matrix <- makeContrasts("TypeTA_WT - TypeSol_WT", "
    TypeGas_WT - TypeSol_WT", "TypeGas_cSix1KO - TypeGas_WT",
     levels=design)

fit <- lmFit(normData.entrez$eset, design)
fit2 <- contrasts.fit(fit, cont.matrix)
fit2 <- eBayes(fit2, trend=TRUE)

summary(decideTests(fit2))
summary(fit2$coefficients)
topTable(fit2, coef=1, number=100, genelist=tmp4$SYMBOL)

### export entire results to text file
### remember to adjust the coef value to the comparison you
     want
### coef=1 is for TA vs Sol
### coef=2 is for GAS vs Sol
### coef=3 is for Gas cSix1KO vs WT

write.table(topTable(fit2, coef=3, number=50000, genelist=
    tmp4$SYMBOL), file="output.cSix1KO-WT.entrez.txt", quote=
    FALSE, sep="\t")


##################
### Make heatmap just with the genes going UP or DOWN in cSix1KO
#(0.585 means a 50% change, 1 means a 2-fold change; 2 means a 4-
    fold change)

                    genes.to.plot3 <- topTable(fit2, coef=3, p.
                        value=0.05, adjust.method="BH", lfc=0.585,
                        number=5000, genelist=tmp4$SYMBOL, resort.
                        by="logFC")

                    selected.ids <- c(rownames(genes.to.plot3))

                    forCoolMap <- exprs(normData.entrez$eset)[
                        selected.ids,]

                    # give names matching those rows - using the
                        "mapIds()" function, adding also the logFC
                        , p.value and average expression
```

```
tab <- topTable(fit2, coef=3, number=40000,
   genelist=tmp4$SYMBOL)

rownames(forCoolMap) <- paste(mapIds(
   mogene10sttranscriptcluster.db, keys =
   selected.ids, keytype="PROBEID", column = "
   SYMBOL", multiVals="first"), signif(tab[
   selected.ids,]$logFC, 3), signif(tab[
   selected.ids,]$adj.P.Val, 3), signif(tab[
   selected.ids,]$AveExpr, 3), mapIds(
   mogene10sttranscriptcluster.db, keys =
   selected.ids, keytype="PROBEID", column = "
   ENTREZID", multiVals="first"), selected.ids
   , sep="|")

### subtract median from each row
### this is to make a median-centered heatmap
        # use function for med subtraction
        medsub <- function(z) {
                rowmed <- apply(z, 1,
                   median)
                rv <- sweep(z, 1, rowmed,
                   "-") #subtracting
                   median expression
                return(rv)
                }
        forCoolMap.medsub <- medsub(forCoolMap)

### make heatmap
    # create annotation
    ha = HeatmapAnnotation(df = data.frame(Tissue
       = factor(SDRFtext[,"Tissue"]), Genotype =
       factor(SDRFtext[,"Genotype"])), col = list(
       Genotype = c("WT" = "black", "cSix1KO" = "
       gray"), Tissue = c("Gas"="blue", "Sol"="red
       ", "TA"="lightblue")))

    # create the heatmap
```

```
ht1 <- Heatmap(forCoolMap.medsub, col =
    colorRamp2(c(-2, 0, 2), c("blue", "white",
    "red")), name="Log2␣med-centered␣expr.",
    column_title="Genes␣differentially␣
    expressed␣in␣cSix1␣and␣WT␣gastrocnemius\
    nChange␣by␣1.5-fold␣or␣more,␣corrected␣p␣
    value␣<␣0.05", column_title_side = "top",
    column_title_gp = gpar(fontsize = 10,
    fontface = "bold"), row_names_gp = gpar(
    fontsize = 4), clustering_distance_rows = "
    pearson", clustering_method_rows = "
    complete", top_annotation = ha, heatmap_
    legend_param = list(at = c(-2, -1, 0, 1, 2)
    ), cluster_columns = FALSE)

# create row boxplot, using data that has NOT
    been median-centered
ha_boxplot = HeatmapAnnotation(boxplot = anno_
    boxplot(forCoolMap, which = "row"), which =
    "row", width = unit(2, "cm"))

# prepare to write to file
# remember to adjust file name
pdf(file = "heatmap_new.cSix1-WT.AllData.
    entrez.BH0.05.pdf", height = 11, width =
    8.5, family = "Arial", paper = "special",
    onefile = FALSE)

# plot the heatmap
draw(ha_boxplot + ht1, heatmap_legend_side = "
    left", annotation_legend_side = "top")

dev.off()


##################
### Make heatmap just with the genes going UP or DOWN in TA or GAS
    versus Sol
#(0.585 means a 50% change, 1 means a 2-fold change; 2 means a 4-
    fold change)

genes.to.plot1 <- topTable(fit2, coef=1, p.
    value=0.05, adjust.method="BH", lfc=1,
    number=5000, genelist=tmp4$SYMBOL, resort.
    by="logFC")
```

```
genes.to.plot2 <- topTable(fit2, coef=2, p.
    value=0.05, adjust.method="BH", lfc=1,
    number=5000, genelist=tmp4$SYMBOL, resort.
    by="logFC")

selected.ids <- c(rownames(genes.to.plot1),
    rownames(genes.to.plot2))

# dael with duplicatess
# those duplicated are the probes that are
    deregualted in BOTH the TA vs Sol and the
    Gas vs Sol comparison
selected.ids.duplicated <- selected.ids[
    duplicated(selected.ids)]

# those unique are the probes that are
    deregulated in EITHER the TA vs Sol or the
     Gas vs Sol comparison
selected.ids.unique <- unique(selected.ids)

### graph for duplicated probes (differential
     expression in both fast muscles compared
    to SOL)
forCoolMap <- exprs(normData.entrez$eset)[
    selected.ids.duplicated,]

# give names matching those rows - using the
    "mapIds()" function, adding also the logFC
    , p.value and average expression
tab <- topTable(fit2, coef=1, number=40000,
    genelist=tmp4$SYMBOL)

rownames(forCoolMap) <- paste(mapIds(
    mogene10sttranscriptcluster.db, keys =
    selected.ids.duplicated, keytype="PROBEID",
     column = "SYMBOL", multiVals="first"),
    signif(tab[selected.ids.duplicated,]$logFC,
     3), signif(tab[selected.ids.duplicated,]$
    adj.P.Val, 3), signif(tab[selected.ids.
    duplicated,]$AveExpr, 3), mapIds(
    mogene10sttranscriptcluster.db, keys =
    selected.ids.duplicated, keytype="PROBEID",
     column = "ENTREZID", multiVals="first"),
    selected.ids.duplicated, sep="|")


### subtract median from each row
            # use function for med subtraction
```

```
        medsub <- function(z) {
                    rowmed <- apply(z, 1,
                       median)
                    rv <- sweep(z, 1, rowmed,
                       "-") #subtracting
                       median expression
                    return(rv)
                    }
        forCoolMap.medsub <- medsub(forCoolMap)

### make heatmap
    # create annotation
    ha = HeatmapAnnotation(df = data.frame(Tissue
       = factor(SDRFtext[,"Tissue"]), Genotype =
       factor(SDRFtext[,"Genotype"])), col = list(
       Genotype = c("WT" = "black", "cSix1KO" = "
       gray"), Tissue = c("Gas"="blue", "Sol"="red
       ", "TA"="lightblue")))

    # create the heatmap
    ht1 <- Heatmap(forCoolMap.medsub, col =
       colorRamp2(c(-2, 0, 2), c("blue", "white",
       "red")), name="Log2 med-centered expr.",
       column_title="Genes differentially
       expressed in Gas vs Sol and in TA vs Sol\
       nChange by 2-fold or more, BH pvalue < 0.05
       for each comparison", column_title_side =
       "top", column_title_gp = gpar(fontsize =
       10, fontface = "bold"), row_names_gp = gpar
       (fontsize = 2), clustering_distance_rows =
       "pearson", clustering_method_rows = "
       complete", top_annotation = ha, heatmap_
       legend_param = list(at = c(-2, -1, 0, 1, 2)
       ), cluster_columns = FALSE)

    # create row boxplot, using data that has NOT
        been median-centered
    ha_boxplot = HeatmapAnnotation(boxplot = anno_
       boxplot(forCoolMap, which = "row"), which =
        "row", width = unit(2, "cm"))

    # prepare to write to file
    pdf(file = "heatmap_new.DiffExp_in_TAvsSOL_and
       _GASvsSOL.entrez.pdf", height = 11, width =
        8.5, family = "Arial", paper = "special",
       onefile = FALSE)

    # plot the heatmap
```

```
draw(ha_boxplot + ht1, heatmap_legend_side = "
    left", annotation_legend_side = "top")

dev.off()


##################
### Make heatmap just with the genes going UP or DOWN in TA or GAS
    versus Sol
# but also filter with genes with a Six1 BS within 50 kb of TSS in
    primary myotubes
# use Six1_MT_splitter_c50_summits_FC.bed
# use GREAT version 3.0.0
# Species assembly: mm9
# Association rule: Basal+extension: 5000 bp upstream, 1000 bp
   downstream, 50000 bp max extension,
# curated regulatory domains included
# Genes_with_Six1_MT_peaks.GREAT.txt

genes.to.plot1 <- topTable(fit2, coef=1, p.
    value=0.05, adjust.method="BH", lfc=1,
    number=5000, genelist=tmp4$SYMBOL, resort.
    by="logFC")
genes.to.plot2 <- topTable(fit2, coef=2, p.
    value=0.05, adjust.method="BH", lfc=1,
    number=5000, genelist=tmp4$SYMBOL, resort.
    by="logFC")

selected.ids <- c(rownames(genes.to.plot1),
    rownames(genes.to.plot2))

# deal with duplicates
# those duplicated are the probes that are
    deregualted in BOTH the TA vs Sol and the
    Gas vs Sol comparison
bothdereg.ids <- selected.ids[duplicated(
    selected.ids)]

# gene gene symbols for those probes
bothdereg.ids.annot <- as.data.frame(mapIds(
    mogene10sttranscriptcluster.db, keys = as.
    vector(bothdereg.ids), keytype="PROBEID",
    column = "SYMBOL", multiVals="first"))
colnames(bothdereg.ids.annot) <- "Symbols"

    ### introduce Six1-bound genes
    bound <- read.table("Genes_with_Six1_MT
        _peaks.GREAT.txt")
```

```
                colnames(bound) <- "SYMBOL"

            ### Now retain only the deregualted genes
                that have a symbol also found in the list
                of Six1-bound genes
                    bothdereg.bound.ids <- rownames(subset(
                        bothdereg.ids.annot, bothdereg.ids.
                        annot$Symbols %in% bound$SYMBOL))

            ### graph for duplicated (diff expression in
                both fast muscles)
221         forCoolMap <- exprs(normData.entrez$eset)[
                bothdereg.bound.ids,]

            # give names matching those rows - using the
                "mapIds()" function, adding also the logFC
                , p.value and average expression
            # values for the TA vs Sol comparison
            tab <- topTable(fit2, coef=1, number=40000,
                genelist=tmp4$SYMBOL)

            rownames(forCoolMap) <- paste(mapIds(
                mogene10sttranscriptcluster.db, keys =
                bothdereg.bound.ids, keytype="PROBEID",
                column = "SYMBOL", multiVals="first"),
                signif(tab[bothdereg.bound.ids,]$logFC, 3),
                 signif(tab[bothdereg.bound.ids,]$adj.P.Val
                , 3), signif(tab[bothdereg.bound.ids,]$
                AveExpr, 3), mapIds(
                mogene10sttranscriptcluster.db, keys =
                bothdereg.bound.ids, keytype="PROBEID",
                column = "ENTREZID", multiVals="first"),
                bothdereg.bound.ids, sep="|")

        ### subtract median from each row
                    # use function for med subtraction
231                 medsub <- function(z) {
                                rowmed <- apply(z, 1,
                                    median)
                                rv <- sweep(z, 1, rowmed,
                                    "-") #subtracting
                                    median expression
                                return(rv)
                                }
                    forCoolMap.medsub <- medsub(forCoolMap)

### make heatmap
            # create annotation
```

```
ha = HeatmapAnnotation(df = data.frame(Tissue
   = factor(SDRFtext[,"Tissue"]), Genotype =
   factor(SDRFtext[,"Genotype"])), col = list(
   Genotype = c("WT" = "black", "cSix1KO" = "
   gray"), Tissue = c("Gas"="blue", "Sol"="red
   ", "TA"="lightblue")))

# create the heatmap
ht1 <- Heatmap(forCoolMap.medsub, col =
   colorRamp2(c(-2, 0, 2), c("blue", "white",
   "red")), name="Log2␣med-centered␣expr.",
   column_title="Six1-bound␣genes␣
   differentially␣expressed␣in␣Gas␣vs␣Sol␣and␣
   in␣TA␣vs␣Sol\nChange␣by␣2-fold␣or␣more,␣BH␣
   pvalue␣<␣0.05␣for␣each␣comparison", column_
   title_side = "top", column_title_gp = gpar(
   fontsize = 10, fontface = "bold"), row_
   names_gp = gpar(fontsize = 4), clustering_
   distance_rows = "pearson", clustering_
   method_rows = "complete", top_annotation =
   ha, heatmap_legend_param = list(at = c(-2,
   -1, 0, 1, 2)), cluster_columns = FALSE)

# create row boxplot, using data that has NOT
    been median-centered
ha_boxplot = HeatmapAnnotation(boxplot = anno_
   boxplot(forCoolMap, which = "row"), which =
    "row", width = unit(2, "cm"))

# prepare to write to file
pdf(file = "heatmap_new.DiffExp_in_TAvsSOL_and
   _GASvsSOL.entrez+Six1Bound.pdf", height =
   11, width = 8.5, family = "Arial", paper =
   "special", onefile = FALSE)

# plot the heatmap
draw(ha_boxplot + ht1, heatmap_legend_side = "
   left", annotation_legend_side = "top")

dev.off()
```

Sample and Data Relationship Format Annotation File

```
File Name Type Replicate Tissue Genotype
TA_WT_1 GSM1125060_ctl1_MoGene-1_0-st-v1_.CEL TA_WT_1 TA_WT 1 TA WT
TA_WT_2 GSM1125062_ctl2_MoGene-1_0-st-v1_.CEL TA_WT_2 TA_WT 2 TA WT
Sol_WT_1 GSM1212589_ctrl_1_sol_MoGene-1_0-st-v1_.CEL Sol_WT_1
   Sol_WT 1 Sol WT
Sol_WT_2 GSM1212590_ctrl_2_sol_MoGene-1_0-st-v1_.CEL Sol_WT_2
   Sol_WT 2 Sol WT
Sol_WT_3 GSM1212591_ctrl_3_sol_MoGene-1_0-st-v1_.CEL Sol_WT_3
   Sol_WT 3 Sol WT
Gas_WT_1 GSM1125095_2_ctl1_GAS_MoGene-1_0-st-v1.CEL Gas_WT_1 Gas_WT
    1 Gas WT
Gas_WT_2 GSM1125096_2_ctl2_GAS_MoGene-1_0-st-v1.CEL Gas_WT_2 Gas_WT
    2 Gas WT
Gas_WT_3 GSM1125097_ctl3_GAS_MoGene-1_0-st-v1_.CEL Gas_WT_3 Gas_WT
   3 Gas WT
Gas_cSix1KO_1 GSM1125098_cSix1_1_GAS_MoGene-1_0-st-v1_.CEL
   Gas_cSix1KO_1 Gas_cSix1KO 1 Gas cSix1KO
Gas_cSix1KO_2 GSM1125099_cSix1_2_GAS_MoGene-1_0-st-v1_.CEL
   Gas_cSix1KO_2 Gas_cSix1KO 2 Gas cSix1KO
Gas_cSix1KO_3 GSM1125100_cSix1_3_GAS_MoGene-1_0-st-v1_.CEL
   Gas_cSix1KO_3 Gas_cSix1KO 3 Gas cSix1KO
```

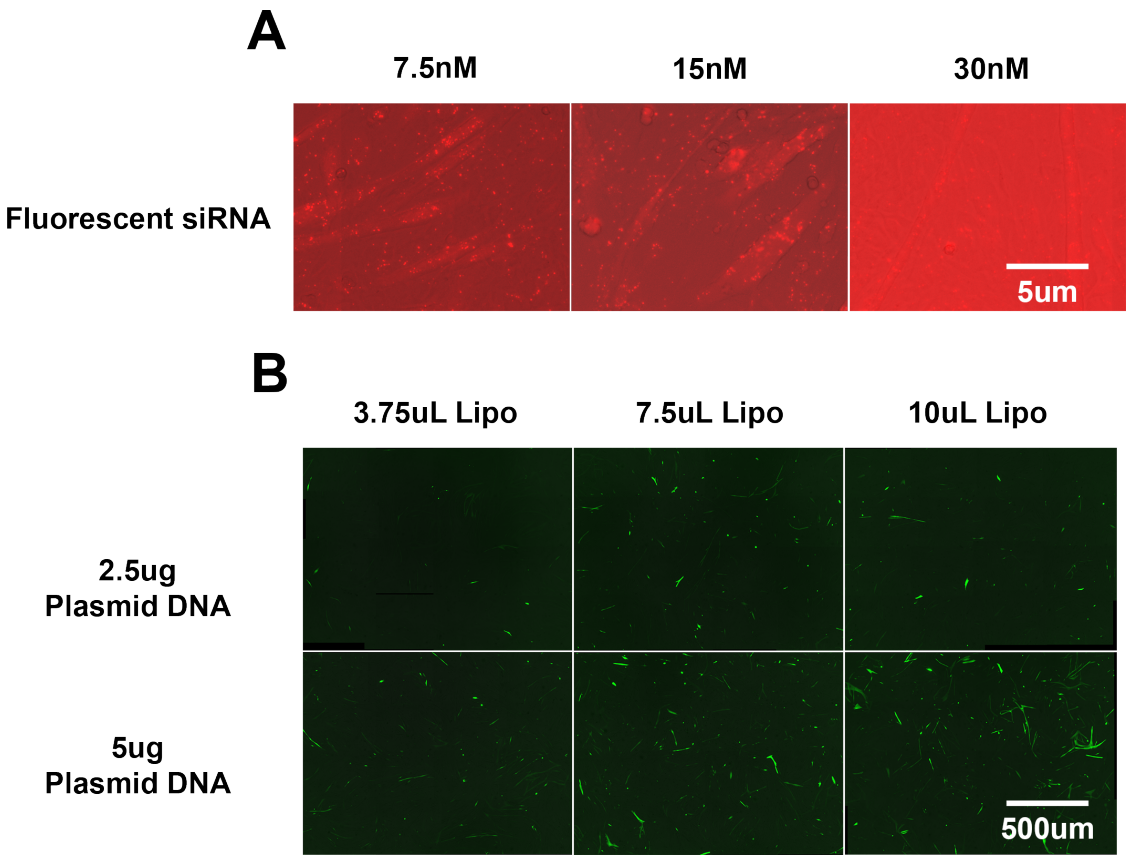

Figure 29: **Optimization of *in vitro* transfection efficiency**
(**A**) Representative microscopy of Alexa Fluor 555-conjugated fluorescent siRNA signal in transfected C2C12 Myotubes. From left to right, panels exhibit increased starting concentrations of transfected siRNA used to optimize siRNA transfection efficiency.
(**B**) Representative microscopy of GFP signal in transfected C2C12 Myotubes. Two different concentrations of plasmid DNA were administered, along with 3 different amounts of Lipofectamine transfection reagent (Lipo), in order to optimize plasmid DNA transfection efficiency.

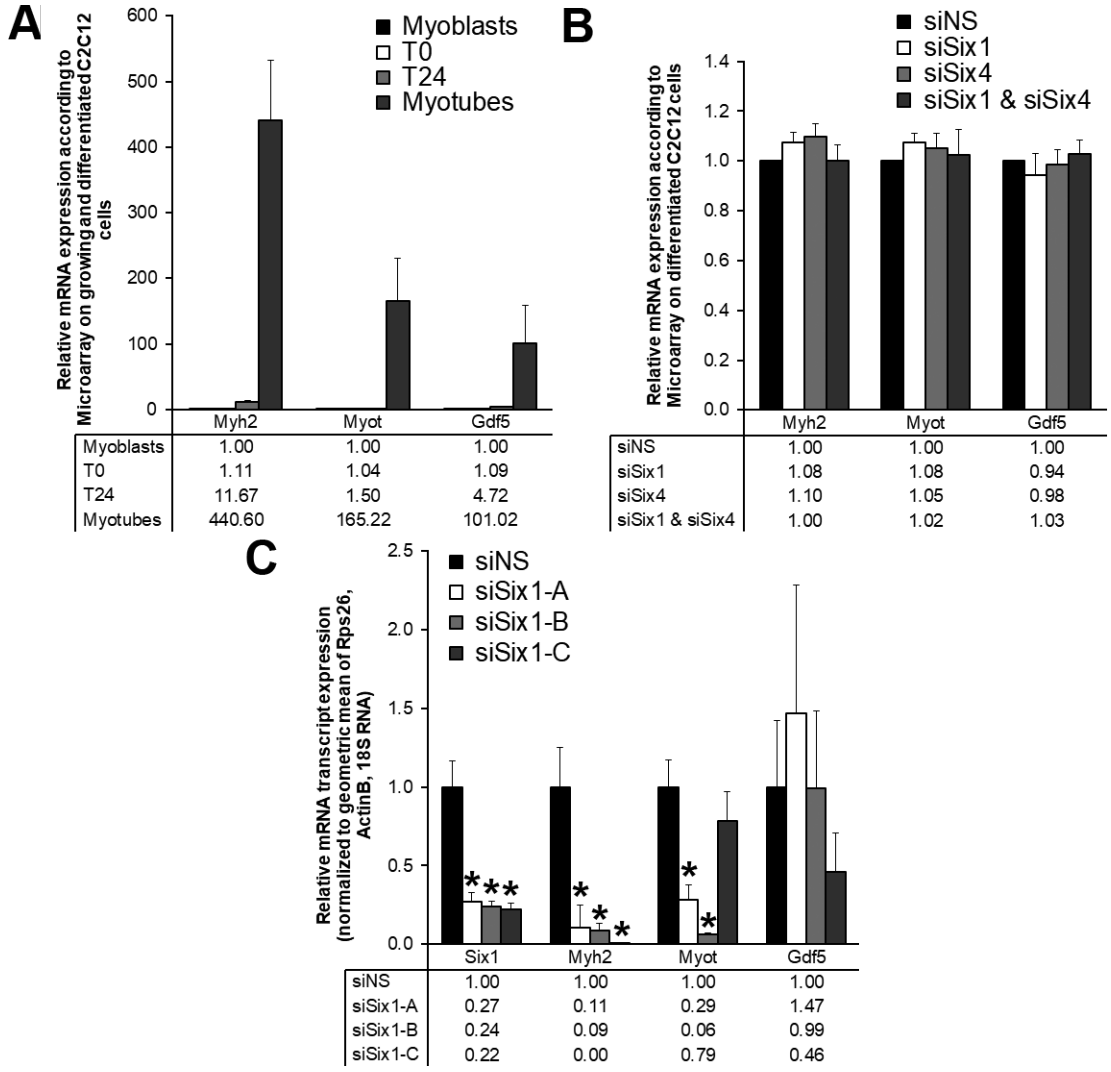

Figure 30: **C2C12 Myotubes are a poor model for studying adult muscle**
(**A**) Determination of late-induced differentiation genes based on Microarray time-course analysis of differentiating C2C12 cells.
(**B**) Determination of late-induced differentiation genes unaffected by Six1 knockdown based on Microarray knockdown analysis of T24 differentiating C2C12 cells.
(**C**) Analysis of Six1 knockdown resistant late differentiation genes at T144 of differentiating C2C12 cells under Six1 knockdown conditions. Data represents an average of 3 biological replicates (A), 4 biological replicates (B), and 5 biological replicates (C). SIX1-A, -B and -C represent three distinct siRNA duplexes with the ability to induce Six1 mRNA knockdown (sequences found in Table 3). siNS represents a control siRNA targeting a non-specific sequence. Error bars indicate the SEM. * Represents statistically significant changes in levels of expression as determined by a two-tailed paired Student's T-Test relative to siNS (p-value $<$ 0.05).

Tables

Table 3: List of used oligonucleotides for qPCR and siRNA

Name	Sequence	Application
18S Forward	CCTGCGGCTTAATTTGACTC	qRT-PCR
18S Reverse	AACTAAGAACGGCCATGCAC	qRT-PCR
Atp1b4 Forward	GACCCGGAGAAAAGGATGTC	qRT-PCR
Atp1b4 Reverse	AGCCAGGGAGGCATAGAAG	qRT-PCR
Atp2a1 Forward	TGTCCCTCCACTTCCTCATC	qRT-PCR
Atp2a1 Reverse	TCCGAGCAATGAACTTGAGA	qRT-PCR
Beta Actin Forward	ATCGCTGACAGGATGCAGAAG	qRT-PCR
Beta Actin Reverse	AGAGCCACCAATCCACACAGA	qRT-PCR
Dio2 Forward	TCTTGACTTTGCCAGTGCAG	qRT-PCR
Dio2 Reverse	GCAGTTGCCTAGTGAAAGGTG	qRT-PCR
Dio3 Forward	GCTCTGGTCCTGGACACTATG	qRT-PCR
Dio3 Reverse	GCCACTCTGGATGACGTAGAG	qRT-PCR
Gdf5 Forward	GTAACAGCAGCGTGAAGTTGG	qRT-PCR
Gdf5 Reverse	CACGTACCTCTGCTTCCTGAC	qRT-PCR
Glut4 Forward	TTGGGAACACTCAACCAACTG	qRT-PCR
Glut4 Reverse	GTAGCTGTGCCCAGCATAGAC	qRT-PCR
HoxD10 Forward	GAGAAATCGGACTCACCTTCC	ChIP-qPCR
HoxD10 Reverse	CACATACCCAGGCAGAACG	ChIP-qPCR
Ifitm1 Forward	CCGTGAAGTCTAGGGACAGG	qRT-PCR
Ifitm1 Reverse	ACAGGGAGCTGATGTTCAGG	qRT-PCR
Irf7 Forward	CACCCCCATCTTCGACTTC	qRT-PCR
Irf7 Reverse	TGTAGTGTGGTGACCCTTGC	qRT-PCR
Irf9 Forward	CAAGCAAGACTTCCGAGAGG	qRT-PCR
Irf9 Reverse	TCCCCATCTTTGTGCTTTTC	qRT-PCR
Mb Forward	CAAGATCCCGGTCAAGTACC	qRT-PCR
Mb Reverse	GAGCATCTGCTCCAAAGTCC	qRT-PCR
MCT10	GCGUCUUCACAAUCCUGCUCCCUUU	Stealth siRNA
MCT10 Forward	ACAACATGGCCTTCAAGACAG	qRT-PCR
MCT10 Reverse	CCGTGAAGACACTCACGATG	qRT-PCR
MCT10 Forward	GGATATTGTTGGACCCATGC	ChIP-qPCR
MCT10 Reverse	AAACTGGAGACATGGGGTTG	ChIP-qPCR
MCT8 Forward	AAAAATCGCCAAGTGGAGTTC	qRT-PCR
MCT8 Reverse	TCACAATGGGAGAACAGAAGAAG	qRT-PCR
Me1 Forward	TTTCGAACGACTGAACTCTGAC	qRT-PCR
Me1 Reverse	ATGAGCACGCTGTAGAAGAGC	qRT-PCR
Mef2D Forward	CGTGGCAACACCAAGTTTAC	qRT-PCR
Mef2D Reverse	GGAGGATAGCTCTGCACTGG	qRT-PCR
Meg3 Forward	CTGCAGCTCTTCCAGAAACC	qRT-PCR
Meg3 Reverse	GGTGTGAGCCGATGATGTC	qRT-PCR
Myh1 Forward	ACCGCAAGAATGTTCTCAGG	qRT-PCR
Myh1 Reverse	ATTTGGCCAGGTTGACATTG	qRT-PCR

Myh2 Forward	AGGCAACTTCTGGCAAAATG	qRT-PCR
Myh2 Reverse	TGTCATTCCTCACGGTCTTG	qRT-PCR
Myh3 Forward	TTTGATGCCAAAACCTACTGC	qRT-PCR
Myh3 Reverse	ATGGCATACACGTCCTCTGG	qRT-PCR
Myh4 Forward	CATGAACCCTCCCAAGTACG	qRT-PCR
Myh4 Reverse	TGACGGTGACACAAAAGAGG	qRT-PCR
Myh7 Forward	AGGGCGACCTCAACGAGAT	qRT-PCR
Myh7 Reverse	CAGCAGACTCTGGAGGCTCTT	qRT-PCR
Myog Forward	CAGTGAATGCAACTCCCACA	qRT-PCR
Myog Reverse	ACCCAGCCTGACAGACAATC	qRT-PCR
Myog Forward	AGAGGGAAGGGGAATCACAT	ChIP-qPCR
Myog Reverse	TGGCATGAACCCAGAGATAA	ChIP-qPCR
Myot Forward	CCGTCTCAACCCGATTACTG	qRT-PCR
Myot Reverse	GGATGACATGGCATTTACAGG	qRT-PCR
Myoz1	GGAGGAAGUCAAGCAAACUGAUUAU	Stealth siRNA
Myoz1 Forward	GAGGAGGAAGTCAAGCAAACTG	qRT-PCR
Myoz1 Reverse	TGATCTTCTTGCCCAGGTTC	qRT-PCR
Myoz1 Forward	CCACCCAGTGTAACCAGACC	ChIP-qPCR
Myoz1 Reverse	TAGCCCTTCTGCAGGATCAG	ChIP-qPCR
Rcan1 Forward	TGGGGAAGGAAATGAAGTTG	qRT-PCR
Rcan1 Reverse	GGGGAGATGAGGAACTGTTTG	qRT-PCR
Rcan2 Forward	TTATGCTGTGGCCAAACTAGG	qRT-PCR
Rcan2 Reverse	CTGTCACACACATGCACCAC	qRT-PCR
Rps26 Forward	GCCATCCATAGCAAGGTTGT	qRT-PCR
Rps26 Reverse	GCCTCTTTACATGGGCTTTG	qRT-PCR
Runx1 Forward	CCGTGCTACCCACTCACTG	qRT-PCR
Runx1 Reverse	ATGACGGTGACCAGAGTGC	qRT-PCR
Six1 Forward	TTTTACGCAAGAGCAAGTGG	qRT-PCR
Six1 Reverse	CTCTCGTTCTTGTGCAGGTG	qRT-PCR
SIX1-A	GCGAGGAGACCAGCUACUGCUUUAA	Stealth siRNA
SIX1-B	ACUCCUCCUCCAACAAGCAGAAUCA	Stealth siRNA
SIX1-C	GCAACUUCCGCGAGCUCUACAAGAU	Stealth siRNA
Six4 Forward	CGAGACCCAGTCCAAAAGC	qRT-PCR
Six4 Reverse	GCTAGAGAGGCTGAGGTTGG	qRT-PCR
SIX4-B	UAAGGAAGACAGGUGAAGUACUUGC	Stealth siRNA
Thra Forward	AGGCCTTCAGCGAGTTTACC	qRT-PCR
Thra Reverse	ATGATCTGGTCTTCGCAAGG	qRT-PCR
Thrb Forward	ACCAGAGTGGTGGATTTTGC	qRT-PCR
Thrb Reverse	AAGGGACATGATCTCCATGC	qRT-PCR
UCP3 Forward	TGCACTGTATGCTGAAGATGG	qRT-PCR
UCP3 Reverse	AAACATCATCACGTTCCAAGC	qRT-PCR
Utrophin Forward	TCCAGCTCAGATCCTGAAGTC	qRT-PCR
Utrophin Reverse	CACCTGCAGATTTCTTTGCTC	qRT-PCR
Zdbf2 Forward	GCTTGCTCTTTTCTGCTCAAG	qRT-PCR
Zdbf2 Reverse	TGCAATACCCTTGCCTTTTC	qRT-PCR

Table 4: List of used Antibodies and Dilutions

Antibody	Dilution	Source or Product Number	Manufacturer
B-Tubulin	1:1000	Hybridoma Cells Clone 9E7	DSHB
Myosin I	1:100	BA-D5	DSHB
Myosin IIa	1:100	SC-71	DSHB
Myoz1	1:500	Clone 8 SC-136429	Santa Cruz
Six1	1:500	Purified from immunized rabbits	Open Biosystems
Six4	1:1000	Purified from immunized rabbits	Open Biosystems
Utrophin (IF)	1:100	NCL-DRP2	Leica Biosystems
Utrophin (WB)	1:800	H-300 SC-15377	Santa Cruz